Photo-Assisted Atomic Layer Deposition and Chemical Vapor Deposition of Metal and Metal Oxide Thin Films

Katja Marianne Väyrynen

M.Sc. Thesis

Laboratory of Inorganic Chemistry

Department of Chemistry

University of Helsinki

10 / 2015

HELSINGIN YLIOPISTO – HELSINGFORS UNIVERSITET – UNIVERSITY OF HELSINKI

Tiedekunta/Osasto – Fakultet/Sektion – Faculty/Section	Laitos – Institution – Department
Faculty of Science	Department of Chemistry

Tekijä – Författare – Author
Katja Marianne Väyrynen

Työn nimi – Arbetets titel – Title
Photo-Assisted Atomic Layer Deposition and Chemical Vapor Deposition of Metal and Metal Oxide Thin Films

Oppiaine – Läroämne – Subject
Inorganic Chemistry

Työn laji – Arbetets art – Level	Aika – Datum – Month and year	Sivumäärä – Sidoantal – Number of pages
M.Sc. Thesis	10 / 2015	140

Tiivistelmä – Referat – Abstract

The deposition of high-quality metal thin films is an integral part of the modern microelectronic industry. As the downscaling of feature sizes continues, there is a constant demand for more accurate film deposition methods. Owing to its atomic level accuracy, atomic layer deposition (ALD) is a thin film deposition technique that has gained growing interest among researchers since it was patented in the 1970s. The ALD method is based on sequential saturating surface reactions that lead to a self-limiting growth mechanism and thus enable the deposition of conformal films even on complex structures. The impetus behind this thesis was to develop ALD processes for the deposition of as thin, continuous, and conducting metal films as possible. Thermally driven metal ALD processes are typically carried out at high temperatures increasing the extent of coarsening and thus limiting the deposition of thin yet continuous films. Plasma-enhancement has been employed to lower the deposition temperatures but with limited success. Photo-assistance could potentially be utilized to lower the deposition temperatures and thus provide an alternative for the use of plasma. So far, photo-ALD has mainly been utilized to merely enhance existing thermal ALD processes. The majority of the studied materials are oxides, but with the right tools and precursors the method could turn out suitable for metal deposition as well.

Since there are no reports on the photo-ALD of metals, the literature review of this thesis concentrates on photochemical vapor deposition (photo-CVD) instead. The main motivation was to gain insight into the photochemistry occurring in the metal photo-CVD processes and then put this knowledge into practice in photo-ALD. Although most of the processes introduced in the literature review rely on gas-phase irradiation of the metal precursor or thermal decomposition achieved by the use of intense laser light, both of which may lead to CVD-type growth and are thus usually considered as undesirable effects in terms of ALD, valuable information regarding e.g. potential precursor candidates as well as reactor configurations for photo-ALD was acquired.

The first part of the experimental section focuses on setting up the photo-ALD reactor the operation of which was then tested with a single-source Ta_2O_5 process known from literature. Analogous processes were developed for Nb_2O_5, TiO_2, ZrO_2, and HfO_2 using the corresponding alkoxides as precursors. All the processes were identified as light induced based on area-selective deposition achieved with the use of near-contact masks. For the Ta_2O_5 process, the photolytic nature was further demonstrated with optical filtering and conformality studies. The deposition of Ru, Ag, Mo, Ti, and Cu was attempted using a variety of precursors. The depositions were carried out either by using the single-source approach or in the presence of a co-reactant. Mirror-like metal growth was observed only for Ru and Ag and furthermore, only on certain substrates. Neither Ru nor Ag was deposited on metals, and on oxides the growth appeared to stop after the formation of a continuous metal film. The film formation in the case of metals was found to be highly dependent on the substrate; however, further mechanistic investigation is necessary. Several explanations were proposed, but the answer remains ambiguous.

Avainsanat – Nyckelord – Keywords
Atomic Layer Deposition, ALD, Photo-ALD, Photo-CVD, UV irradiation, Thin film, Metal, Metal oxide

Säilytyspaikka – Förväringställe – Where deposited
Kumpula Campus Library / E-thesis

Muita tietoja – Övriga uppgifter – Additional information

Contents

Abbreviations

acac	acetylacetonate
AES	Auger emission spectroscopy
ALD	atomic layer deposition
BTMSE	bis(trimethylsilyl)ethane
chd	cyclohexadiene
COD	1,5-cyclooctadiene
Cp	cyclopentadienyl
CVD	chemical vapor deposition
cw	continuous-wave
DEZn	diethylzinc
DIBAH	diisobutylaluminum hydride
DMAH	dimethylaluminum hydride
DMCd	dimethylcadmium
DMEAA	dimethylethylamine alane
DMZn	dimethylzinc
DRAM	dynamic random access memory
EBECHRu	(ethylbenzyl)(1-ethyl-1,4-cyclohexadienyl)Ru(0)
EDS	energy-dispersive X-ray spectroscopy
fod	2,2-dimethyl-6,6,7,7,8,8,8-heptafluorooctane-3,5-dionato
FRAM	ferroelectric random access memory
GIXRD	grazing incidence X-ray diffraction
hfac	hexafluoroacetylacetonate
IR	infrared
LCVD	laser-assisted chemical vapor deposition
LHAR	lateral high aspect ratio
MHY	2-methyl-1-hexene-3-yne

MOSFET	metal-oxide-semiconductor field-effect transistor
PEALD	plasma-enhanced atomic layer deposition
pta	pivaloyltrifluoroacetonate
PVD	physical vapor deposition
QCM	quartz crystal microbalance
SAM	self-assembled monolayer
SEM	scanning electron microscopy
TEAA	triethylamine alane
thd	2,2,6,6-tetramethyl-3,5-heptadionate
TIBA	triisobutylaluminum
TMA	trimethylaluminum
TMAA	trimethylamine alane
TMVS	trimethylvinylsilane
TOF-EI-MS	time-of-flight electron ionization mass spectrometry
TOF-ERDA	time-of-flight elastic recoil detection analysis
TOF-SIMS	time-of-flight secondary ion mass spectrometry
UV	ultraviolet
VUV	vacuum ultraviolet
XES	X-ray emission spectroscopy
XPS	X-ray photoelectron spectroscopy
XRD	X-ray diffraction
XRR	X-ray reflectivity
YBCO	yttrium barium copper oxide

1 Introduction

Deposition of metal thin films and coatings is essential for a myriad of applications including coatings resistant to oxidation, corrosion, and abrasion, reflective coatings, electrodes, as well as electronic contacts.[1] A significant field of application lies in the development of efficient interconnects for microelectronic devices. In order to increase the number of components on an integrated circuit and thus improve the performance of an electronic device, feature sizes must be reduced. Scaling down requires accurate deposition techniques yielding materials of high quality in a well-defined manner.

The deposition of metal films is often done by physical vapor deposition (PVD) methods such as evaporation and sputtering. However, as line-of-sight techniques these methods provide poor step coverage, and the uniform coating of complex structures is thus nigh impossible. Chemical vapor deposition (CVD) is a technique based on the reactions or decomposition of volatile precursors on a heated substrate, which ultimately results in film formation. Although superior to the PVD methods with respect to conformality, the rate and extent of film formation in CVD is difficult to control making it inadequate a method to rise up to the demands set by future microelectronics.

Atomic layer deposition (ALD), which is a modification of the CVD technique, relies on sequential saturating surface reactions leading to the self-limiting growth mechanism characteristic to ALD.[2–6] A typical ALD cycle consists of alternating precursor pulses separated by purge gas flows that eliminate gas-phase reactions. ALD is the ultimate method for depositing conformal films with an atomic level accuracy even at the bottom of high-aspect-ratio trenches. The unparalleled conformality explains the increasing research on the ALD method driven by the demands arising from the industry. ALD has been employed to deposit a plethora of materials ranging from pure elements to oxides, nitrides, chalcogenides, and many others.[7] The deposition of metal films by conventional ALD has, however, been quite restricted due to a lack of suitable precursors and reducing agents as well as the insufficient amount of energy provided by thermal activation. Thermal ALD processes are mostly found for noble metals such as Ru and Ir.[8,9] The deposition of electropositive metals, such as Ti and Ta, has proven to be quite challenging by conventional ALD but has been achieved by supplying additional energy to the process via plasma discharges in plasma-

enhanced ALD (PEALD).[10] On the other hand, the use of aggressive plasma species may lead to issues with conformality and film damage.

Photo-assisted atomic layer deposition employs ultraviolet (UV) radiation and/or visible light to activate the film forming reactions. Due to the additional energy provided by photons, depositions may potentially be carried out at lower temperatures compared to thermal ALD enabling the use of thermally unstable precursors and substrates. Photons do not cause film damage to the same extent as the aggressive plasma species in PEALD. Other beneficial aspects of photo-ALD include selective area film growth, modified film properties, and the possibility to use single-source precursors. The amount of impurities can also be reduced although some electronically active defects may appear.

Only a limited number of articles regarding photo-ALD have been published. The studied materials include GaAs, ZnO, Ta_2O_5, ZrO_2, BN, TiO_2, and Al_2O_3.[11–23] The majority of these processes are merely enhancements of the earlier established corresponding thermal ALD processes with lower deposition temperatures and increased growth rates. Up to date, no reports on the photo-ALD of metals exist although the method might turn out to be quite suitable for metal deposition since the use of photons facilitates the removal of ligands and can be employed to generate efficient reducing species such as hydrogen and methyl radicals. The main motivation behind the development of metal photo-ALD is the desire to obtain as thin, continuous, and conducting metal films as possible. Because photo-ALD processes can potentially be carried out at lower temperatures, the extent of coarsening should be reduced and continuous films thus obtained at lower thicknesses compared to thermal ALD.

Due to the nonexistence of metal photo-ALD processes, the literature review of this thesis concentrates on the deposition of metals via photo-CVD. The photo-CVD of metals has been extensively scrutinized and applied for a wide selection of metals providing valuable information on the photochemistry that is likely to occur in photo-ALD as well. The experimental section of this thesis revolves around the photo-ALD of ruthenium and silver. The first part of the research focused on setting up the photo-ALD reactor and its testing with several metal oxide processes using the corresponding metal alkoxides as precursors analogous to that reported for Ta_2O_5 by Lee *et al.*[18]

Literature review

2 Fundamentals of photochemical vapor deposition

2.1 Basic principle

CVD is a thin film deposition method where one or several vapor-phase precursors are transported into a reactor where they produce material on a heated substrate via chemical reactions that can occur both on the surface as well as in the gas phase.[1,24] Gas-phase reactions may lead to particle formation resulting in films of lower quality and are thus usually undesirable. Furthermore, keeping in mind the goal of this thesis, the development of photo-ALD, the examination of surface chemistry is far more essential than detailed assessment of gas-phase reactions. Figure 1 illustrates a number of steps characteristic to a typical CVD process.[1]

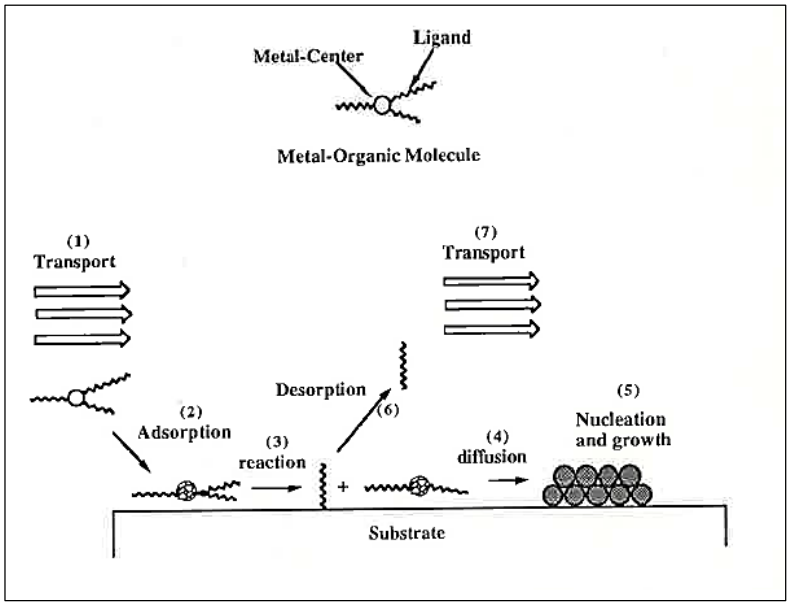

Figure 1. Different steps occurring in a typical CVD system.[1] Reproduced with permission from Jairath, R., Jain, A., Tolles, R.D., Hampden-Smith, M.J. and Kodas, T.T. in *The Chemistry of Metal CVD*, chapter 1, p. 30. Copyright 1994 VCH Verlagsgesellschaft mbH.

While conventional CVD processes rely on thermal energy, there are alternative forms of energy that can be utilized to enhance the film growth. Due to reactive radical species, plasma-assisted depositions can generally be carried out at lower temperatures and with higher growth rates than thermal depositions. Film density can also be improved, however, film damage caused by the energetic species may appear. Besides plasma, CVD processes can also be activated with photons. Photo-CVD was of great scientific interest especially in the ‘80s and ‘90s, during which time many a review article was published.[25–28] As with plasma enhancement, a potential advantage also with light inducement is the lowered deposition temperatures which allow the utilization of thermally unstable substrates. It is also possible to employ precursors with poor thermal stability without increasing the extent of decomposition and thus the amount of defects caused by particles.

Photo-assistance is typically carried out by applying photons the wavelength of which varies from the UV range to the visible region (100–700 nm). Light is usually obtained either from a UV lamp or a laser as discussed in more detail in Section 3.2. Photon activation can occur directly via absorption by precursor molecules, indirectly via reaction intermediates, or by substrate absorption. A molecule can absorb radiation either in the gas phase or on the surface after adsorption. The absorption behavior of a molecule may change drastically upon adsorption, which must be taken into account in the assessment of a process. In a favorable case, the absorption of a photon at a given wavelength excites the precursor molecule to a higher energy state. After the excitation, the molecule may undergo dissociation or react with other species present in the system potentially resulting in deposition of the desired material. In order for the dissociation to occur, the incident photons must be energetic enough to break bonds, typically meaning operation in the UV region. Dissociation may follow either single-photon absorption or the absorption of multiple photons. Single-photon processes generally operate at lower energy densities suppressing excess heating of the substrate; thus, undesired diffusion processes and thermal decomposition of the precursor can be avoided.

In some cases, lasers operating in the infrared (IR) regime have been utilized to generate vibrational excitations within a molecule leading to its dissociation and, further on, film formation. Moreover, even when working in the UV or visible region, there is some thermal component involved and the film growth typically results from the combination of both photolysis and pyrolysis. The two mechanisms are difficult to distinguish but can be qualitatively studied by using optical filters excluding the longer wavelengths contributing

to most of the heating or by measuring the temperature of the substrate. The extent of heating can also be minimized by the proper choice of substrate. Metals, for instance, absorb light efficiently and are thus heated more than the optically transparent quartz. Deposition rates in photo-CVD processes may be independent of temperature, increase, or even decrease as a function of temperature depending on the growth mechanism. With increasing temperature the extent of pyrolysis typically increases, which often translates into higher growth rates. A decreasing trend in the growth rate is observed if the process relies on the photolysis of adsorbed species because their surface coverage decreases with increasing temperature. Deposition rates are also affected by reactant pressures.[27] At low reactant pressures, film growth is dominated by surface photolysis generally producing films with good morphology and low resistivity. In contrast, high reactant pressures lead to increased gas-phase photolysis yielding deposits of poor quality at high growth rates.

One of the greatest assets of photo-CVD is the lowered deposition temperature enabling the use of thermally unstable substrates and precursors. The method may also allow the deposition of materials that are not readily accessible by thermal CVD. In some cases, photo-CVD has been utilized to generate a film that acts as a nucleation layer for subsequent thermal deposition. Photo-CVD also allows area-selective deposition either by the use of masks or by laser beam scanning. Area-selectivity via masking is possible if the process is governed by the photolysis of surface species. Laser writing is based on the local heating of the substrate causing pyrolysis of the adsorbed precursor molecules. Provided that the diffusion of gas-phase photofragments is minimized, well-defined lines can be deposited. Major drawbacks that have limited the development of photo-CVD include complex reaction chemistry and reactor design, alongside the lack of suitable precursors. Precursor chemistry is assessed in more detail in the forthcoming section.

2.2 Precursors

Precursor chemistry is an integral part of the overall design of CVD processes.[1,24,29] There is a wide selection of requirements common for all CVD precursors that can be further categorized into essential and desirable features. Sufficient volatility ensures efficient and reproducible precursor supply. High vapor pressure gases and liquids can be delivered at a constant flux and are thus generally favored over solids. The precursors should be stable and of high purity to minimize the inclusion of impurities in the deposits. Moderate reactivity suppresses gas-phase reactions; thus, particle formation can be avoided. To abide by the principles of sustainable development, non-toxic, recyclable, and low-cost precursors are typically preferred.

Compounds serving as precursors for thermal CVD can also be utilized in laser driven processes where deposition occurs via pyrolysis at localized hot spots. In photolytic processes, however, film formation is governed by the optical properties of the compound and precursors suitable for thermal CVD may be of no utility for photo-CVD. Determination of the absorption spectrum of a compound is the most vital step when evaluating its applicability for photo-CVD.[30] The precursor candidate should have strong absorption at the wavelengths emitted by the light source in use. As mentioned in the previous section, the absorption behavior of a compound may be significantly different in the gas phase and on the substrate surface.[26] The altered photochemistry of the adsorbed species may arise from surface relaxation or a different decomposition pathway.[27] The extinction coefficient of the compound should also be taken into account since the effectiveness of photo-enhancement increases as a function of absorbed radiation. Absorption properties depend on the bonding in a given compound. Tightly bound σ-electrons require more energy and thus shorter wavelengths for excitation than the less tightly held π-electrons. The absorption of photons must lead to a reaction path that ultimately results in film formation. Precursors having the metal at a low oxidation state are generally favored since the reduction of these compounds to metallic form occurs more readily as opposed to high-valent metal precursors.

Metal alkyls have been utilized to deposit e.g. aluminum, zinc, and cadmium films via photo-CVD (discussed in more detail in Section 4).[27] Several metal alkyls dissociate upon absorption of 257 nm photons making them highly compatible with a frequency-doubled Ar^+ laser operating at 257.3 nm. Metal alkyls are readily available and their photochemistry is

well-understood, which explains their abundant utilization as photo-CVD precursors. However, alkyl compounds decompose to reactive alkyl radicals upon absorption, which may produce films with high carbon contents. A significant amount of carbon generally has a deteriorating effect on film properties such as resistivity. Another downside related to the alkyl precursors is their pyrophoricity meaning that extra caution has to be taken towards safe handling.

Metal carbonyls have been applied as precursors for the photo-CVD of e.g. chromium, molybdenum, and tungsten. Metal carbonyls are relatively volatile compounds at a zerovalent state. Moreover, metal carbonyls are known for their reactivity towards light, a topic which has been reviewed on several occasions.[31–33] Metal films deposited from the corresponding carbonyl complexes are often highly contaminated with carbon and oxygen impurities.[34] Possible explanations for the contamination include incomplete decarbonylation of the precursor and adsorption of CO molecules released during gas-phase dissociation.

Metal β-diketonates are volatile compounds and show strong absorption at wavelengths above 250 nm due to the resonance structure depicted in Figure 2.[30] The absorption wavelength can be modified with the choice of proper substituents, which facilitates matching a precursor with a suitable light source. The most studied metals deposited from the corresponding β-diketonate complexes include e.g. copper and platinum.

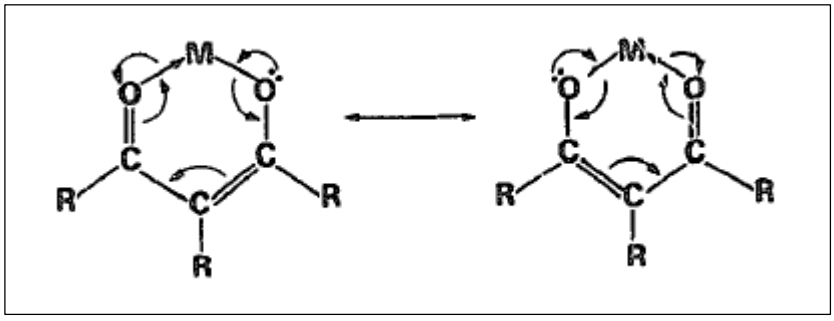

Figure 2. The resonance structure of a metal β-diketonate complex.[30] Reproduced with permission from Trundle, C. and Brierley, C.J. *Appl. Surf. Sci.* ***36*** 102. Copyright 1989 Elsevier.

Cyclopentadienyl (Cp) complexes have been employed in the photo-CVD of e.g. iron and nickel. The main advantage of metallocenes as opposed to alkyl and carbonyl compounds is their non-pyrophoricity. According to Stauf *et al.*, the direct photodecomposition of metallocenes leads to the cleavage of the bond between the metal atom and the Cp ligand.[35] The Cp ring is stable and volatile enabling its feasible removal from the metal surface. However, at high temperatures there is a possibility of fragmentation leading to carbon contamination.

If carbon contamination of the deposits is of critical concern, a metal halide precursor can be utilized instead of a carbon-containing one.[27] Halide precursors have been employed as metal sources for the deposition of e.g. tungsten and aluminum. Metal halides are often highly volatile and generally absorb radiation in the UV range making them compatible with photo-CVD. The main advantage of halide precursors is the exclusion of carbon impurities although trace amounts of halogen species may appear instead.

3 Reactors for photochemical vapor deposition

3.1 Reactor design

CVD reactors can roughly be categorized into two groups: hot- and cold-wall reactors.[1,24] In hot-wall reactors, the entire reactor chamber is heated ensuring uniform temperature throughout the system, which further permits orientational variation of the substrate with respect to the gas flow. In cold-wall reactors, a heater is utilized to localize the heating only to a restricted area where the sample is placed. As follows, film formation on the reactor walls can be minimized and frequent maintenance of the chamber thus avoided. Deposition throughout the chamber is especially detrimental in photo-CVD reactors having an optical window integrated into the system, a topic assessed in Section 3.3. The downside of the cold-wall reactors arises from the steep temperature gradients over the substrate causing severe convection and, in consequence, non-uniform films. Cold walls also increase the probability of precursor condensation. Both reactor types have been utilized in photo-CVD, however, the cold-wall reactors are more abundant on the grounds of window protection. Analogous to conventional CVD, precursors in photo-CVD are admitted into the system either parallel to (cross-flow reactor) or atop the substrate (showerhead reactor). The latter is more tolerant to non-ideal chemistry but is slower due to fewer collisions of precursor molecules between the substrate and the reactor walls.

In addition to the basic components of a CVD reactor (reaction chamber, carrier gas supply, precursor delivery, and vacuum system), a photo-CVD reactor is typically composed of a light source and an optically transparent window. The types of light sources and windows are more thoroughly discussed in the forthcoming sections. Radiation is most often directed perpendicularly with respect to the substrate. Figure 3 represents a typical photo-CVD setup where the radiation is obtained from a light source directly above the susceptor and the precursors are delivered from the side of the reaction chamber.[36] Parallel irradiation may produce films the morphology of which differs greatly from that of films deposited via perpendicular irradiation. The light source may also be held at some fixed angle as shown in Figure 4.[37] Another option is to tilt the susceptor with respect to the irradiation source as depicted in Figure 5.[38]

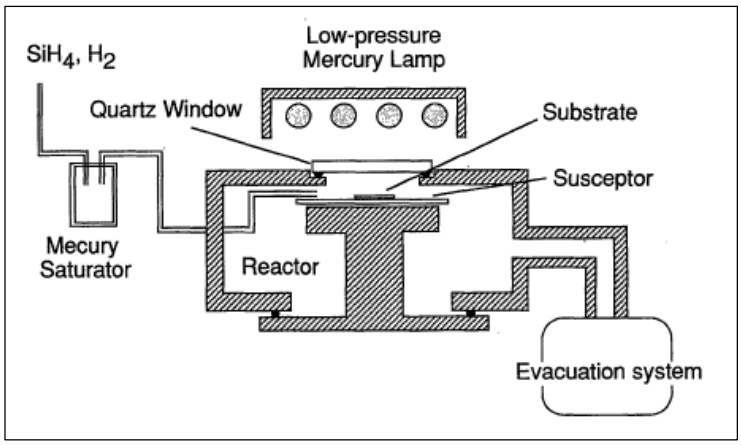

Figure 3. A typical photo-CVD apparatus.[36] Reproduced with permission from Oshima, T., Yamada, A. and Konagai, M. *Jpn. J. Appl. Phys.* ***36*** 6481. Copyright 1997 The Japan Society of Applied Physics.

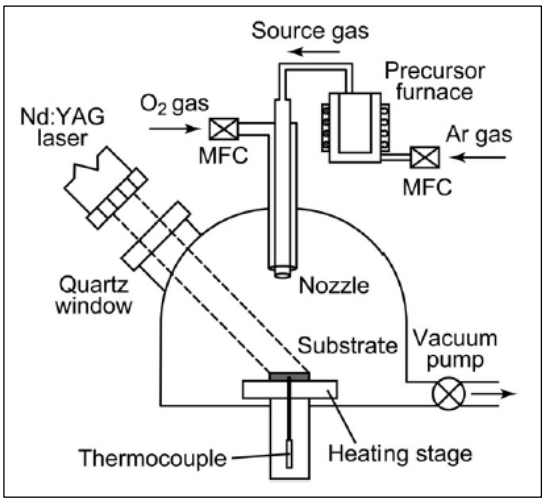

Figure 4. A reactor equipped with a laser at a 45° angle with respect to the substrate.[37] Reproduced with permission from Kadokura, H., Ito, A., Kimura, T. and Goto, T. *Surf. Coat. Technol.* ***204*** 2302. Copyright 2010 Elsevier.

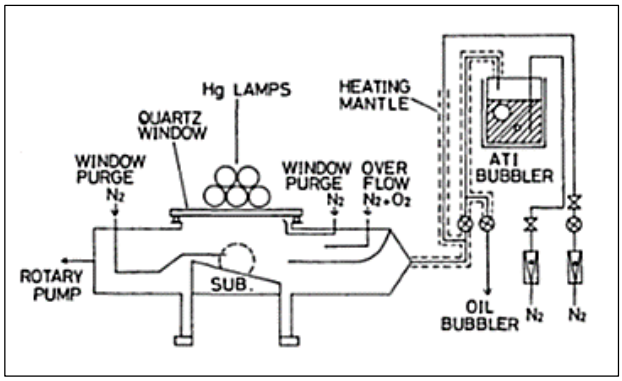

Figure 5. A photo-CVD reactor with a tilted susceptor.[38] Reproduced with permission from Fukushima, Y., Higashino, T., Matsumura, N. and Saraie, J. *Jpn. J. Appl. Phys.* ***31*** L261. Copyright 1992 The Japan Society of Applied Physics.

3.2 Light sources

Photo-CVD experiments are typically carried out with the aid of UV radiation and/or visible light obtained either from a lamp or a laser. When a laser is utilized as the light source, the method is often referred to as laser-assisted CVD (LCVD) instead of photo-CVD. Commonly employed lasers are listed in Table 1.[24,39] Most CVD precursors absorb light in the UV-C region corresponding to wavelengths between 100 and 280 nm. In some cases, lasers emitting IR radiation have been utilized to locally heat the substrate and induce pyrolytic decomposition of the precursor. A combined effect of both photolysis and pyrolysis may be present with other light sources, especially in the case of lasers due to the high intensity of the localized beam. At high laser intensities, the temperature increase at the center of the beam may become significant enough to cause volcano-type growth due to evaporation of the deposited material. Interference of a polarized laser beam with waves reflected from the underlying substrate surface may induce ripple structures, observed e.g. in the case of molybdenum (Section 4.12). Lasers can be utilized for direct writing of metal lines by focusing the beam to a single spot which is scanned along the surface by moving either the susceptor or the beam. The monochromatic laser light can be leveraged to produce material at a high efficiency, provided that the precursor in question has a high absorption cross-section at that specific wavelength.

Table 1. Commonly utilized lasers and their representative line wavelengths.[24,39]

Laser type	Wavelength (nm)
He_2^*	74
Ne_2^*	83
Ar_2^*	126
Kr_2^*	146
F_2	157
Xe_2^*	172 & 175
ArF	193
CaF_2	193
KrCl	222
KrF	248
Cl_2	259
XeBr	282
XeCl	308
N_2	337
XeF	351
Kr^+	357
Ar^+	488 & 514.5
Cu vapor	511
Nd : Glass	1060
Nd : YAG	1060
CO_2	10600

UV lamps typically provide a wide output spectrum, which is beneficial in the investigation of different precursors or if the absorption behavior of a precursor is unknown. Frequently employed UV lamps include e.g. xenon, mercury, and deuterium lamps (Figures 6–8).[40–42] Both irradiation sources, lamps and lasers, can be either continuous-wave (cw) or pulsed sources. If a cw light source is utilized, pulsing can be achieved via mechanical shutters setting additional demands for the apparatus design. Pulsing is essential if irradiation is needed only during certain periods of the deposition. Pulsing is especially vital in photo-

ALD where radiation applied simultaneously with the metal precursor pulse might destroy the self-limiting growth mechanism or cause particle formation.

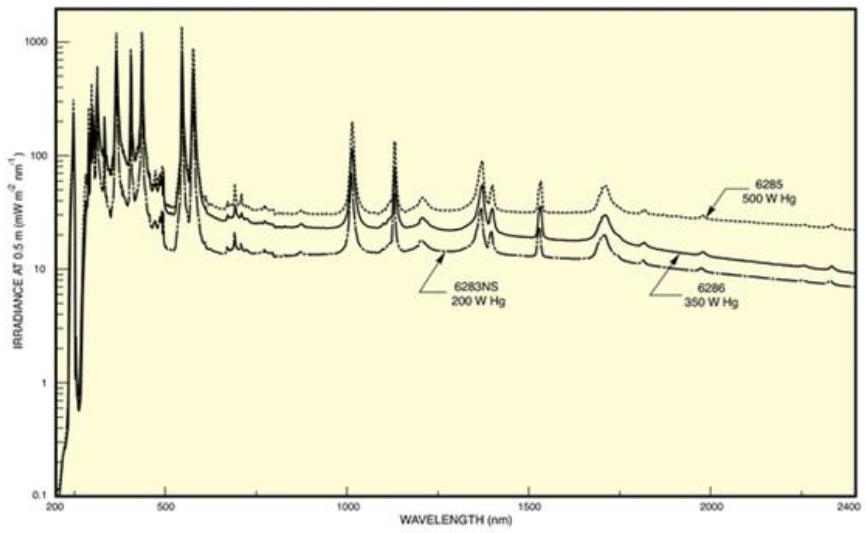

Figure 6. Output spectrum of a mercury lamp at 200, 350, and 500 W.[40] Reproduced with permission from Newport Corporation.

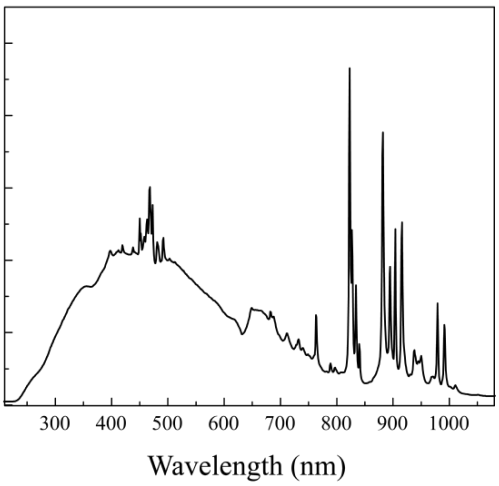

Figure 7. Output spectrum of a xenon lamp.[41] Image free for reproduction.

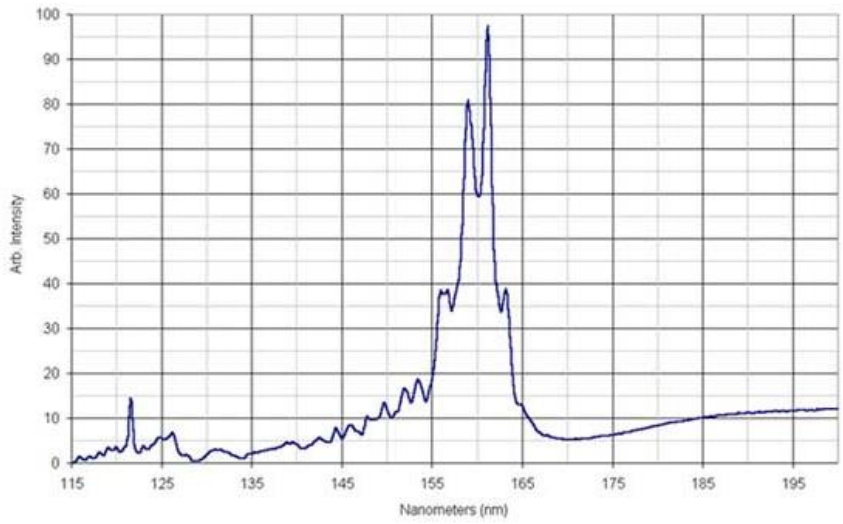

Figure 8. Deuterium lamp emission spectrum.[42] Reproduced with permission from McPherson, Inc.

3.3 Windows for light entrance

There are two major challenges regarding the windows in photo-CVD reactors possibly also explaining the scarcity of photo-ALD processes: transparency at the wavelengths of interest and protection against film growth. Firstly, the acquisition of short wavelengths required for the photolysis of numerous precursors may, in some cases, turn out to be quite difficult. As shown in Table 1, a number of lasers emit radiation at wavelengths well below 190 nm, however, the admittance of these wavelengths into the reaction chamber can be challenging. The selection of a window material is essential for the proper operation of a photo-CVD apparatus. Quartz is the most abundantly utilized window material but has a UV cut-off wavelength at 190 nm restricting its application in the far UV or vacuum UV (VUV) regime. At wavelengths below the transparency of quartz, fused silica, and fluoride materials, such as MgF_2 or LiF, are typically employed. Even with the latter two, the transmittance of 120 nm photons is only 70 % for LiF and 50 % for MgF_2.[43] In addition, the price of these window materials is much higher than that of quartz, which may become a major issue if frequent replacement of the window is required. In order to utilize VUV radiation efficiently, Tarui's group has proposed a windowless reactor where gases are discharged by microwave radiation and the generated plasma is utilized as the light source (Figure 9).[43]

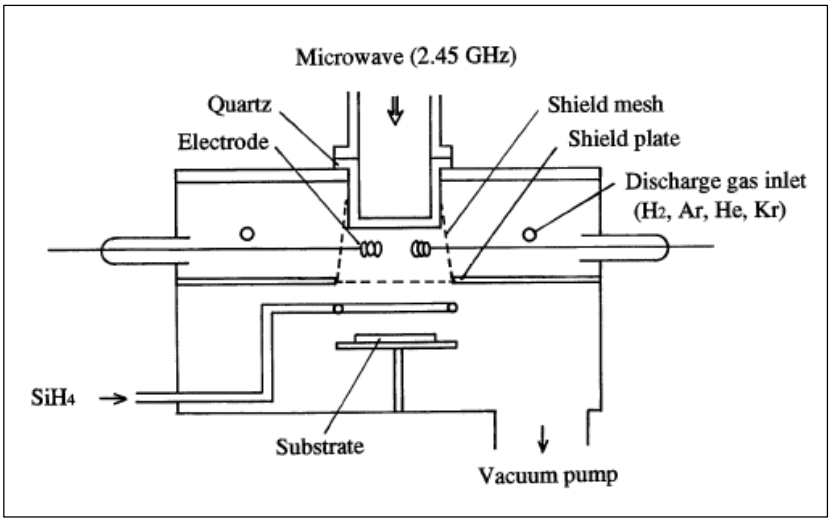

Figure 9. A windowless photo-CVD reactor with an internal plasma light source.[43] Reproduced with permission from Kuroiwa, K., Yamazaki, H., Tsuchiya, S., Kamisako, K. and Tarui, Y. *Jpn. J. Appl. Phys.* ***31*** L518. Copyright 1992 The Japan Society of Applied Physics.

The second limiting factor related to both photo-CVD and photo-ALD is film growth on the optical window. Film formation on the window surface reduces the flux of transmitted photons leading to changing deposition conditions and thus providing inconsistent results. The deposition of a metal film on the window surface eventually blocks the light altogether. In order to avoid incessant cleaning or replacing of the window, a myriad of preemptive measures have been developed. The depositions are often carried out in cold-wall reactors where the amount of gas-phase reactions is minimized. However, this does not eliminate film growth on the reactor walls completely, and complementary window protection is thus necessary. The most widespread shielding method is the utilization of an inert gas flow in the vicinity of the window surface. The proper choice of gas is essential since e.g. VUV radiation may be energetic enough to excite inert N_2 molecules causing undesired side reactions. In some cases, film formation onto the window has been minimized by condensing most of the precursor molecules onto the substrate by cooling the susceptor.[44] Window contamination has also been suppressed by coating the window with a thin layer of low vapor pressure fluorinated lubricant such as Fomblin®.[45,46] Rocheleau *et al.* have patented a photo-CVD apparatus equipped with a moveable, roll-shaped Teflon curtain that eliminates window contamination altogether (Figure 10).[47,48] Prior to this, a resembling apparatus was also patented by Peters *et al.*[49]

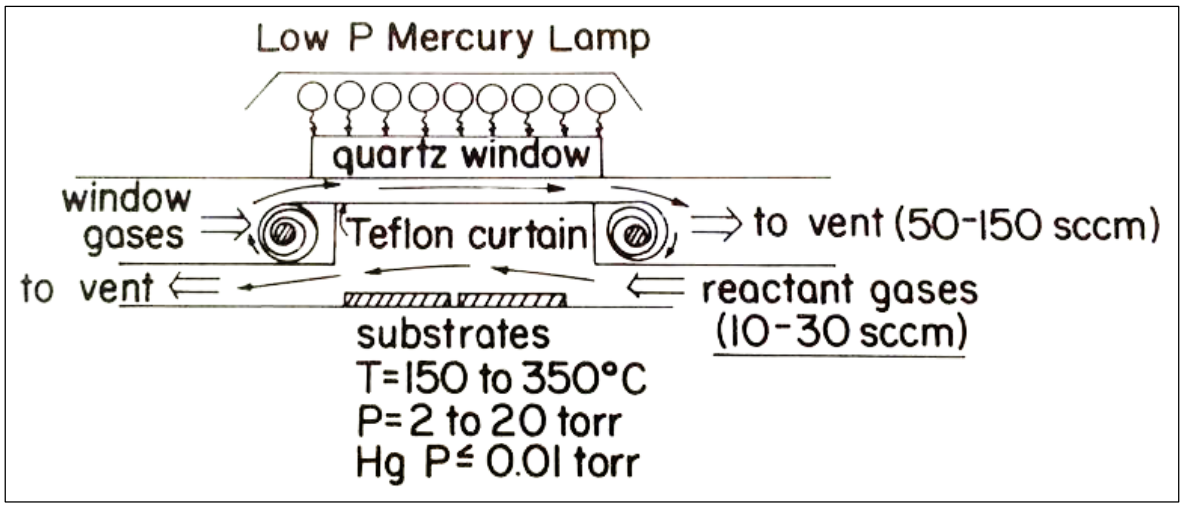

Figure 10. A photo-CVD reactor equipped with a moveable UV-transparent Teflon curtain utilized for window protection.[48] Reproduced with permission from Rocheleau, R.E., Hegedus, S.S., Buchanan, W.A. and Jackson, S.C. *Appl. Phys. Lett.* ***51*** 133. Copyright 1987 AIP Publishing LLC.

4 Metals grown by photochemical vapor deposition

4.1 General outlook

An article on the laser direct writing of metals in 1979 by Deutsch *et al.* triggered a boom in the field of metal photo-CVD.[50] Since then, a wide selection of metals have been deposited with the aid of a laser or a UV lamp as highlighted in Figure 11. The impetus behind the majority of the studies was to develop laser-induced processes for applications such as the repair of defects in circuits and lithographic masks as well as the deposition of interconnects for integrated circuits. Photo-CVD has also been applied to a variety of other materials including e.g. silicon, carbon, oxides, nitrides, carbides, and even more complex compounds such as yttrium barium copper oxide (YBCO), but these are not within the scope of this thesis. The forthcoming section will scrutinize the photo-CVD of metals one material at a time following the order of increasing atomic number. Each subheading contains information on the precursors, light sources, deposition conditions, and results concerning the metal under study.

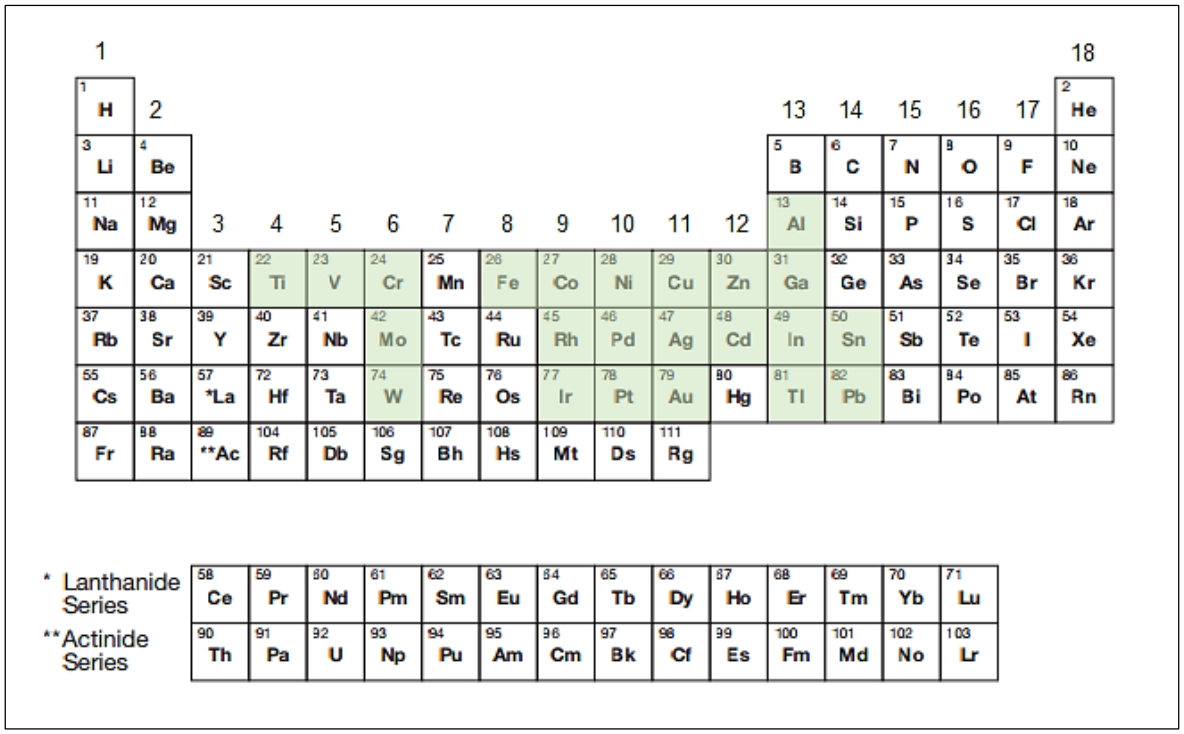

Figure 11. Metals deposited by photo-CVD (highlighted).

4.2 Aluminum

Because of its low resistivity (2.74 μΩcm), aluminum is an appealing material for interconnects in microelectronic devices.[24] Other applications include metallized polymers, gas diffusion barriers, optical coatings, and adhesion promoters. Over the years, a significant number of reports concerning the LCVD of Al films from trialkylaluminum precursors have been published.[50–61] The majority of these studies have concentrated on trimethylaluminum (TMA) due to its commercial availability and importance on the industrial scale. In order to obtain films with low resistivity, incorporation of carbon impurities should be minimized, which has proven to be of great difficulty with the trialkylaluminum precursors. The amount of residual carbon has been reduced by employing H_2 as the carrier gas or by using precursors without a direct Al–C bond.[62–67]

The photolysis mechanism of TMA has been extensively studied and the consensus appears to be that dissociation occurs via two competing single-photon processes in the wavelength regime of 190–270 nm.[68–70] The $Al(CH_3)_3$ monomer absorbs a photon, which results in the formation of Al and $AlCH_3$ fragments as depicted below with Equations 1–3. At shorter wavelengths, mechanism 2 begins to dominate, and at 190 nm mechanism 1 is suppressed almost entirely. According to Higashi, complete photodissociation of an alkylaluminum compound is challenging to achieve because the first excited state is not a directly dissociative one but rather a weakly bound state with a surface lifetime of possibly many picoseconds.[71,72]

Mechanism 1: $Al(CH_3)_3 + h\nu \rightarrow Al(CH_3)_2^* + CH_3$ (1)

$Al(CH_3)_2^* \rightarrow Al + C_2H_6$ (2)

Mechanism 2: $Al(CH_3)_3 + h\nu \rightarrow Al(CH_3) + CH_3 + CH_3$ (3)

The absorption spectrum of TMA vapor is illustrated in Figure 12.[73] The precursor is dimerized at room temperature and completely in a monomer form at 130 °C. The absorption by the monomer is more efficient compared to the dimer and extends to longer wavelengths.

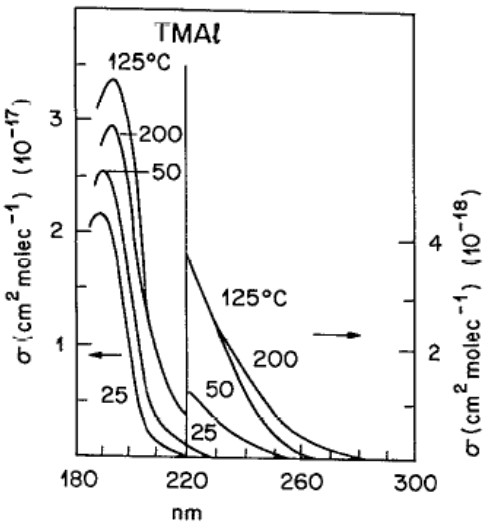

Figure 12. Absorption spectrum of TMA vapor at 25–200 °C.[73] Reproduced with permission from Okabe, H., Emadi-Babaki, M.K. and McCrary, V.R. *J. Appl. Phys.* ***69*** 1730. Copyright 1991 AIP Publishing LLC.

The LCVD of aluminum from TMA was first reported in 1979 by Deutsch *et al.* who carried out their depositions using a frequency doubled Ar^+ laser operating at 257.2 nm as well as a pulsed ArF excimer laser emitting 193 nm photons.[50] Rytz-Froidevaux and coworkers employed a Kr^+ laser at 520.8–568.2 nm to heat GaAs surfaces and deposit aluminum via laser pyrolysis.[51] One mW was responsible for a temperature rise of 3.3 °C. Arai *et al.* studied the LCVD of aluminum using an ArF excimer laser at 193 nm.[53] In order to accelerate the film growth, the substrate was heated to a temperature of 200 °C. The average laser power was 1 mW which was moderate enough not to cause a significant temperature rise on the substrate. The film growth was more accurately confined by using a heavy buffer gas, such as argon, reducing the diffusion of the Al photofragments more efficiently than a light buffer gas. Suppression of the diffusion of photofragments was even more efficient when an electric field was applied suggesting that positive ions form alongside radicals upon irradiation. Calloway and colleagues also applied a negative potential of 200 V to the substrate stage and observed an increase in the deposition rate.[52]

The resistivity measured by Arai *et al.* was about 50 μΩcm being almost 20 times the bulk value.[53] Shanov *et al.* obtained a resistivity of 90 μΩcm at the lowest via pyrolysis of TMA utilizing visible radiation from a copper laser. Resistivity was found to decrease with

increasing writing speed, which was assigned to the decreasing grain size producing denser aluminum layers.

Seki and coworkers produced aluminum films from TMA using 193 and 248 nm radiation obtained from ArF and KrF excimer lasers, respectively.[55] Fused silica, which is transparent at these wavelengths, was chosen as the substrate material in order to circumvent laser induced heating. Film formation occurred faster at 150 °C compared to room temperature due to the stronger absorption of the monomerized precursor dominant at elevated temperatures. When exposed to radiation at 248 nm, deposition was over seven times faster from the monomer than from the dimer. The composition of samples grown at 150 °C was determined by Auger electron spectroscopy (AES). The aluminum content was 95 % with traces of oxygen (4 %) and carbon (< 1 %) impurities, independent of the applied wavelength.

Shi *et al.* employed a 30 W deuterium arc lamp emitting light at 180–500 nm to deposit aluminum films from TMA. The depositions were carried out at room temperature on top of different self-assembled monolayers (SAMs) adsorbed on gold substrates.[56] SAMs consist of organic molecules and can be utilized to deposit highly oriented films in a selective manner. Light was directed parallel to the substrate in order to avoid photo-oxidation of the SAMs. Film growth was observed only on –COOH- and –OH-terminated SAMs and not on $–CH_3$-surfaces. As can be determined from the time-of-flight secondary ion mass spectrometry (TOF-SIMS) data represented in Figure 13, the rate of Al formation was about 1.7 times faster for samples exposed to UV radiation.[56] Similar behavior was also noticed for the –OH-terminated samples. The growth mechanism of Al without UV exposure was not speculated.

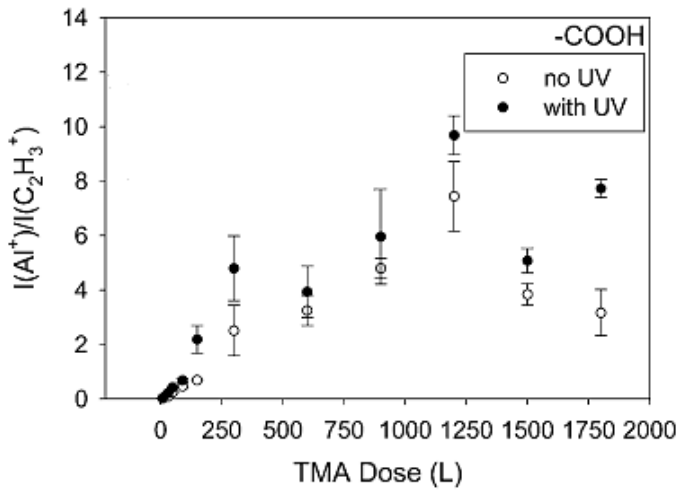

Figure 13. TOF-SIMS ion intensity ratio $Al^+/C_2H_3^+$ as a function of TMA dose indicating the relative amount of deposited aluminum with and without UV exposure on –COOH-terminated SAMs.[56] Reproduced with permission from Shi, Z., Lu, P. and Walker, A.V. *Langmuir **28*** 16909. Copyright 2012 American Chemical Society.

Tsao and Ehrlich have employed a frequency doubled Ar^+ laser at 257.2 nm to deposit thin aluminum stripes from triisobutylaluminum (TIBA) as nucleation promoters for subsequent thermal deposition realized with a CO_2 laser.[57] TIBA can be utilized to deposit aluminum of high quality but at a limited rate due to its relatively low vapor pressure.[61] However, slowness is not of major concern in the generation of thin nucleation layers which was also the motivation behind the studies carried out by Fleming's group who deposited aluminum from TIBA using a KrF excimer laser at 248 nm.[58,59] Unlike Tsao and Ehrlich, Fleming's group heated the substrate during LCVD to a temperature of 250 °C. According to Tsao and Ehrlich, the initiation of film growth was slower at high temperatures because of desorption of TIBA. This was contradictory to the observations made by Fleming's group who explained their findings by the formation of diisobutylaluminum hydride (DIBAH) which has a lower vapor pressure than TIBA and is hence more prone to adsorption. The pattern resolution was maintained even without diffusion suppression by a buffer gas suggesting that deposition occurred mainly via surface reactions. Growth rate was found to vary between 30 and 1000 Å/min depending on the partial pressure of the precursor controlled by hydrogen dilution. Mantell also studied the suitability of the LCVD process using TIBA for nucleation promotion and observed that despite the high level of carbon and oxygen impurities in the photodeposited aluminum film, the subsequent thermal deposition was

successful.[60] Lee and Allen deposited aluminum lines with a low resistivity of 5.6 μΩcm by irradiating a thin layer of liquid TIBA with 514.5 nm photons obtained from an Ar^+ laser.[61] The method was claimed to be analogous to conventional LCVD since the irradiation of the precursor resulted in the formation of a bubble; hence, the deposition occurred at the solid-gas interface.

Aluminum film formation has also been achieved using dimethylaluminum hydride (DMAH). Osgood's group employed an Ar^+ laser operating at 275 nm, a frequency-doubled Ar^+ laser emitting photons at 257.2 nm, and a pulsed KrF excimer laser at 248 nm.[74,75] Zhu *et al.* utilized the LCVD of aluminum lines using DMAH to deposit a seed layer in order to achieve subsequent thermal growth in a selective manner at low temperatures (110–180 °C).[75] Hanabusa *et al.* carried out their experiments using a 150 W deuterium lamp or an ArF laser in order to obtain photons at wavelengths below 200 nm.[76] Since the absorption cross-section of DMAH increases drastically below 220 nm (Figure 14), the utilization of short wavelengths is essential for aluminum deposition.[74] The deposition was supposed to occur via a surface photochemical pathway since at low laser powers, the film thickness increased linearly with increasing laser power and below the decomposition temperature of the precursor (250 °C), film formation was obtained only on irradiated areas. At a substrate temperature of 200 °C, Hanabusa and coworkers measured a growth rate of 190 Å/min and 0.6 Å/pulse with the lamp and the laser, respectively.[76] The values of resistivity were about 2–3 times that of bulk aluminum, which is consistent with the reasonably low impurity levels (carbon content 2–3 %). A much higher resistivity of 140 μΩcm was observed at the same temperature (~260 °C) without irradiation.

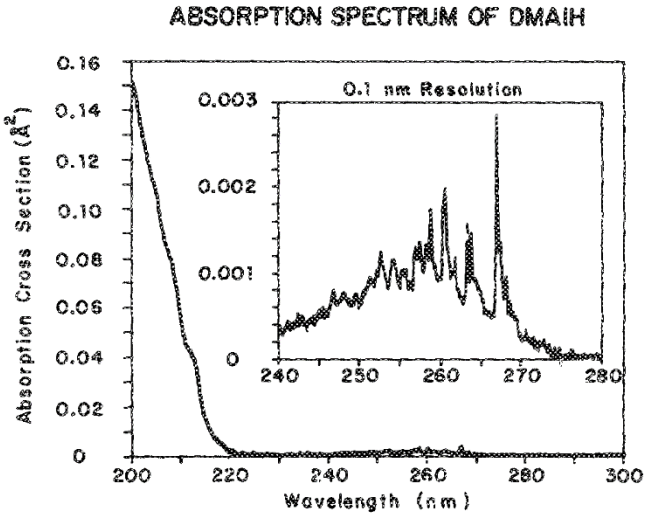

Figure 14. Absorption spectrum of gaseous DMAH.[74] Reproduced with permission from Cacouris, T., Scelsi, G., Shaw, P., Scarmozzino, R. and Osgood, R.M. *Appl. Phys. Lett.* ***52*** 1865. Copyright 1988 AIP Publishing LLC.

Baum *et al.*, Frugier *et al.*, as well as Stuke's group have reported a process for the LCVD of high-purity aluminum lines using trimethylamine alane (TMAA) and an Ar^+ laser (514.5 nm).[62–65] Popov *et al.* also deposited aluminum from TMAA but employed visible light from a copper bromide vapor laser instead of an Ar^+ laser.[66] Because of the high vapor pressure of TMAA, high deposition rates can be attained. The decomposition temperature of TMAA is ~100 °C which is easily accessible with the aid of a laser.[66] Contrary to the trialkylaluminum precursors, TMAA is nonpyrophoric and yields films with lower carbon contents due to the absence of a direct Al–C bond. The incorporation of excess oxygen is inhibited by the formation of nonvolatile Al–OH species and high concentration of hydrogen at the surface. The decomposition of TMAA is proposed to proceed via laser pyrolysis as represented by Equations 4–5.

$$AlH_3(NMe_3)_2 \leftrightarrow AlH_3(NMe_3) + NMe_3 \quad (4)$$

$$AlH_3(NMe_3) \rightarrow AlH_3 + NMe_3 \rightarrow Al + \frac{3}{2}H_2 + NMe_3 \quad (5)$$

The height of the deposited stripes was found to vary as a function of laser power density, scanning speed, and precursor vapor pressure. The higher the laser power density, the higher the temperature at the substrate, which in turn led to an increased deposition rate. The height of the stripes decreased as the scanning speed increased due to the shorter laser exposure time and thus lower substrate temperature. No carbon contamination was detected by Baum *et al.* who reported oxygen incorporation (3–5 at.%) upon exposure to ambient air as the only impurity.[62] However, Popov *et al.* observed relatively high carbon contents attributed to the dissimilarity of the utilized Ar^+ and copper bromide vapor lasers, respectively.[66] The reported resistivities were consistently 1.5–4 times higher compared to the bulk value (2.8 μΩcm). The lowest value of 4.0 μΩcm was obtained by Popov and colleagues. In addition to TMAA, Foulon and Stuke deposited aluminum also from triethylamine alane (TEAA) and observed lower deposition rates because of the lower vapor pressure and thus lower dose of TEAA.[63] They also investigated the resistivity of the deposited aluminum lines from both precursors as a function of laser power (Figure 15).[63] When approaching the threshold power density required for film formation (0.6 MW/cm^2), a steep increase in the resistivity was observed, which was most likely caused by poor packing of the crystallites. The resistivity also increased with high laser powers because of the local heating at the center of the stripe causing an increase in the grain size.

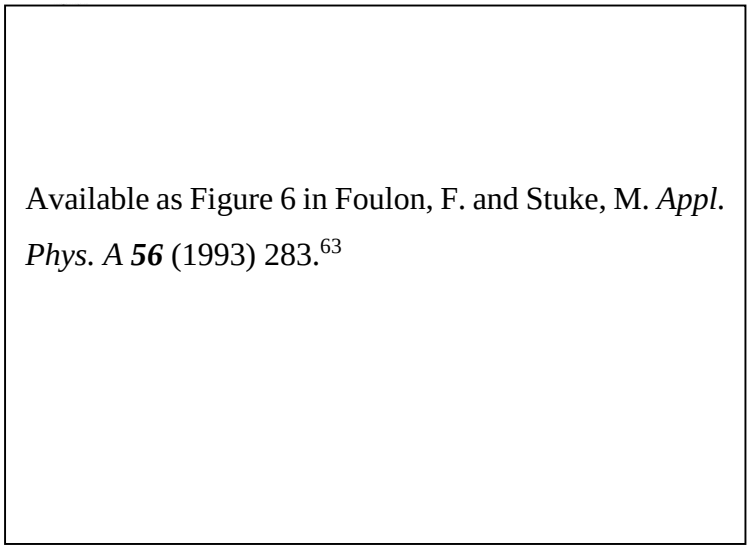

Figure 15. Resistivity of aluminum as a function of laser power at a scanning speed of 25 μm/s.[63]

Han *et al.* deposited aluminum films via pyrolytic LCVD using dimethylethylamine alane (DMEAA) and a 514 nm Ar^+ laser.[67] The motivation for the study was to create a patterned nucleation layer of aluminum in a simple manner without masks. No traces of carbon and oxygen were detected by AES, which is in correlation with the low resistivity (3.6 μΩcm) measured for a film deposited at a laser power of 2.7 kW/cm^2.

Geohegan and Eden deposited aluminum thin films by dissociative photoionization of AlI_3 using an ArF excimer laser operating at 193 nm or a 150 W Xe lamp.[77] The absorption of a photon led to the production of an ion pair, and the formed metal cations were then collected on a metal (Ni, Cu, or Ag) coated stainless steel cathode. Similar photochemistry was also employed for the photolytic deposition of indium and thallium films for which a growth rate of 420 Å/h was recorded. Properties of the Al deposits were not reported but at least for In and Tl, only trace amounts of iodine were detected by AES. The photochemistry of metal iodides is discussed in more detail in Section 4.11.[78]

To conclude, the photo-CVD of aluminum has been thoroughly studied from various precursors including TMA, TIBA, and TMAA. The resistivity values varied a lot depending on the deposition conditions such as the applied wavelength. The lowest resistivity (3.6 μΩcm) was obtained by Han *et al.* using DMEAA and an Ar^+ laser at 514.5 nm. The amount of residual carbon could be reduced by using precursors without a direct Al–C bond.

4.3 Titanium

Titanium oxidizes readily upon exposure to ambient air, which makes the deposition of pure metallic titanium challenging. Titanium thin films are employed as adhesion layers, metal foils, and corrosion resistant coatings.[24] Tsao *et al.* and Izquierdo *et al.* have investigated the photolytic deposition of titanium coatings using $TiCl_4$ as the precursor and a UV laser as the light source.[79,80] The goal of these studies was to develop a method for the direct writing of titanium lines on $LiNbO_3$ to produce optical waveguides. Chou and coworkers have published a paper on the LCVD of titanium using $TiBr_4$ and a CO_2 laser.[81]

According to the absorption spectrum measured by Alderdice, $TiCl_4$ vapor has two absorption peaks below 300 nm (Figure 16).[82] Both peaks were assigned to ligand-to-metal charge transfer transitions.

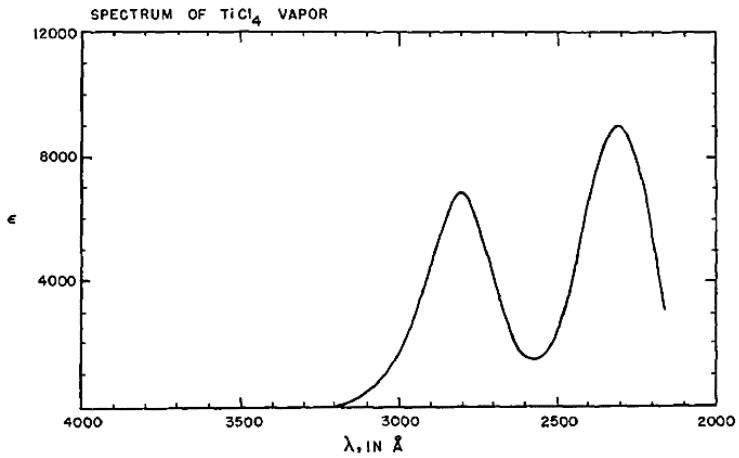

Figure 16. Absorption spectrum of $TiCl_4$ vapor.[82] Reproduced with permission from Alderdice, D.S. *J. Mol. Spectrosc.* ***14*** 509. Copyright 1965 Elsevier.

Tsao *et al.* carried out their depositions in a vacuum vessel utilizing a frequency-doubled 514.5 nm Ar^+ laser (effective wavelength 257.2 nm) focused to a spot size of 4 μm in diameter.[79] The depositions were carried out at a low temperature but absolute values were not specified. The laser power at the substrate surface was measured to be 50 kW/cm^2 producing a temperature rise of less than 30 °C. The use of 514.5 instead of 257.2 nm radiation resulted in local heating of the substrate causing pyrolysis of the precursor and severe damage to the $LiNbO_3$ substrate. Gas-phase reactions and deposition on the window surface were suppressed by maintaining a modest $TiCl_4$ vapor pressure of 0.5 Torr. Figure 17 depicts the deposition rate of titanium as a function of both laser intensity and precursor vapor pressure. The linear dependence of the growth rate on the laser intensity was assigned to a single-photon process where the photon absorption is the rate-limiting step. On the grounds of the $TiCl_4$ pressure dependence of the deposition rate, the photoreaction was suggested to occur by an autocatalytic mechanism confined to the sample surface. The knee in Figure 17b can be explained by the saturation of the chemisorbed monolayer followed by a more gradual increment caused by the successive physisorbed layers.

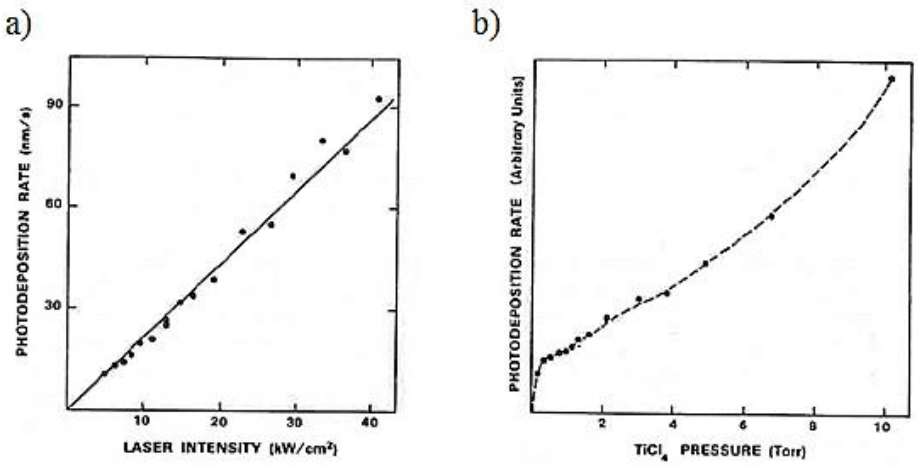

Figure 17. Deposition rate of titanium as a function of a) laser intensity and b) $TiCl_4$ vapor pressure.[79] Reproduced with permission from Tsao, J.Y., Becker, R.A., Ehrlich, D.J. and Leonberger, F.J. *Appl. Phys. Lett.* ***42*** 559. Copyright 1983 AIP Publishing LLC.

The deposition of titanium lines on $LiNbO_3$ has also been studied by Izquierdo *et al.* who employed $TiCl_4$ and a KrF excimer laser operating at a wavelength of 248 nm.[80] The laser beam was focused to a spot size of 20 µm. All lines were deposited at laser energies below 100 nJ/pulse in order to avoid heating of the thermally sensitive substrate. The thermal dissociation of $TiCl_4$ requires a high temperature of 600 °C. A temperature of 600 °C would cause severe damage to the substrate in use. Since no thermal damage was observed, the process was proposed to be photolytic. The thickness of the deposited lines increased linearly with increasing pulse energy and $TiCl_4$ pressure (Figure 18).[80] The films contained low concentrations of chlorine (below 2 at.%).

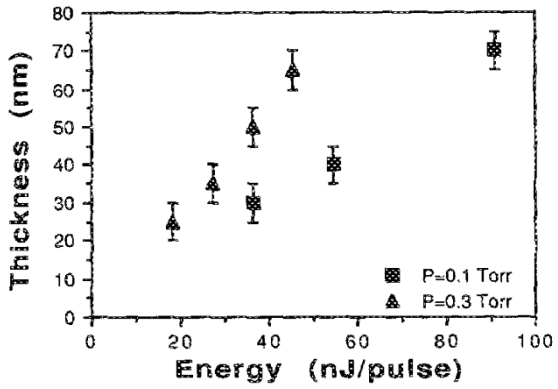

Figure 18. Ti line thickness as a function of laser pulse energy and $TiCl_4$ vapor pressure.[80] Reproduced with permission from Izquierdo, R., Lavoie, C. and Meunier, M. *Appl. Phys. Lett.* ***57*** 647. Copyright 1990 AIP Publishing LLC.

Chou *et al.* have deposited titanium thin films via decomposition of $TiBr_4$ vapor with the aid of a CO_2 laser.[81] Since the light source operates in the IR region (10.6 µm), the dominant reaction mechanism was thermal rather than photolytic. The laser power was set to 850 W, and the beam was focused to an area of 2 mm in diameter. The precursor was evaporated at a temperature of 40 °C corresponding to a vapor pressure of 0.462 Torr. The depositions were carried out at chamber temperatures of 55, 70, and 85 °C. Figure 19 depicts the titanium film thickness as a function of both irradiation time and total chamber pressure.[81] The increase in growth rate after 6 seconds of irradiation was suggested to derive from a threshold temperature needed for the film formation to occur pyrolytically. No exact value for the threshold temperature was reported but it was predicted to be below the temperature required for the thermal CVD process using $TiBr_4$ and H_2 (1200 °C). As shown in Figure 19b, the film thickness also increased with increasing total pressure. The deposition rate of the photo-CVD process was 190 µm/h yielding an increase of two orders of magnitude when compared to conventional CVD.

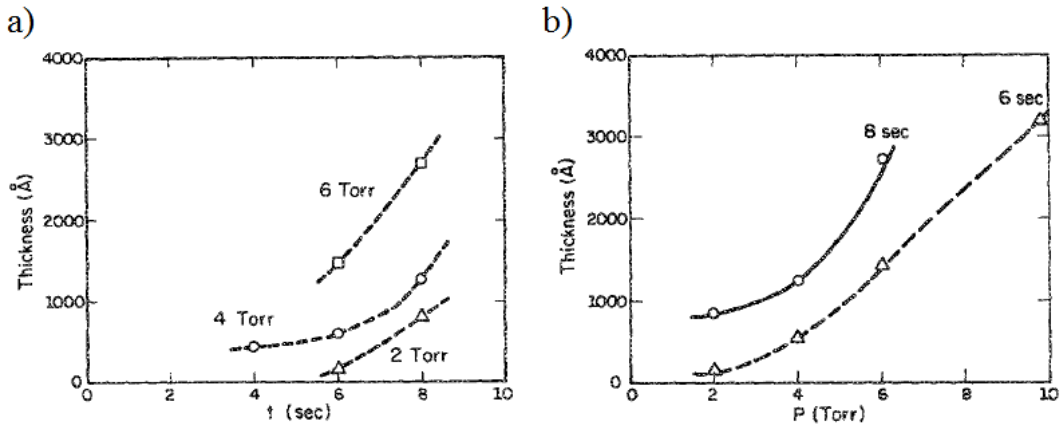

Figure 19. Thickness of the deposited Ti film as a function of a) irradiation time and b) total chamber pressure at a chamber temperature of 70 °C.[81] Reproduced with permission from Chou, W.B., Azer, M.N. and Mazumder, J. *J. Appl. Phys.* ***66*** 191. Copyright 1989 AIP Publishing LLC.

According to AES measurements, the films contained over 90 at.% of titanium after 28 minutes of sputtering at a sputtering rate of 30 Å/min. Oxygen and carbon impurities were present on the film surface and most likely incorporated upon exposure to the atmosphere or due to residual gases in the vacuum system. Despite its high probability, bromine contamination was not reported.

To conclude, titanium has been photolytically deposited from $TiCl_4$ and via laser pyrolysis from $TiBr_4$. In all cases, the deposition rate increased with increasing precursor vapor pressure and irradiation time. The growth rate of titanium in the $TiBr_4$ photo-CVD process was over two orders of magnitude greater than reported for conventional CVD.

4.4 Vanadium

High-purity vanadium is difficult to obtain, and therefore it is mostly applied in alloys combined with a wide range of metals the most important being iron.[83] At a commercial scale, vanadium is deposited via thermal decomposition of the corresponding halides. A handful of reports on the thermal decomposition of organometallic vanadium compounds also exist and have been reviewed by Kodas and Hampden-Smith.[1]

Turney *et al.* have published a low-temperature process for the deposition of vanadium thin films from the corresponding hexacarbonyl complex using a 10 Hz pulsed laser source.[44] $V(CO)_6$ has 17 electrons making it a paramagnetic compound. The electronic structure of the employed precursor differs from other hexacarbonyls, which was suspected to translate into increased reactivity. Wavelengths of 562 and 281 nm were obtained from a Nd:YAG laser combined with a dye laser. The laser beam was held at a right angle with respect to the substrate surface. The precursor was evaporated at 0 °C, and the vapor pressure was measured to be 250 mTorr. Due to the poor thermal stability of $V(CO)_6$, the substrate was kept at room temperature or cooled with liquid nitrogen. Cooling led to condensation of the precursor on the substrate surface, which was required to avoid deposition on the reactor window when the 281 nm radiation was applied. The absorbance of metal hexacarbonyls is negligible at visible wavelengths; hence, cooling was unnecessary under the 562 nm irradiation. Figure 20 shows the absorption spectrum of gaseous $V(CO)_6$ measured by Haas and Sheline as well as the absorption spectrum of $V(CO)_6$ in cyclohexane provided by Rubinson.[84,85] The intense peaks near 260 nm were assigned to charge-transfer transitions, and the weaker features at longer wavelengths are caused by metal-centered d–d transitions.

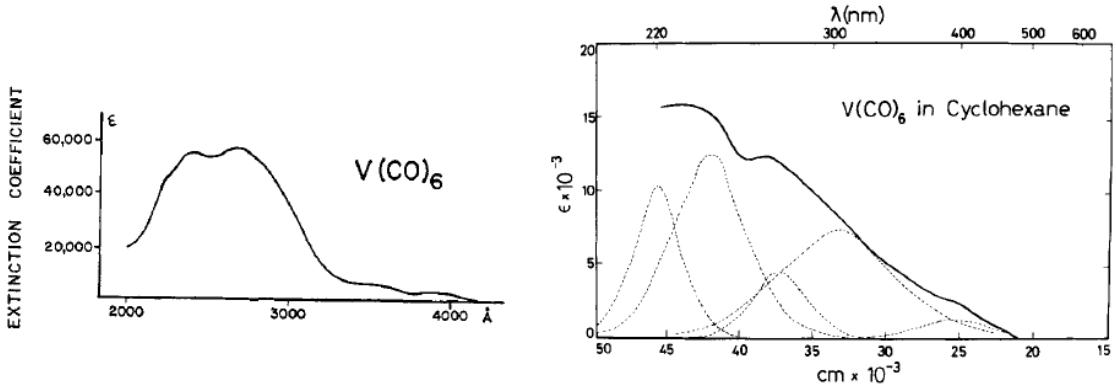

Figure 20. Absorption spectrum of $V(CO)_6$ both in the gas phase (left) and in cyclohexane (right).[84,85] Reproduced with permission from Haas, H. and Sheline, R.K. *J. Am. Chem. Soc.* ***88*** 3219 and Rubinson, K.A. *J. Am. Chem. Soc.* ***98*** 5188. Copyright 1966 and 1976 American Chemical Society.

Turney *et al.* observed a growth rate of approximately 3 Å/s for the LCVD process of $V(CO)_6$. This was to some extent higher than the values determined for W and Mo probably due to the greater vapor pressure and thus higher concentration of $V(CO)_6$ compared to the other hexacarbonyls. Another possible explanation mentioned by the authors was the greater reactivity of the vanadium precursor with the underlying vanadium thin film. As mentioned in Section 2.2, films deposited from metal carbonyls often contain high levels of carbon and oxygen impurities. As could be expected, AES measurements on the deposited V thin films revealed significant concentrations of incorporated carbon and oxygen. The results indicated a loss of approximately five CO units per metal atom leading to a stoichiometry of VCO. The film composition remained constant throughout the entire film thickness.

4.5 Chromium

Chromium is a refractory metal which can be utilized in various applications including optical coatings for infrared lasers and reflectors for VUV radiation, protectors against corrosion and oxidation, metal contacts in microelectronics, and silicide contact layers.[1] The LCVD of chromium films from the corresponding hexacarbonyl complex has been extensively studied using a number of different lasers.[86–96] The absorption spectrum of $Cr(CO)_6$ in cyclohexane is displayed in Figure 21.[82] According to Gray and Beach, the intense peaks at 225 and 280 nm correspond to the allowed metal-to-ligand charge transfer transitions.[97]

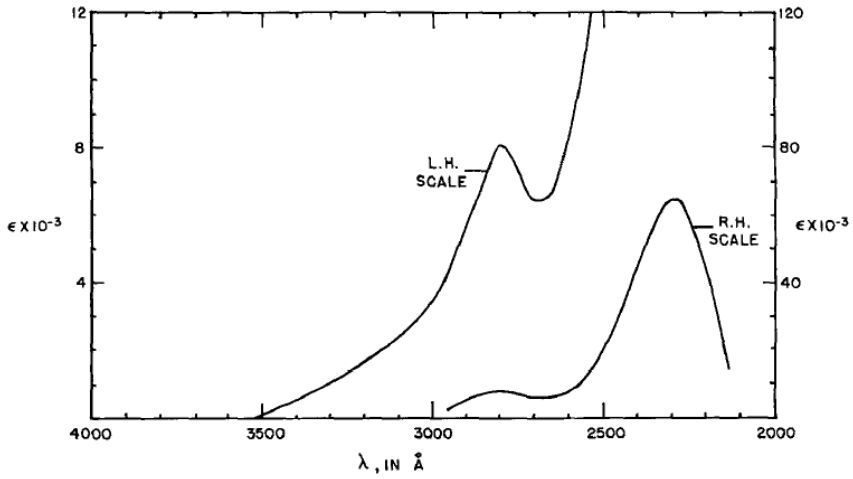

Figure 21. Absorption spectrum of $Cr(CO)_6$ in cyclohexane solution (L.H. = left hand scale, R.H. = right hand scale).[82] Reproduced with permission from Alderdice, D.S. *J. Mol. Spectrosc.* ***14*** 509. Copyright 1965 Elsevier.

Tyndall and Jackson studied the multi-photon dissociation process of $Cr(CO)_6$ using a KrF excimer laser operating at a wavelength of 248 nm.[98] The complex was found to dissociate via two distinct pathways depicted in Equations 6 and 7. The absorption of a single photon results in the formation of a dissociative continuum. The excited intermediate $Cr(CO)_4^{\dagger}$ absorbs a sequential photon producing Cr*. According to Mayer *et al.*, the formation of the resonant dissociative species at wavelengths above 300 nm requires an absorption of at least two photons.[88] It was observed that to complete the dissociation of $Cr(CO)_6$ into Cr*, 3 photons are needed at 280 nm or at 350 nm, and 4 photons at 500 nm.

$$Cr(CO)_6 + h\nu \rightarrow Cr(CO)_4^{\dagger} + 2\ CO \quad (6)$$

$$Cr(CO)_4^{\dagger} + h\nu \rightarrow Cr^* + 4\ CO \quad (7)$$

Chromium was deposited using several lasers listed in Table 2. Femtosecond pulses of 400 nm radiation obtained from a frequency-doubled Ti:sapphire laser were found to initiate the photolytic dissociation of $Cr(CO)_6$ with high efficiency due to the exceptionally high intensities produced by the ultrashort light pulses.[95,96] Film formation was not observed when an Ar^+ laser was employed without frequency doubling at 514 nm.[92]

Table 2. Lasers utilized to deposit chromium by LCVD.

Laser	**Wavelength** [nm]	**References**
F_2 excimer	157	[89]
ArF excimer	193	[87,89,91]
KrF excimer	248	[87,89–91,93]
Cu^+	260	[86]
XeCl excimer	308	[89]
XeF excimer	308	[91]
Frequency-doubled Ar^+	257	[87,92,94]
Dye laser combined with a frequency-doubled Nd : YAG	280–350	[88]
Frequency-doubled Ti:sapphire	400	[95]

All of the studies were carried out near room temperature, and the $Cr(CO)_6$ precursor was evaporated without external heating yielding a vapor pressure of about 0.2 Torr. Flynn *et al.* investigated the wavelength dependence of the deposition process and observed the deposition rate to increase with increasing number of pulses independent of the pulse frequency.[91] The measured growth rates were 0.05, 0.28, and 0.10 Å/pulse at 308, 249, and 193 nm, respectively. Yokoyama and coworkers, however, observed a decreasing trend in the growth rate with increasing repetition rate.[90] Gluck *et al.* measured a deposition rate of 1–2 Å/s at a wavelength of 257 nm and a laser power of 1 W/cm^2.[92] The highest deposition rate (33 Å/s) was observed by Solanki *et al.* at 248 nm.[89] Nowak *et al.* studied the temperature dependence of the process and observed a constant nucleation time of 5 seconds up to the temperature of 50 °C (Figure 22) suggesting that the primary contribution to the nucleation arises from the adsorption of fragments generated by the photolytic dissociation.[93] After the initial phase, the growth rate was found to increase linearly with increasing substrate temperature possibly due to activated chemisorption or pyrolytic film formation.

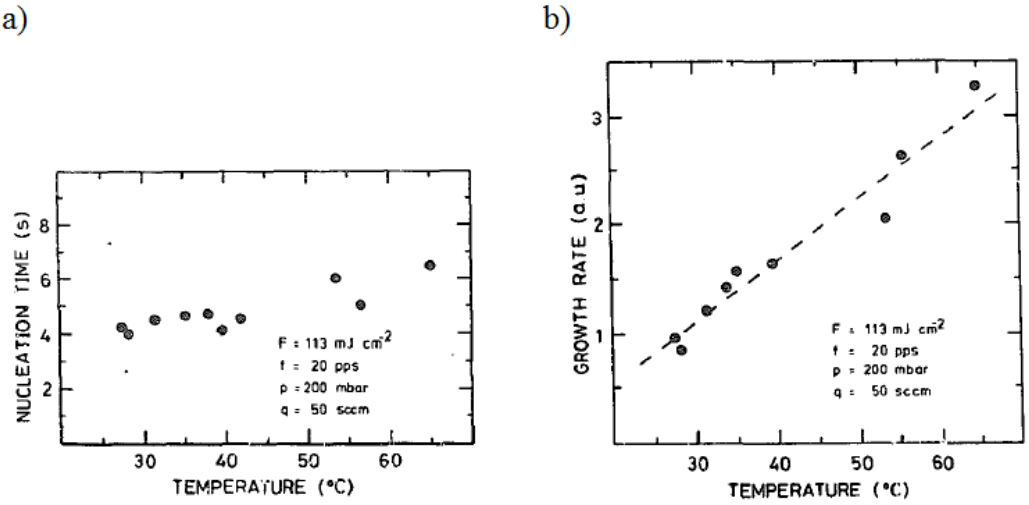

Figure 22. a) Cr nucleation time and b) growth rate as a function of substrate temperature.[93] Reproduced with permission from Nowak, R., Konstantinov, L. and Hess, P. *Appl. Surf. Sci.* ***36*** 177. Copyright 1989 Elsevier.

The incidence angle of the laser beam was found to have a significant effect on the film morphology.[89,91] When light was directed perpendicularly to the substrate, metallic films with good adhesion properties were obtained. However, parallel orientation produced black, particulate films. At low laser intensities, the film surface consisted of aggregates of large grains. Small, densely packed grains were obtained upon increasing the laser intensity.

As can be expected for a process that relies on a carbonyl precursor, carbon and oxygen impurities were present in all deposits. Solanki *et al.* observed relatively pure chromium films with a carbon content of 0.8 % and an oxygen content of less than 7 %.[89] For a film of 350 nm thickness, the resistivity was 210 μΩcm which is 20 times the value of bulk chromium (12.9 μΩcm). The resistivity observed by Flynn *et al.* was 37.5 μΩcm for a 250 nm film but the impurity levels were not reported.[91] Yokoyama *et al.* obtained a chromium content of 50 % at best, translating into a resistivity of 6000 μΩcm which is 500 times the bulk value.[90] According to Hess's group, the purity of the film could be increased by using hydrogen as the buffer gas instead of helium or argon.[34] Gluck *et al.* employed nitrogen as the buffer gas and obtained films containing only 30–38 % chromium and over 60 % oxygen.[92] Analysis of the buffer gas showed a trace amount of oxygen (< 1 ppm) which was enough for the formation of Cr_2O_3 instead of metallic chromium. Background gases and

exposure to air after the deposition were also the reason for the poor stoichiometry obtained by Singmaster and coworkers.[94]

To conclude, the LCVD of chromium films from $Cr(CO)_6$ has been extensively studied at numerous wavelengths. The incidence angle of the laser beam had a significant effect on film morphology. The values of resistivity were generally quite high due to the high degree of carbon and oxygen impurities incorporated into the films.

4.6 Iron

Iron is a useful material for metal alloys and metal silicide diffusion barriers.[1] The most abundantly employed precursor for the LCVD of iron is $Fe(CO)_5$, the absorption spectrum of which is depicted in Figure 23.[99] Absorption peaks at 245 and below 200 nm were classified as metal-to-ligand charge transfer transitions. Ray *et al.* investigated the photodissociation of $Fe(CO)_5$ and drew a conclusion that the absorption of a single photon leads to the formation of $Fe(CO)_2$.[100] The absorption of a sequential photon results in the elimination of the remaining carbonyl ligands producing metallic iron and carbon monoxide.

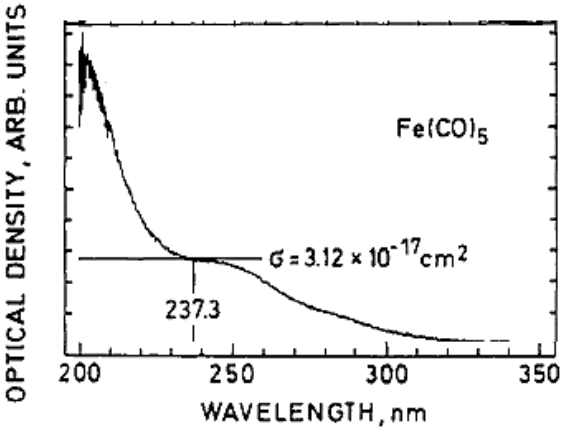

Figure 23. Absorption spectrum of $Fe(CO)_5$ vapor.[99] Reproduced with permission from Kotzian, M., Roesch, N., Schröder, H. and Zerner, M.C. *J. Am. Chem. Soc.* ***111*** 7687. Copyright 1989 American Chemical Society.

Ehrlich *et al.* obtained iron deposits using excimer lasers at 193 and 248 nm as well as a frequency-doubled Ar^+ laser emitting 257 nm photons.[87] The beam was directed perpendicularly to the substrate, and the $Fe(CO)_5$ vapor pressure was fixed at 0.5 Torr. The formation of iron particles was not restricted only to the irradiated areas but the photofragments produced in the gas phase scattered throughout the vicinity of the stripes. This undesirable effect could be minimized by reducing the laser intensity and precursor vapor pressure and by introducing an inert buffer gas into the reaction system. The diffusion of iron particles was also a concern for Jackman and Foord who carried out their depositions using a 18 W cw Ar^+ laser at 488–514 nm at a substrate temperature of 227 °C.[101] The particle formation in the gas phase could, however, be avoided by reducing the absorption path down to 10 mm by using a continuous precursor flow instead of a static fill. The lines deposited under the constant $Fe(CO)_5$ flow exhibited a low resistivity of 30 μΩcm and good adhesion to the SiO_2 substrate. A periodic ripple structure appearing in the deposits was assigned to the changing absorption coefficient of the deposit and the exothermic formation of iron silicate verified with AES measurements. Maxwell *et al.* deposited three-dimensional iron structures in the same wavelength region of 488–514 nm at a high axial deposition rate (along the beam axis) of up to 45 μm/s.[102]

Xu and Steinfeld observed iron silicide formation at the interface of the metal film and the underlying silicon substrate when applying 193 and 248 nm radiation from an ArF and a KrF laser, respectively.[103] The deposited iron films were of high purity with C/Fe and O/Fe ratios below 3 %. The deposition rate was estimated at 0.6–1 Å/pulse at a precursor partial pressure of ~50 mTorr. Armstrong *et al.* also carried out their depositions using a 193 nm ArF laser.[104] The precursor vapor pressure was ~0.1 Torr, and the laser fluence at the substrate was 14 mJ/cm^2. At a repetition rate of 50 Hz, 20,000 pulses produced a film with a thickness of 2.6 μm. Metallic films with good adhesion were obtained. According to the X-ray diffraction (XRD) measurements, the deposits were polycrystalline (Figure 24), and this was also confirmed by Mössbauer spectroscopy.[104]

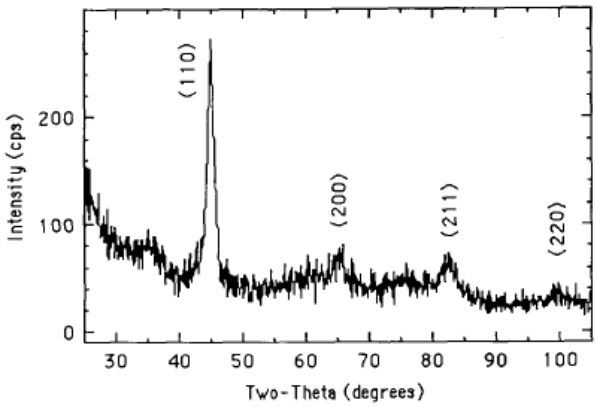

Figure 24. X-ray diffractogram of iron deposited from $Fe(CO)_5$.[104] Reproduced with permission from Armstrong, J.V., Enrech, M., Decrouez, C., Lunney, J.G. and Coey, J.M.D. *IEEE Trans. Magn.* ***26*** 1629. Copyright 1990 IEEE.

Allen and Tringubo studied the deposition of iron lines and spots from $Fe(CO)_5$ using a CO_2 laser at 10.6 µm.[105] According to the authors, the minimum temperature for the thermal CVD process using $Fe(CO)_5$ is 370 °C. The precursor vapor pressure was held at 27 Torr. Both the film thickness and the deposition rate are depicted as a function of irradiation time in Figure 25.[105] The longer the irradiation was applied on the sample, the thicker the films grew, although the apparent deposition rate decreased due to the lower surface temperature caused by the increasing reflectivity of the growing film. The deposits were adherent and hard but exhibited high resistivity the value of which, however, was not reported.

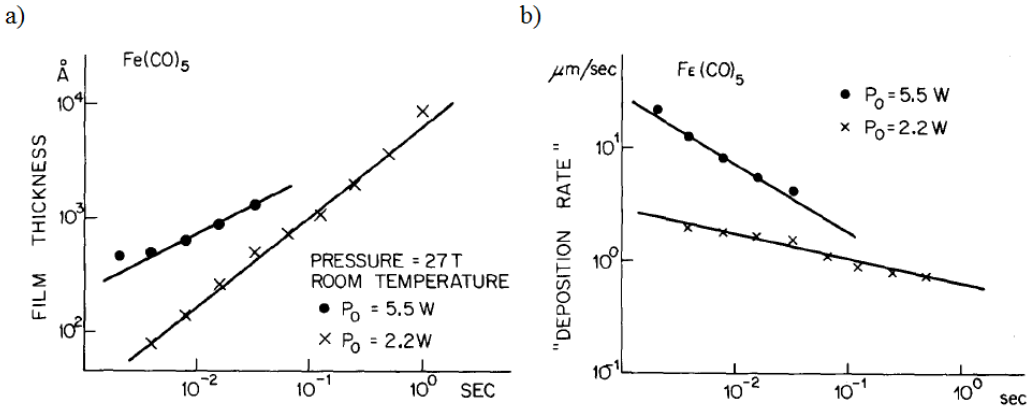

Figure 25. a) Fe film thickness and b) deposition rate as a function of irradiation time.[105] Reproduced with permission from Allen, S.D. and Tringubo, A.B. *J. Appl. Phys.* ***54*** 1641. Copyright 1983 AIP Publishing LLC.

Bottka *et al.* as well as Foord and Jackman deposited iron films from $Fe(CO)_5$ using a mercury lamp at 253.7 nm.[106,107] In order to circumvent pyrolysis and film formation on the reactor window, the gaseous precursor molecules were first condensed on a substrate cooled to a temperature of -196 °C followed by irradiation. The $Fe(CO)_5$ vapor pressure was held below 30 Torr to confine the condensation only on the substrate surface.

Stauf and Dowben deposited iron films from ferrocene using 337 nm radiation obtained from a N_2 laser.[108] The absorption spectrum of ferrocene is illustrated in Figure 26.[35] The laser beam was focused to a spot size of 1.26×10^6 μm^2 resulting in a laser power density of 0.434 W/cm^2. The ferrocene vapor pressure was held at 1 mTorr leading to a growth rate of 100 Å/h.

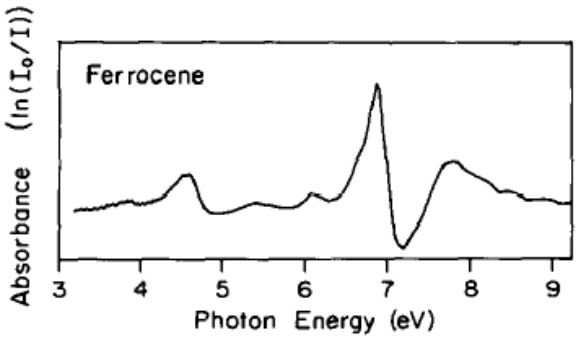

Figure 26. Absorption spectrum of ferrocene vapor between 3 and 9 eV (corresponding to 413 and 138 nm, respectively).[35] Reproduced with permission from Stauf, G.T., Driscoll, D.C. and Dowben, P.A. *Thin Solid Films* ***153*** 421. Copyright 1987 Elsevier.

To conclude, iron deposition has been realized from both $Fe(CO)_5$ and ferrocene. With $Fe(CO)_5$, the confinement of the photofragments only to the irradiated areas was challenging. Laser orientation on the substrate had a significant effect on the film morphology. The resistivity values varied accordingly with impurity levels, and a resistivity of 30 μΩcm was obtained at best.

4.7 Cobalt

Cobalt is utilized as a catalyst for electroless plating and in interconnects in microelectronic devices.[1] The LCVD of cobalt has been studied from $Co_2(CO)_8$ using an Ar^+ laser emitting visible light.[109,110] The transmission spectrum of $Co_2(CO)_8$ vapor and the laser wavelengths employed by Rothschild *et al.* are depicted in Figure 27.[109] Intense absorption occurs below 400 nm but a tail ranging up to 600 nm can be observed. Photodecomposition of the precursor at the selected wavelengths was confirmed by mass spectrometry. The deposition process occurred by an initial photolytic step followed by a growth period sustained by a combination of photolytic and pyrolytic mechanisms.

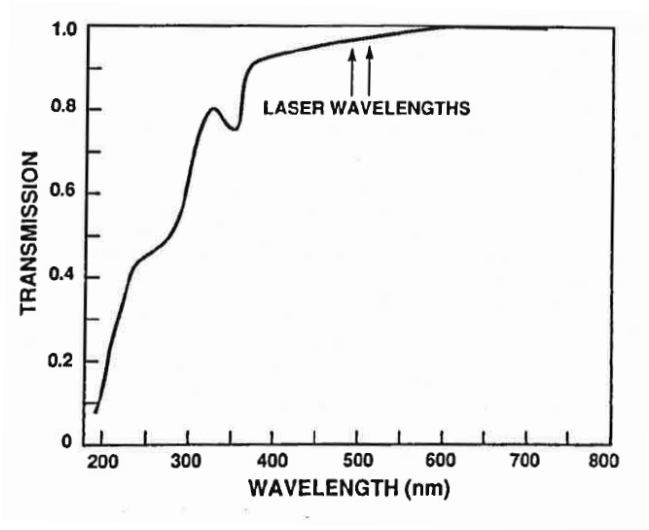

Figure 27. Transmission spectrum of $Co_2(CO)_8$ vapor along with the laser wavelengths utilized by Rothschild *et al*.[109] Reproduced with permission from Rothschild, M., Sedlacek, J.H.C, Shaver, D.C. and Ehrlich, D.J. *Mat. Res. Soc. Symp. Proc.* ***158*** 79. Copyright 1990 Cambridge University Press.

Rothschild *et al.* carried out their depositions at low laser powers of a few mW.[109] The precursor was evaporated at room temperature resulting in a vapor pressure of 0.3–0.7 Torr. A cobalt content of 100 % was detected utilizing AES. A resistivity of 13 μΩcm, which is twice the value determined for bulk cobalt, was measured (thickness not reported). This difference was assigned to the crystalline defects present in the films deposited via LCVD.

At room temperature and an Ar^+ laser power of 0.2 W, Reisse *et al.* obtained adhesive cobalt films on SiO_2 substrates with a growth rate of 5 μm/s.[110] The partial pressure of $Co_2(CO)_8$ was 0.1 Torr. The deposited films exhibited a resistivity of 20 μΩcm. Depositions on Si substrates at a higher laser power of 0.65 W yielded films at a lower growth rate of 0.75 μm/s. This was assigned to the more moderate temperature rise and consequently smaller contribution arising from the pyrolytic reaction pathway on the Si substrates that have higher thermal conductivity than SiO_2.

On the grounds of these observations, a conclusion can be drawn stating that high-purity cobalt films with low values of resistivity can be deposited by the photodecomposition of the corresponding carbonyl complex using an Ar^+ laser operating at visible wavelengths.

4.8 Nickel

Nickel films are utilized as metal contacts in microelectronics, catalysts, as well as protective and decorative coatings.[24] The LCVD of nickel revolves mainly around the decomposition of $Ni(CO)_4$ induced by a localized hot spot created by the incident laser beam.[111–118] Nickel films have also been deposited by the photodecomposition of nickelocene.[108]

The decomposition of $Ni(CO)_4$ is a well-understood process and is industrially used for the purification of nickel (Mond process). Equation 8 is a simplified representation of the overall decomposition of the tetracarbonyl into metallic nickel and carbon monoxide.[111] Based on literature, Tonneau *et al.* made an assumption that during Ar^+ laser irradiation, the reaction occurs through the decomposition of the two dominant intermediate surface species, $Ni(CO)_2$ and Ni(CO), which are produced in the dissociative adsorption of $Ni(CO)_4$.[117]

$$Ni(CO)_4 \xrightarrow{140\ ^\circ C} Ni + 4\ CO \qquad (8)$$

Figure 28 shows the absorption spectrum of $Ni(CO)_4$ vapor.[99] Intense absorption occurs at a wavelength of 207 nm, which was assigned to the metal-to-ligand charge transfer transitions. However, none of the reported depositions employed radiation below 476.2 nm.

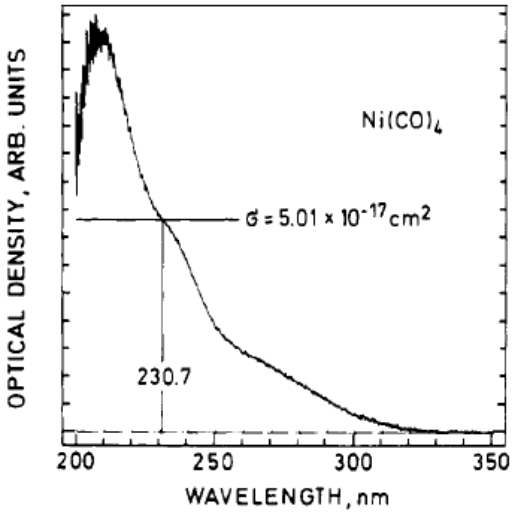

Figure 28. Absorption spectrum of $Ni(CO)_4$ vapor.[99] Reproduced with permission from Kotzian, M., Roesch, N., Schröder, H. and Zerner, M.C. *J. Am. Chem. Soc.* ***111*** 7687. Copyright 1989 American Chemical Society.

Nickel formation from $Ni(CO)_4$ was observed with a CO_2 laser operating at 10.6 µm and with visible light obtained from a Kr^+ or an Ar^+ laser. The IR radiation was admitted to the reaction chamber through a NaCl or a KCl window. According to Allen, the precursor vapor absorbs only 1 % of the photons at 10.6 µm, and deposition occurs due to the heating of the substrate.[111] Kräuter *et al.* reported the overall deposition rate to be independent of the laser wavelength confirming the process to be thermally driven.[112] They also observed a decrease in the deposition rate when the total pressure of the carrier gas was increased due to more efficient cooling of the substrate. The deposition rate was found to increase with increasing laser power and precursor vapor pressure and with decreasing scan speed. Because of its lower thermal conductivity, on glass the deposition rate of nickel was over ten times greater as opposed to SiO_2 on silicon.[112] The rate of film formation decreased with increasing metal film thickness due to the increased reflectivity and thus lower temperature of the surface.[111] The deposition rate is strongly influenced by the reaction conditions but, as an example, Allen measured growth rates of 60 and 1000 µm/min at laser powers of 0.5 and 5 W, respectively.[111] According to Kräuter *et al.*, the deposition rates via LCVD are three or four orders of magnitude greater compared to the rates obtained by conventional CVD.[112]

The films deposited from $Ni(CO)_4$ typically exhibited excellent physical properties including hardness and good adhesion to the substrate.[111,112,115] For a 55 nm film, Allen measured a resistivity of 40 μΩcm which is about six times the resistivity of bulk nickel (6.84 μΩcm).[111] Beleznai *et al.* obtained nickel lines with a resistivity similar to that of bulk metal.[118] Kräuter *et al.* detected no carbon contamination in the films deposited at room temperature using visible wavelengths from a Kr^+ laser, and a resistivity of 19 μΩcm was measured.[112] Using a cw Ar^+ laser at 488–514 nm, Tonneau and coworkers also measured a low carbon content of only 0.5 at.%.[117] The laser power was 0.2–3 W and the deposition temperature between 200 and 400 °C. Contrary to the other studies, the nickel films deposited by Jervis contained 10 % of carbon resulting in poor crystallinity.[115] In most cases however, polycrystalline nickel deposits were obtained.[112,113,117]

Stauf and Dowben have reported an article on the LCVD of nickel using nickelocene as the organometallic precursor.[108] Figure 29 shows the absorption spectrum of nickelocene vapor.[35] The decomposition of nickelocene was achieved at room temperature with a N_2 laser emitting 337 nm photons at a power density of 0.434 W/cm^2 and a frequency of 10 Hz. The laser beam was directed onto the substrate through a quartz window and focused to a spot size of 1.26×10^6 μm^2. When the precursor vapor pressure was less than 1 mTorr, nickel was formed at a deposition rate of approximately 300 Å/h. Near contact masks were used to deposit arrays of 400 μm^2 nickel squares with an edge resolution of less than 1 μm (Figure 30)[108]. The distance between the mask and the substrate was not reported.

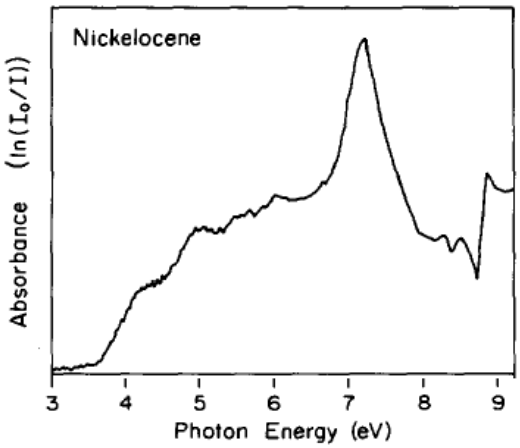

Figure 29. Absorption spectrum of nickelocene vapor between 3 and 9 eV (corresponding to 413 and 138 nm, respectively).[35] Reproduced with permission from Stauf, G.T., Driscoll, D.C. and Dowben, P.A. *Thin Solid Films* ***153*** 421. Copyright 1987 Elsevier.

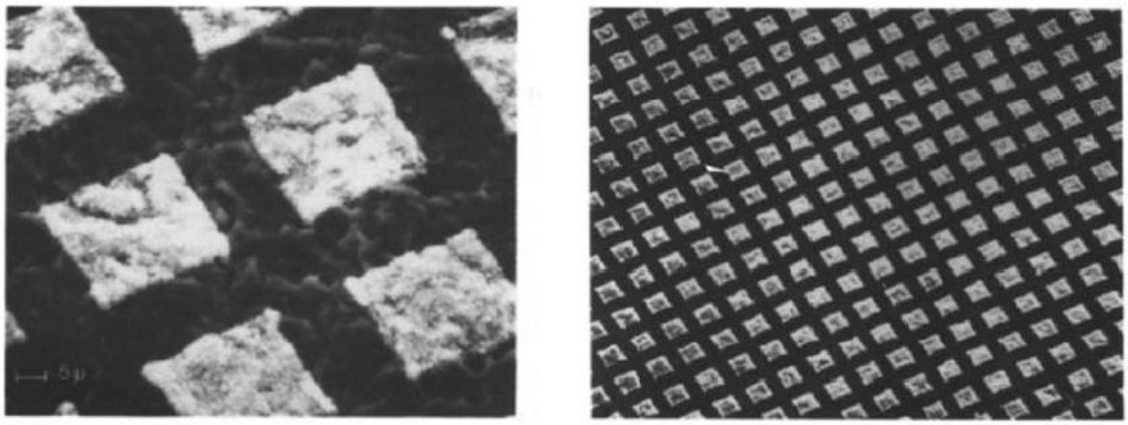

Figure 30. A matrix consisting of 20 µm × 20 µm nickel squares with a thickness of 60 nm.[108] Reproduced with permission from Stauf, G.T. and Dowben, P.A. *Thin Solid Films* ***156*** 31. Copyright 1988 Elsevier.

The LCVD studies of nickel have mainly concentrated on the carbonyl precursor, $Ni(CO)_4$, but a study on nickelocene has also been published. Although carbonyl precursors in general are prone to produce highly contaminated films, deposits without detectable carbon levels were in some cases obtained. The films typically exhibited excellent physical properties, and the deposition rates were significantly improved compared to conventional CVD.

4.9 Copper

Out of all the metals deposited by photo-CVD, copper is by far the most scrutinized one. Copper is the dominant material in intergrated circuit metallization. The motivation behind a great share of the copper photo-CVD studies has been the low deposition temperatures enabling the coating of thermally sensitive substrates such as polymers. Another desirable aspect related to photo-CVD is the possibility of laser direct writing potentially allowing straightforward circuitization and mask repair. The pioneering studies on the photo-CVD of copper were carried out by Houle *et al.* in 1985.[119] In the year 2000, Maury and coworkers published a comprehensive review on all the copper photo-CVD processes reported so far.[120]

Although the research on photo-CVD has waned since its golden years, a few articles on the photo-CVD of copper have emerged also during the 21st century.[121–123]

Precursors for the photo-CVD of copper can be classified in two groups: Cu(I) and Cu(II) complexes. Most of the studies have revolved around the Cu(II) precursors belonging to the group of metal β-diketonates. On account of their resonance structure (Section 2.2), Cu(II) β-diketonates absorb strongly in the UV region. Although not employed to the same extent, many Cu(I) complexes are reactive towards light as well. Figure 31 illustrates the spectral matching of the most utilized precursors with a mercury lamp.[120]

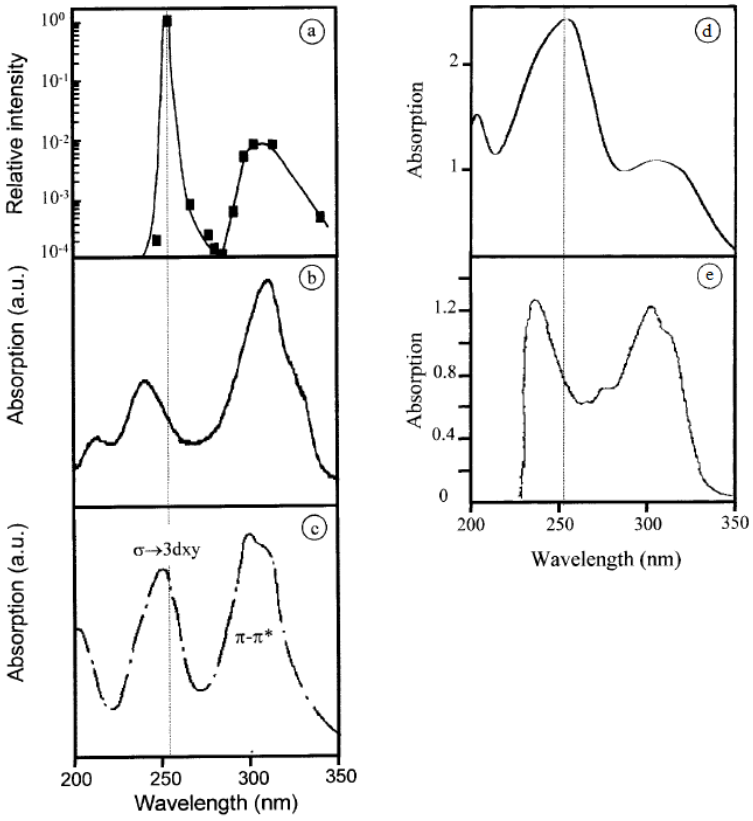

Figure 31. a) Hg lamp output and absorption spectra of b) $Cu(hfac)_2$, c) $Cu(thd)_2$, d) (hfac)CuCOD, and e) (hfac)Cu(TMVS) in n-hexane (hfac = hexafluoroacetylacetonate, thd = 2,2,6,6-tetramethyl-3,5-heptanedionate, COD = 1,5-cyclooctadiene, TMVS = trimethylvinylsilane). With b) and c), absorptions at 250 and 320 nm were assigned to ligand-to-metal charge transfer and π–π* excitation, respectively. With d) and e), absorption is due to excitations from delocalized bonding molecular orbitals to antibonding orbitals at the Cu(hfac) fragment.[120] Reproduced with permission from Maury, F., Vidal, S. and Gleizes, A. *Adv. Mater. Opt. Electron.* ***10*** 123. Copyright 2000 Wiley-VCH Verlag GmbH & Co. KGaA.

Deposition conditions and the most pivotal results using both Cu(II) and Cu(I) precursors are summarized in Tables 3 and 4.[120] The general trends are essentially the same as for most metal photo-CVD processes. With both photolytic and pyrolytic deposition schemes, the growth rate increased with increasing laser power and precursor dose. The quality of deposits grown by photolysis at low laser powers was improved in the presence of a reducing agent such as ethanol or H_2. In the case of $Cu(hfac)_2$, a reducing agent or moderate heating of the substrate was vital for film formation. Because there is no direct Cu–C bond in the β-diketonate complexes, a reducing carrier gas or reactant is often utilized to facilitate the deposition. Pyrolytic deposition realized at high laser powers produced films even without a reducing agent. Pyrolysis generally produced films of lower resistivity. Bulk resistivity (1.7 μΩcm) was reached using $Cu(thd)_2$, a mercury lamp at 254 nm, and a growth temperature of 350 °C.[124] As shown in Figure 32, Wu *et al.* reported good step-coverage for a film deposited at 125 °C using (hfac)Cu(TMVS) and a filtered Hg lamp (250–950 nm).[122]

Table 3. Data on copper photo-CVD utilizing Cu(II)β-diketonates (hfa = hfac, tfa should be pta = pivaloyltrifluoroacetonate, acac = acetylacetonate). References correspond to references in the review article by Maury, not to references within this thesis.[120] Reproduced with permission from Maury, F., Vidal, S. and Gleizes, A. *Adv. Mater. Opt. Electron.* ***10*** 123. Copyright 2000 Wiley-VCH Verlag GmbH & Co. KGaA.

Precursor	UV source	λ (nm)	Carrier gas/ co-reactant	Growth temperature (°C)	Substrate	Dominant process*	Resistivity† (μΩ.cm)	References
$Cu(hfa)_2$	Ar^+ laser	514	None	~250‡	Si; SiO_2	Pyro	3.6	12,13
	ArF; KrF laser	193; 249	EtOH	~20	Si; quartz	Photo	–¶	14–16
	KrF laser	249	None	~20	[d]	Photo	–¶	17
	Ar^+ laser	257	EtOH	~20	Si; quartz	Photo	–¶	14,18
	Ar^+ laser	–¶	None	–¶	Pyrex glass	Pyro	~5	19
	Ar^+ laser	488–514	Ar/H_2	130–200	Si; SiO_2	Pyro	–¶	20
	XeCl laser	308; 350	None; Ar	~20	–§	Photo	–¶	21
	Hg lamp	254	EtOH	~20	Si; quartz	Photo	–¶	14
	Hg lamp	254	He	300–350	Si; Al alloy	Photo/pyro	2.3	9
	Xe lamp	335	EtOH; H_2	100	Polyimide	Photo/pyro	–¶	5
$Cu(thd)_2$	Hg lamp	254	Ar	250–350	Al_2O_3	Photo/pyro	1.7	23
	Hg lamp	254	He; H_2	150–390	Si; Si_3N_4; Al alloy	Photo/pyro	1.9	9,10,24
$Cu(tfa)_2$	CO_2 cw laser	10 600	None; Ar; EtOH	380–600‡	Quartz	Pyro	12	22
$Cu(acac)_2$	Xe lamp	147	O_2	200–350	Si; SiO_2	Photo	–¶	25

* Photochemical decomposition (photo) and pyrolytic deposition (pyro) due to the heating of the substrate induced by the absorption of high power density light.
† Value determined for films grown under optimal conditions.
‡ Calculated substrate temperature.
§ Mechanistic study without substrate.
¶ Not reported.

Table 4. Photo-CVD of Cu using Cu(I) complexes (MHY = 2-methyl-1-hexene-3-yne)[120] Reproduced with permission from Maury, F., Vidal, S. and Gleizes, A. *Adv. Mater. Opt. Electron.* ***10*** 123. Copyright 2000 Wiley-VCH Verlag GmbH & Co. KGaA.

Precursor	UV source	λ (nm)	Carrier gas/ co-reactant	Growth temperature (°C)	Substrate*	Dominant process†	Resistivity‡ (μΩ.cm)	References
$CpCu(PEt_3)$	Ar^+ laser	514	None	200–300§	Si; SiO_2; PI	Pyro	~6.7	26
	KrF; XeCl laser	248; 308	None	–¶	Si; SiO_2; PI	Photo/pyro	–¶	26
(hfa)Cu(TMVS)	Ar^+ laser	514	He; H_2	200–500§	Si; Au; W	Pyro	~1.9	27
	KrF laser	248	H_2	60–120	TiN, Teflon	Photo/pyro	41	3, 31
	Ar^+ laser	514	H_2O	>250§	Quartz, Al_2O_3	Pyro	~1.8	30
	Ar^+ laser	488; 514	H_2	–¶	SiO_2; Si_3N_4	Pyro	2.7	28, 29
	Xe lamp	335	H_2	125–175	PEI	Photo/pyro	8.4	5
(hfa)Cu(MHY)	Hg lamp	254	He	120–220	Si; Ag; glass	Photo/pyro	1.9	7
(hfa)Cu(COD)	Hg lamp	254	He	100–180	Si; SiO_2; EC; PS	Photo/pyro	2.3	32, 11

* Polymer substrates: PI polyimide; PEI polyetherimide; FP fluoropolymer; EC epoxy composite reinforced with carbon; PS polystyrene.
† Photochemical decomposition (photo) and pyrolytic deposition (pyro) due to the heating of the substrate induced by absorption of high power density light.
‡ Value determined for films grown under optimal conditions.
§ Calculated substrate temperature.
¶ Not reported.

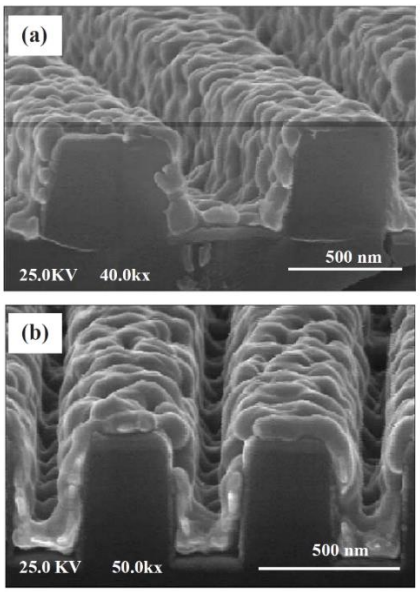

Figure 32. SEM images of Cu-coated a) 0.4 and b) 0.22 μm-width trenches.[122] Reproduced with permission from Wu, Y.-L., Hsieh, M.-H. and Hwang, H.-L. *Thin Solid Films* ***483*** 10. Copyright 2005 Elsevier.

To summarize, the photo-CVD of copper has been thoroughly studied using both Cu(I) and Cu(II) precursors as well as radiation extending from 116 nm to the IR wavelengths. Due to the extensive research, the processes are well-known and have been honed to produce low-resistivity deposits with good morphology and step-coverage at temperatures below the ones employed in thermal CVD.

4.10 Zinc

The key application of zinc is the doping or alloying of GaAs.[1,125] Zinc can also be utilized to form electrical contacts on aluminum through a layer of Al_2O_3 and to alloy aluminum for maskless wet etching through enhanced dissolution of the Al-Zn alloy. The motivation behind the study carried out by Johnson and Schlie was to develop a process for the deposition of high-purity Zn, Se, and eventually ZnSe films for CO_2 and HF lasers.[126] The photo-CVD of zinc has been studied using both dimethylzinc (DMZn) and diethylzinc (DEZn).[51,125,126] The absorption spectrum of DEZn is depicted in (Figure 33).[125] The two broad bands in the region of 200–285 nm in the gas-phase absorption spectrum are characteristic for metal dialkyl compounds. According to spectroscopic studies, the photodissociation of both zinc dialkyls occurs at ~245 nm.[125,126] Absorption of the chemisorbed DEZn layer shifts to shorter wavelengths possibly due to reactions with water or hydroxyl groups adsorbed on the quartz substrate.

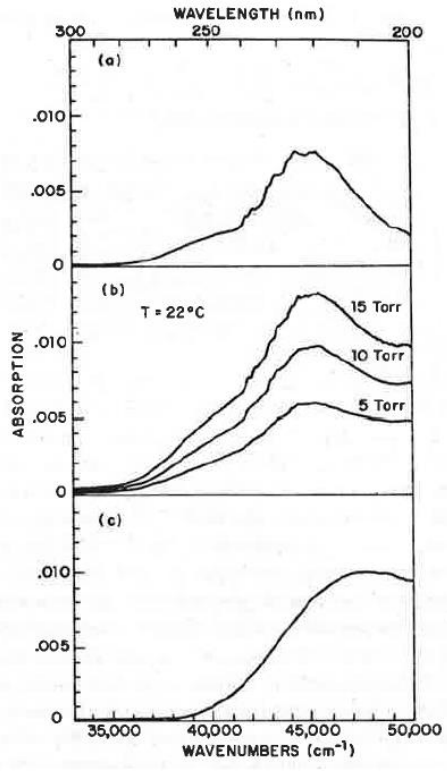

Figure 33. Absorption spectra of DEZn in the a) gas phase b) physisorbed layer, and c) chemisorbed layer.[125] Reproduced with permission from Krchnavek, R.R., Gilgen, H.H., Chen, J.C., Shaw, P.S., Licata, T.J. and Osgood Jr., R.M. *J. Vac. Sci. Technol.* B ***5*** 20. Copyright 1987 American Vacuum Society.

Rytz-Froidevaux *et al.* applied a Kr^+ laser emitting 520.8–568.2 nm radiation to heat the substrate surface and thermally decompose DMZn under H_2 atmosphere.[51] Zinc formation was observed at laser powers between 65 and 190 mW translating into substrate temperatures ranging from 215 to 635 °C. Johnson and Schlie deposited zinc thin films via photodissociation of DMZn at room temperature using a cw Hg/Xe arc lamp.[126] Only wavelengths below 245 nm were admitted into the system in order to avoid pyrolytic growth. A thermocouple was placed in contact with the substrate, and a temperature rise of only 5 °C was observed. At a laser intensity of 0.4 W/cm^2 and a precursor pressure of 10 Torr, deposition occurred at a rate of 1 Å/s. The zinc films were gray instead of lustrous and highly contaminated with carbon arising either from the methyl ligands or from the dissociation of carbon containing impurities in the system. The deposits were flaky but exhibited good adhesion properties.

Krchnavek and coworkers studied the LCVD of zinc using an Ar^+ laser operating at 257.2 nm, a power intensity of 15 kW/cm^2, and the beam focused to a spot size of 3 µm.[125] The temperature rise on the glass substrate was measured to be less than 100 °C being insufficient for pyrolytic deposition. At room temperature and with small spot sizes, the deposition was found to occur at the film surface, whereas at higher temperatures and with larger spot sizes, the deposition proceeded via gas-phase deposition due to decreased surface coverage. All the films were shiny and metallic excluding a darker area exposed to the very center of the beam. The resistivity was approximately 3 times the bulk value (5.96 µΩcm).

4.11 Gallium

Lane *et al.* have published an article about the photo-CVD of gallium thin films using GaI_3 as the precursor.[78] Due to its tendency towards oxidation and low melting point (~30 °C), gallium has little use as a thin film material. However, the studies gave promising results of the exploitation of metal iodides as precursors for photo-CVD in general since similar photochemistry has also been observed for the iodides of Bi, In, and Al.[127] As mentioned in Section 4.2, Geohegan and Eden have deposited Al, In, and Tl thin films photolytically from the corresponding metal iodides.[77] A review by Lüthy lists numerous other metal iodides the photochemistry of which could be applied to metal deposition.[128] It was suggested that gallium formation occurred via a photochemical reaction of an adsorbed monoiodide

intermediate generated by the thermal decomposition of the primary precursor (Equations 9–10).

$$GaI_3 \rightarrow GaI + 2\ I \quad (9)$$

$$GaI \rightarrow Ga + I \quad (10)$$

The resulting films were continuous instead of an assembly of gallium droplets, which partly verifies the presence of an intermediary surface species moderating the surface tension of gallium. The reaction path was also investigated by feeding arsenic into the system. No arsenic was incorporated into the gallium films pointing towards the existence of an intermediary GaI monolayer acting as a barrier against the formation of GaAs. Figure 34 shows the absorption spectra of selected Group 13 metal iodides.[78] The photolytic decomposition of GaI_3 occurs at wavelengths below 220 nm which are not achievable with the high-pressure mercury arc lamp utilized by Lane and coworkers. GaI, on the other hand, has an absorption maximum at 310 nm supporting the proposed reaction mechanism.

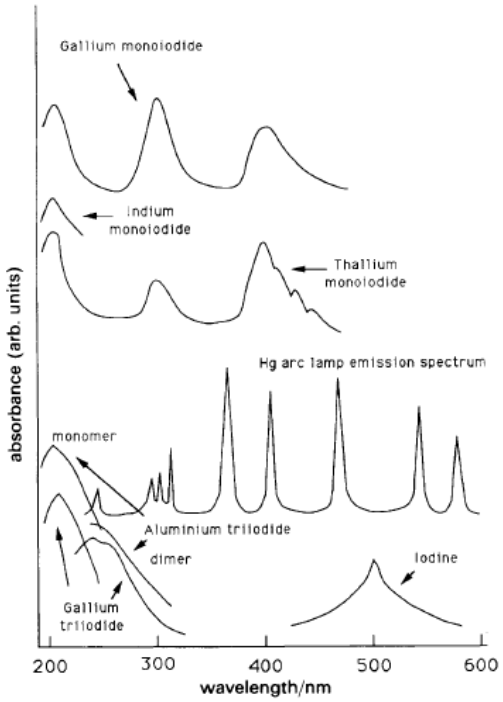

Figure 34. Absorption spectra of selected Group 13 iodide vapors.[78] Reproduced with permission from Lane, S.J. and Green, M. *J. Chem. Soc, Faraday Trans.* ***87*** 995. Copyright 1991 Royal Society of Chemistry.

In order to obtain moisture-free GaI_3 of sufficient purity, the precursor was synthesized *in situ* from the elements. At GaI_3 source temperatures of 220 and 240 °C, the partial pressure of the precursor above the substrate was approximated at 0.11 and 0.27 Torr, respectively. Depositions were carried out in a cold-wall reactor, and the susceptor was tilted in a 45° angle with respect to the light permitting window. A 100 W high-pressure mercury arc lamp was employed as the irradiation source. According to calculations, a maximum photon flux of 3×10^{21} quanta/m was attained at the substrate during a second of irradiation when the wavelength was between 200 and 300 nm and an estimate of 5 eV was used as the photon energy. The process was investigated in the temperature range of 400–600 °C. The irradiation area could be modified using an adjustable aperture. Substrate temperature and light intensity were both found to increase as the aperture size was diminished. Because of the corrosive nature of the precursor, a thermocouple could not be placed in direct contact with the substrate during depositions; thus, the accurate substrate temperature could not be measured.

Because metallic gallium oxidizes readily when exposed to ambient air, sample analysis was done *ex situ* on gallium oxide films. However, the metallic luster of gallium could be visually observed before the sample was removed from the deposition system. Moisture sensitivity of gallium deposits correlates with the amount of iodine present in the films. Since the deposited films were not sensitive to moisture, it was concluded that the iodine concentration was low. This was also confirmed with an electron probe analysis. Figure 35 represents the deposition rate of gallium as a function of substrate temperature at constant illumination intensity.[78] The deposition rate decreased with increasing temperature pointing towards a surface reaction controlled process. At higher temperatures, the rate of desorption increases leading to fewer surface species and therefore lower deposition rates. Photolytic processes that occur in the gas-phase show only weak temperature dependence. In thermal CVD, growth rates typically increase as a function of increasing deposition temperature.

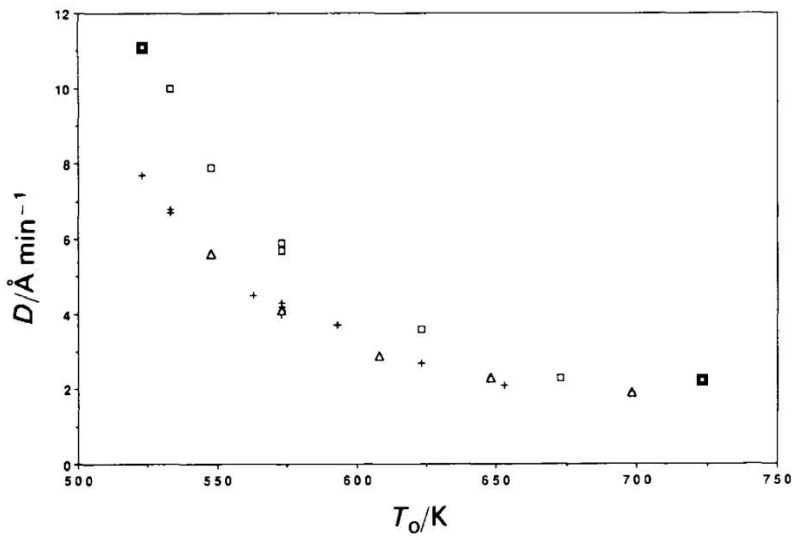

Figure 35. Deposition rate of gallium as a function of substrate temperature. Squares represent depositions on Si and at a precursor partial pressure of 0.27 Torr, crosses correspond to Si substrates and 0.11 Torr, and triangles to GaAs substrates and 0.11 Torr.[78] Reproduced with permission from Lane, S.J. and Green, M. *J. Chem. Soc, Faraday Trans.* ***87*** 995. Copyright 1991 Royal Society of Chemistry.

The deposition rate was also investigated as a function of scaled illumination intensity (Figure 36).[78] The actual illumination intensity is a product of the scaling factor Z and the maximum value Z_0. The deposition rate increased with increasing intensity until a limit above which the rate started to decrease because the surface coverage decreased due to desorption induced by local heating of the substrate. Film growth at a very low deposition rate independent of deposition temperature could be observed even without irradiation. This was consequential of GaI_3 reacting with residual water and oxygen leading to the direct formation of Ga_2O_3.

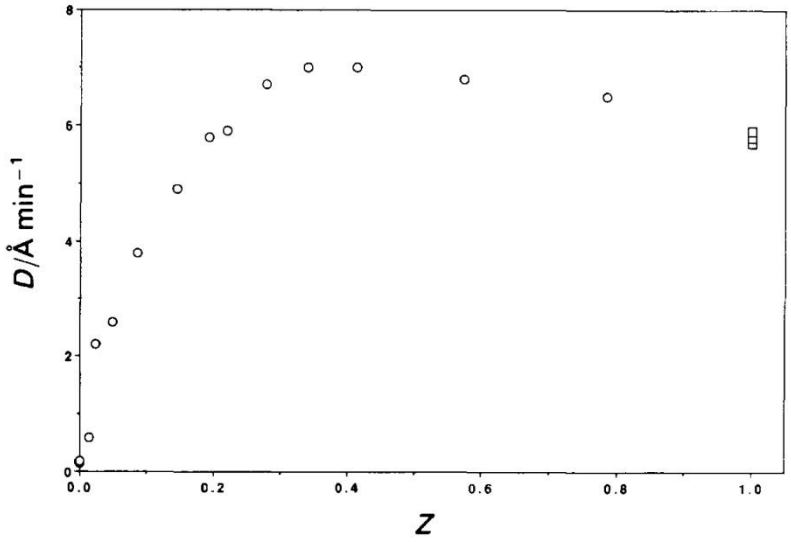

Figure 36. Deposition rate of Ga as a function of scaled illumination intensity at a constant temperature of 300 °C.[78] Reproduced with permission from Lane, S.J. and Green, M. *J. Chem. Soc, Faraday Trans.* ***87*** 995. Copyright 1991 Royal Society of Chemistry.

A conclusion can be drawn that the deposition of gallium is possible by photolytic means. Although gallium thin films have little potential regarding applications, the process could be utilized to deposit high quality GaAs films or as an example for the metal deposition of similar compounds.

4.12 Molybdenum

Molybdenum can be employed in a large number of applications including interconnects, gate and Schottky contact metallizations, wear resistant and laser mirror coatings, as well as IR reflectors.[1] Molybdenum is chemically similar to tungsten apart from its higher propensity towards oxidation.[129] The LCVD of molybdenum focuses mainly on the corresponding hexacarbonyl complex but reports utilizing MoF_6 and $MoCl_5$ also exist.[44,86,89,91,92,110,129–135]

Gray and Beach have measured the absorption spectrum of $Mo(CO)_6$ vapor (Figure 37).[97] Intense absorption bands arising from the allowed metal-to-ligand charge transfer transitions

occur at 286.7 and 228 nm. According to Singmaster *et al.*, the primary photoproducts forming from $Mo(CO)_6$ are $Mo(CO)_4$ and $Mo(CO)_3$.[135]

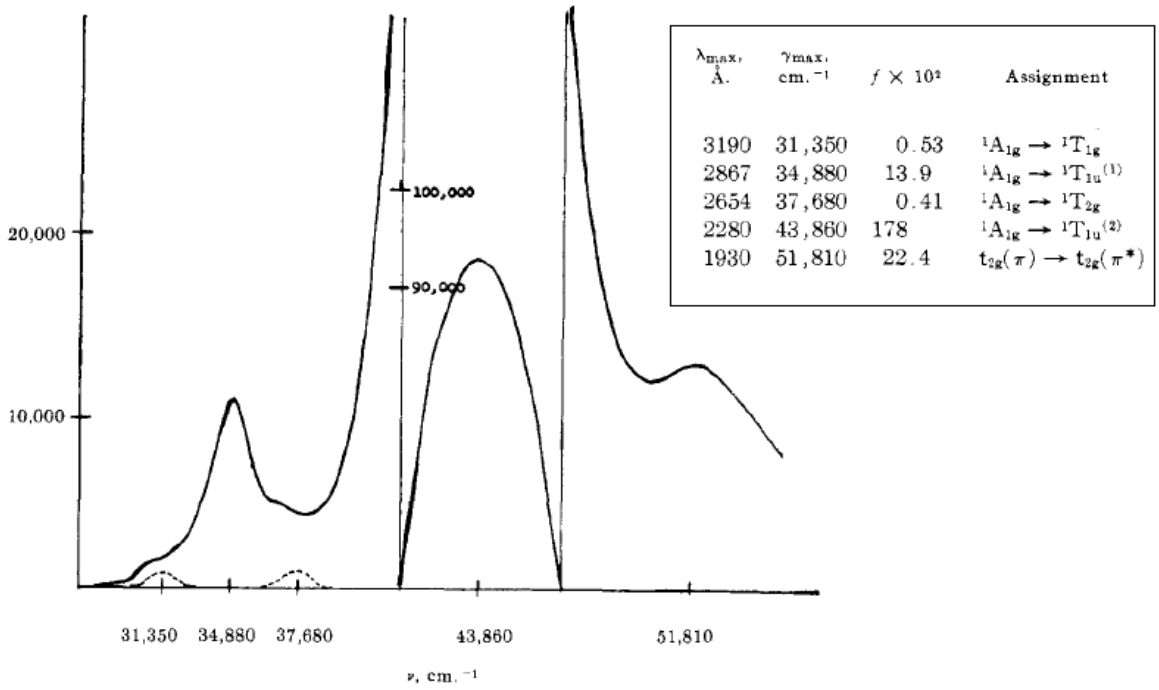

Figure 37. Absorption spectrum of $Mo(CO)_6$ vapor.[97] Reproduced with permission from Gray, B. and Beach, N.A. *J. Am. Chem. Soc.* ***85*** 2922. Copyright 1963 American Chemical Society.

The molybdenum depositions from $Mo(CO)_6$ have been carried out using various wavelengths. Solanki *et al.* employed a Cu^+ laser generating 260 nm photons to deposit molybdenum at room temperature.[86] The same group carried out a more thorough study with the aid of an excimer laser operating at 157, 193, 248, or 308 nm generated by F_2, ArF, KrF, and XeCl transitions, respectively.[89] Laser operation at 248 nm was found the most optimal with respect to film purity and deposition rate (250 nm/min). Nonetheless, the most adhesive films were deposited at 193 nm. A relatively low carbon content of 0.9 % was determined by Auger analysis. However, due to a high degree of oxygen impurities (< 7 %), the resistivity values were 20 times that of bulk (5.2 μΩcm). Flynn and coworkers also utilized 193 and 248 nm radiation in their depositions.[91] Adherent deposits were obtained only when the radiation was applied perpendicularly to the substrate. Deposition rates of 0.13 and 0.15 Å/pulse were observed at 249 and 193 nm, respectively. The deposition rates were

independent of the pulse repetition rate. The resistivity of a 250 nm molybdenum film was 37.5 μΩcm.

Gilgen *et al.* employed longer wavelengths in the range of 350–360 nm provided by an Ar^+ laser.[130] High laser powers were utilized translating into elevated substrate temperatures which, according to the authors, was necessary for achieving complete dissociation of $Mo(CO)_6$ and thus high-quality molybdenum lines. At a laser power of 30 mW, a scan rate of 1 μm/s, and a precursor vapor pressure of 0.17 Torr, a rapid growth rate of 270 nm/s was observed on glass. In contrast, a growth rate of no more than 8 nm/s can be achieved via conventional CVD at temperatures above 450 °C. Due to the high rate of film formation, resistivity of the lines remained at quite a high level of 7–10 times the bulk value.

Consistent with the results of Solanki *et al.*, Gluck and colleagues observed low deposition rates without the use of a buffer gas.[86,92] A buffer gas reduces the mean free path of photofragments produced from $Mo(CO)_6$ in the gas phase, which facilitates the confinement of the deposition. The Mo films deposited by Gluck *et al.* at 257 nm contained significant levels of oxygen (30–40 %) and 10 % carbon also with trace amounts of nitrogen.[92] The oxygen impurities were assigned to air exposure after the deposition and adsorption of oxygen impurities present in the buffer gas.

Jackson and Tyndall studied the LCVD of molybdenum at 257 and 325 nm obtained from a frequency-doubled Ar^+ laser and a He-Cd laser, respectively.[133] According to quartz crystal microbalance (QCM) measurements, the deposition rate increased linearly with increasing $Mo(CO)_6$ vapor pressure. In addition, the log of the deposition rate increased linearly as a function of laser power. The areas exposed to irradiation at 257 nm were heavily cracked and rippled, which was assigned to the interaction between the polarized laser beam and the underlying rough film resulting in the formation of surface waves interfering with the incident light (Figure 38).[133] The ripple structures were not present in the samples deposited with the dual-plane polarized He-Cd laser.

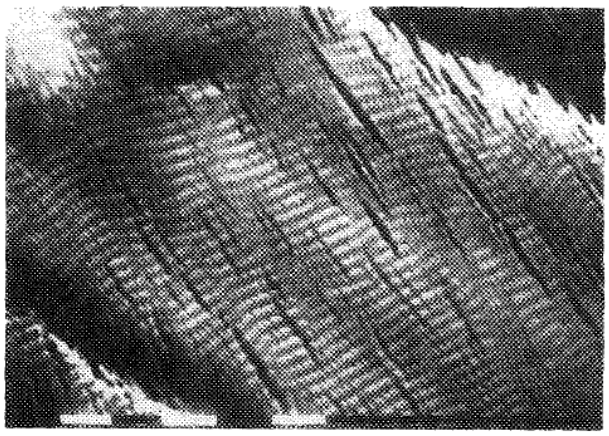

Figure 38. SEM image of a rippled Mo film with cracks. A white bar at the bottom of the image corresponds to 1 µm.[133] Reproduced with permission from Jackson, R.L. and Tyndall, G.W. *J. Appl. Phys.* ***64*** 2092. Copyright 1988 AIP Publishing LLC.

According to Turney *et al.*, the impurity levels of films grown from $Mo(CO)_6$ could be reduced with the application of laser pulses instead of continuous light.[44] However, Radloff *et al.* obtained similar film compositions and deposition rates using both pulsed and continuous lasers.[134] Singmaster and coworkers carried out a thorough study on the LCVD of Mo, W, and Cr from their corresponding hexacarbonyls using cw 257 nm radiation at a low power and obtained even lower molybdenum contents of ~20 % as opposed to prior reports of ~50 %.[135]

Björklund *et al.* deposited molybdenum rods via reduction of MoF_6 using hydrogen and an Ar^+ laser operating at wavelengths of 488 and 514 nm.[129] The depositions were carried out on tungsten wires in a cold-wall reactor. Condensation of the precursor on the chamber walls and the light entrance windows was suppressed by heating. In order to control the deposition temperature, the laser power was varied with the total pressure accordingly. The deposition conditions are summarized in Table 5.[129] The morphology of the deposited structures was found to change depending on the precursor ratio. At high hydrogen concentrations, dendrite-like rods were obtained instead of crystal-shaped ones (growth direction not specified) due to the high thermal conductivity of hydrogen and consequently increased temperature gradients in the system. The deposition rate increased in a linear fashion with increasing hydrogen partial pressure and was independent of the molybdenum content. AES measurements revealed an oxygen content of 2–3 % in the deposits.

Table 5. Conditions applied for the deposition of molybdenum rods.[129] Reproduced with permission from Björklund, K.L., Heszler, P. and Boman, M. *Appl. Surf. Sci.* ***186*** 179. Copyright 2002 Elsevier.

Experimental series No.	Partial MoF_6 pressure (mbar)	Partial H_2 pressure (mbar)	Temperature (K)	Heating of tubing	Heating of windows
1	25	75–425	750	Yes	No
2	50	150–850	750	Yes	No
3	25	75–425	750	Yes	Yes
4	50	150–850	750	Yes	Yes
5	25	125	705–840	Yes	Yes
6	25	125–225	705	Yes	Yes
7	14–41	125	705	Yes	Yes

Duty and colleagues have investigated the pyrolytic LCVD of Mo from $MoCl_5$ using a gas-jet system which facilitates the direction of the precursor flux to the substrate.[132] The precursor was evaporated at 150 °C and introduced into the reaction chamber along with a flow of hydrogen excess. A CO_2 laser was utilized to heat the substrate and trigger a decomposition reaction shown in Equation 11.

$$MoCl_5 + H_2 \rightarrow Mo\ (s) + 5\ HCl \qquad (11)$$

At temperatures above 1150 °C, fibrous and porous deposits were obtained, whereas lower deposition temperatures yielded flat and flaky deposits. According to the data provided by energy dispersive X-ray spectroscopy (EDS), the deposits formed on graphite contained a negligible amount of impurities.

In summary, the LCVD of molybdenum has been studied using $Mo(CO)_6$, MoF_6, and $MoCl_5$. The most often utilized precursor by far has been $Mo(CO)_6$ yielding inconsistent results with respect to deposition rate, film composition, and morphology.

4.13 Rhodium

Noble metals are chemically inert and can maintain their resistance against oxygen even at high temperatures.[8] Thus, noble metals can be applied in integrated circuits as electrodes for dynamic random access memories (DRAMs) and ferroelectric random access memories (FRAMs). Noble metals are also utilized as gate electrodes in metal-oxide-semiconductor field-effect transistors (MOSFETs), activation layers for copper deposition in interconnects, as well as for catalysis and sensors. Suhr's research group has reported a process for the LCVD of rhodium lines from $Rh(CO)_2$(acac), $Rh(CO)_2$(thd), and $Rh(CO)_2$(hfac).[136–138] Cohan *et al.* have investigated the deposition of rhodium thin films via LCVD using $CpRh(C_2H_4)_2$ as the organometallic precursor.[139]

The motivation behind the experiments done by Suhr's group was to develop a process for the laser direct writing of narrow rhodium lines.[136–138] The depositions were carried out using an Ar^+ laser emitting photons at 514.5 nm. A laser beam with a radius of 7 μm was focused onto the substrate surface through a glass window. The lines were generated by moving the entire cell assembly with respect to the laser beam. The deposition followed a pyrolytic mechanism which proceeded through two stages: nucleation and the growth phase. The laser beam triggers decomposition of the precursor leading to the formation of a small deposit which increases the absorptivity of the substrate and therefore causes a temperature rise on the surface. This increase in temperature is essential for the initiation of the growth stage where gaseous precursor molecules approach the surface and decompose to form the metal deposit. Because of the different vapor pressures of the different precursors, evaporation temperatures that produced the stripes with the lowest resistivity were chosen for comparison. These evaporation temperatures were 85, 78, and 40 °C for the acac, thd, and hfac complex, respectively. Figure 39 shows the stripe resistivity compared to the resistivity of bulk rhodium as a function of the laser power.[138] The lowest values were obtained when $Rh(CO)_2$(hfac) was used as the metal precursor. The low resistivity was most likely attributed to the high purity of these lines, which was verified by AES. The low resistivity was also influenced by the regular morphology of the stripes deposited from $Rh(CO)_2$(hfac).

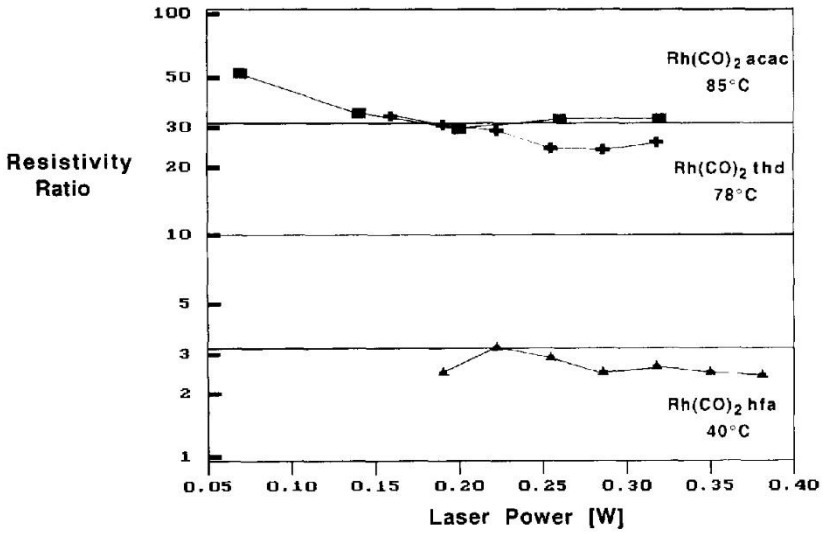

Figure 39. Resistivity ratio (ρ/ρ_0) of the deposited rhodium stripes as a function of laser power. Writing speed = 40 µm/s.[138] Reproduced with permission from Flint, E.B., Messelhäuser, J. and Suhr, H. *Appl. Surf. Sci.* ***54*** 56. Copyright 1992 Elsevier.

The line dimensions depend on the evaporation temperature of the precursor, laser power, and writing speed. It was observed that the stripe dimensions increased as a function of increasing laser power and evaporation temperature (Figures 40 and 41).[138,136] An increase in laser power leads to a higher temperature at the substrate surface causing more decomposition over a wider area. Higher evaporation temperature leads to a higher vapor pressure and thus to a higher precursor dose increasing the line width but only to a certain extent. At a given point, further increase of laser power has no effect on the stripe width because the temperature at the edge of the line falls below the threshold temperature required for the decomposition of the precursor. Line widths are also influenced by the chemical nature of the precursor. Precursors with low decomposition temperatures, for example, yield larger line widths at a certain temperature compared to precursors with higher thermal stability. Also, if the decomposition occurs through a mobile surface intermediate, the line width may increase by the means of diffusion.

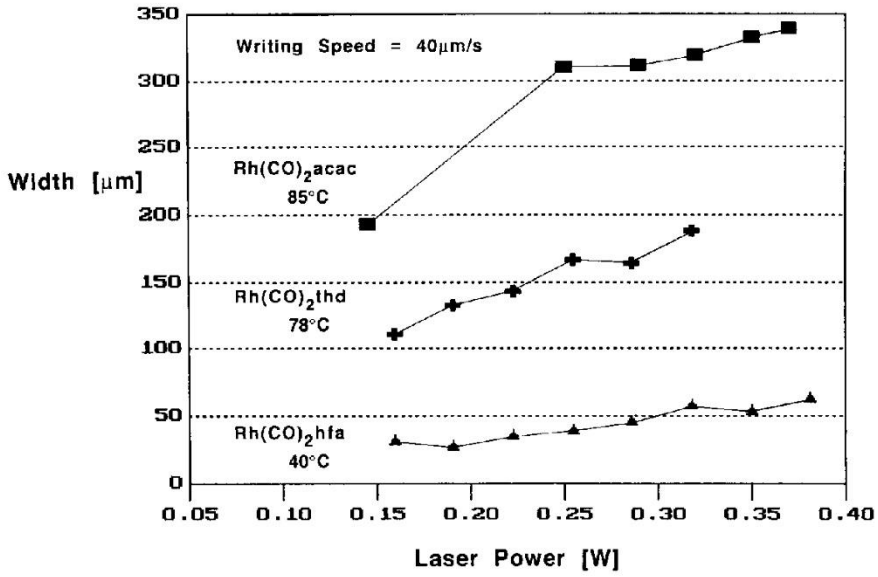

Figure 40. Rhodium line width as a function of laser power for different precursors.[138] Reproduced with permission from Flint, E.B., Messelhäuser, J. and Suhr, H. *Appl. Surf. Sci.* ***54*** 56. Copyright 1992 Elsevier.

Available as Figure 1a in Flint, E.B., Messelhäuser, J. and Suhr, H. *Appl. Phys. A* ***53*** (1991) 430.[136]

Figure 41. Rhodium line width as a function of laser power. $Rh(CO)_2(acac)$ evaporation temperature was varied from 65 to 95 °C.[136]

Cohan *et al.* deposited rhodium thin films using $CpRh(C_2H_4)_2$ as the precursor.[139] The depositions were carried out in an atmosphere of He and H_2 at room temperature and atmospheric pressure. A XeCl excimer laser operating at a wavelength of 308 nm was employed as the irradiation source. No deposition was observed with visible irradiation at wavelengths of 440 or 503 nm indicating the process to be of photochemical nature. Photolysis studies suggest the primary photoactive process to be the cleavage of the metal-ethylene bond. The rhodium films were deposited in a glass cell, and the laser beam was directed into the system through a quartz window located above the sample. The laser frequency was 20 Hz, and the irradiated area was a circle with a diameter of 1 cm. The pulse energy at the substrate was ~20 mJ/pulse. After about 20 minutes of irradiation, a mirror-like rhodium film was obtained on glass and quartz, and a slightly yellow deposit was formed on silicon. After the deposition, the irradiation was continued under H_2 for another 20 minutes. According to X-ray photoelectron spectroscopy (XPS), high-purity rhodium films with less than 1 at.% carbon contamination were obtained. The carbon content was higher if the sample was not irradiated after the deposition. The post-deposition irradiation is most likely required for the removal of the Cp unit from the molecule adsorbed on the Si surface. There is a small visible peak corresponding to rhodium at $2\theta = 41°$ in the X-ray diffractogram suggesting only modest crystallinity (Figure 42).[139]

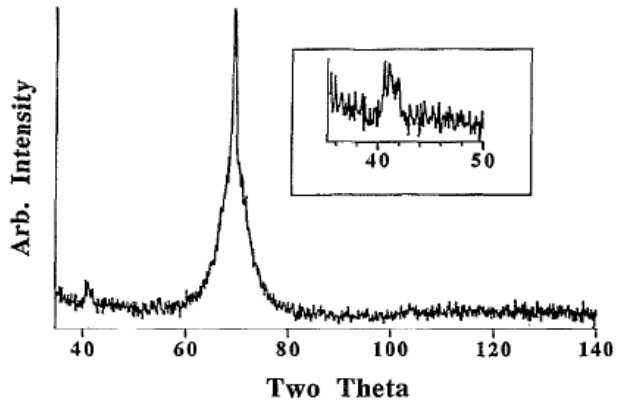

Figure 42. X-ray diffractogram of rhodium film. The intense peak at $2\theta = 70°$ corresponds to the Si substrate.[139] Reproduced with permission from Cohan, J.S., Yuan, H., Williams, R.S. and Zink, J.I. *Appl. Phys. Lett.* ***60*** 1402. Copyright 1992 AIP Publishing LLC.

The LCVD of rhodium has been reported for $Rh(CO)_2(acac)$, $Rh(CO)_2(thd)$, $Rh(CO)_2(hfac)$, and $CpRh(C_2H_4)_2$ precursors. The first three were used to deposit rhodium stripes pyrolytically with an Ar^+ laser operating at 514.5 nm. To conclude, $Rh(CO)_2(hfac)$ was the most promising candidate out of the three precursors in terms with stripe width, resistivity, and operating temperature. The deposition process using $CpRh(C_2H_4)_2$ was photolytic, and rhodium films of high purity were obtained.

4.14 Palladium

Similar to other noble metals, palladium is chemically inert and has a low resistivity making it an attractive material for microelectronic applications. Kuchumov *et al.* have studied a low-temperature photo-CVD process of palladium using $Pd(hfac)_2$ as the precursor.[140] The same precursor was also employed by Cole *et al.* in an attempt to deposit a palladium seed layer for electroless copper plating.[141] Electroless copper plating was also the motivation behind the studies carried out by Thomas and Park who deposited palladium via irradiation of CpPd(allyl).[142] Stauf and Dowben have also utilized CpPd(allyl) as the precursor for the patterned photodeposition of palladium layers.[108]

The main motivation behind the studies done by Kuchumov *et al.* was to develop a low-temperature process for the deposition of palladium that would enable the coating of porous structures with poor thermal stability e.g. polymer substrates.[140] Depositions were carried out in a cold-wall reactor, and $Pd(hfac)_2$ was introduced to the substrate from an evaporator in a 45° angle with respect to the susceptor. Radiation was obtained from a low-power direct-voltage krypton lamp operating at 116 nm and more powerful alternating-voltage argon lamps at 126 nm. A flow of hydrogen was essential for the formation of palladium. No film growth was observed until a temperature of 350 °C without hydrogen under UV stimulation. Deposition without irradiation but with hydrogen could be obtained at 250 °C. With the aid of UV stimulation the deposition temperature could be lowered from 250 °C down to 50 °C. The reactor temperature was lower for the film growth on dielectrics such as polymers, mica, and quartz (50–70 °C) and higher for metal and semiconductor substrates (70–110 °C).

Cole *et al.* investigated the use of palladium as a catalytic layer for the electroless deposition of copper.[141] Electroless plating enables the deposition of uniform and low stress films,

particularly vital in electronic applications where stress relieving mechanisms may lead to short circuiting. A few milligrams of $Pd(hfac)_2$ was placed in a stainless steel vessel heated to a temperature of 70 °C to obtain the desired vapor pressure. An Ar^+ laser beam at a wavelength of 351 nm was directed to the polyimide substrate through a quartz window. Figure 43 shows the schematics of the copper deposition process.[141] Since polyimide has an absorption coefficient of 2.6×10^4 cm^{-1} at 351 nm, most of the radiation is absorbed causing local heating of the substrate. Polyimide withstands temperatures up to 400 °C, but $Pd(hfac)_2$ decomposes already at 225 °C providing a wide temperature window for the process. No film formation was observed on quartz suggesting the deposition mechanism to be pyrolytic rather than photolytic. The laser powers needed for the decomposition of $Pd(hfac)_2$ were high enough to cause damage also to the underlying polyimide substrate having a deteriorating effect on the morphology of the subsequently deposited copper layers.

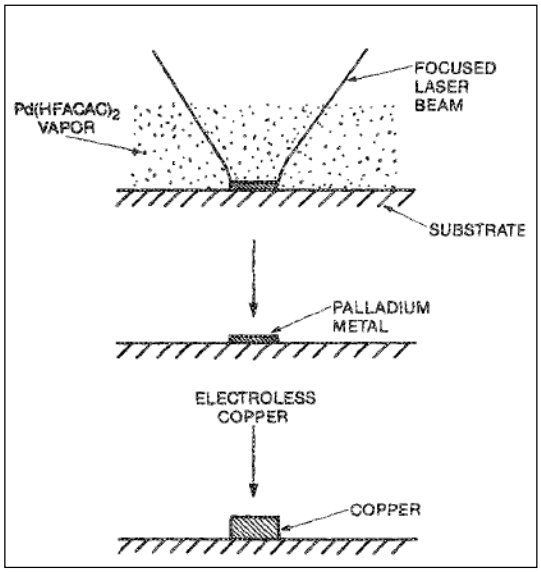

Figure 43. Schematics of the laser-induced palladium deposition process followed by electroless deposition of copper.[141] Reproduced with permission from Cole, H.S., Liu, Y.S., Rose, J.W. and Guida, R. *Appl. Phys. Lett.* ***53*** 2111. Copyright 1988 AIP Publishing LLC.

Stauf and Dowben have published an article on the patterned photodeposition of palladium using CpPd(allyl) as the organometallic precursor.[108] The photolytic dissociation was achieved with a N_2 laser operating at 337 nm. The beam was directed to the silicon wafer through a quartz window and focused to a spot the size of 1.26 mm^2. The laser power density at the substrate was 0.434 W/cm^2, and the laser frequency was 10 Hz. The vapor pressure of

the palladium complex was 1 mTorr. A deposition rate of about 8000 Å/h was measured. Because photo-CVD is a line-of-sight method, near contact masking could be employed to deposit 20 × 20 μm palladium squares (Figure 44).[108] The edge resolution of the squares was less than 1 μm and mainly limited by the resolution of the illuminated patterns rather than photochemistry.

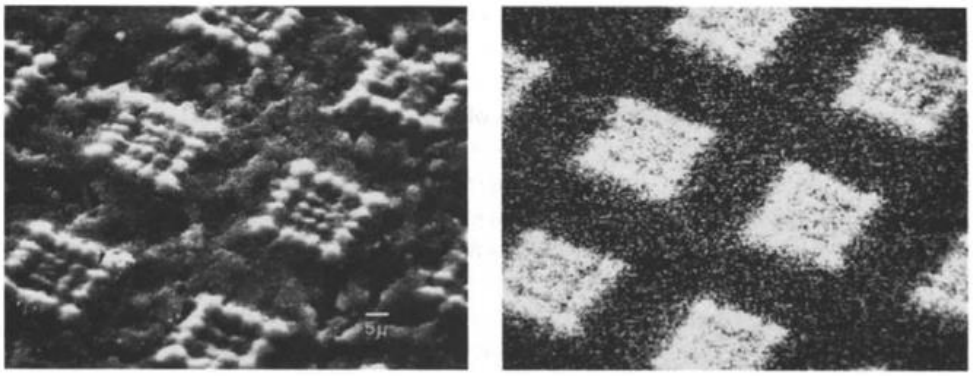

Figure 44. 400 μm^2 palladium squares deposited on silicon by the photodecomposition of CpPd(allyl) through a near contact mask. On the left, a SEM image from the surface. On the right, an elemental map obtained by X-ray electron spectroscopy (XES).[108] Reproduced with permission from Stauf, G.T. and Dowben, P.A. *Thin Solid Films* ***156*** 31. Copyright 1988 Elsevier.

Thomas and Park deposited films containing palladium crystallites of about 1000 Å in diameter homogenously suspended in an organic matrix via irradiation of CpPd(allyl) in the gas phase.[142] The depositions were carried out in a quartz cell at room temperature. The precursor vapor pressure was approximately 20 mTorr. A low-pressure mercury lamp emitting 254 nm photons was employed as the radiation source. The precursor has an absorption maximum at 252 nm suggesting a ligand-to-metal charge transfer band that should lead to the formation of elemental Pd or Pd radicals (Figure 45).[142] The illumination intensity at the substrate surface was 1.5 mW/cm^2. Films thick enough required for the activation of copper deposition were obtained after only 10 minutes of irradiation.

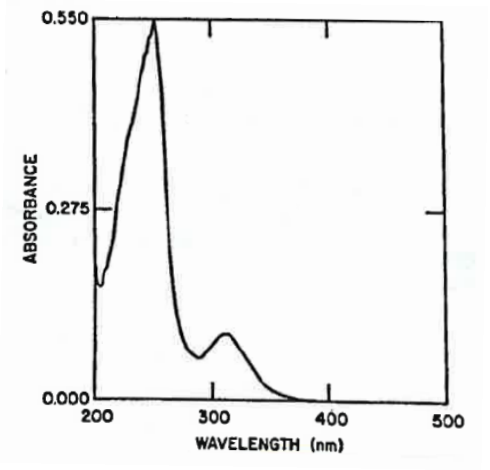

Figure 45. Absorption spectrum of gaseous CpPd(allyl).[142] Reproduced with permission from Thomas, R.R. and Park, J.M. *J. Electrochem. Soc.* ***136*** 1661. Copyright 1989 The Electrochemical Society.

The formation of a brown film was observed only on those parts of the substrate that were exposed to irradiation indicating a photolytic decomposition mechanism. A multi-photon process was discarded since sufficient photon flux was not available from the utilized light source. Figure 46 shows two possible schemes considered for the decomposition mechanism.[142] According to the first presumption, decomposition initiates by the absorption of a photon resulting in the formation of two unstable radical species. The palladium containing unit would further decompose leading to the formation of Pd(0) and a species formed by the coupled ligands. The more likely mechanism involves the formation of an excited state intermediate that would decompose after the adsorption.

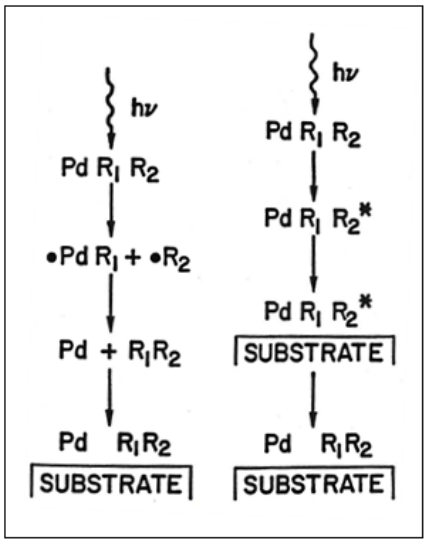

Figure 46. Proposed mechanisms for the photodecomposition of CpPd(allyl).[142] Reproduced with permission from Thomas, R.R. and Park, J.M. *J. Electrochem. Soc.* ***136*** 1661. Copyright 1989 The Electrochemical Society.

To conclude, palladium has been deposited by photochemical vapor deposition from $Pd(hfac)_2$ and CpPd(allyl). The photodecomposition of palladium precursors is an efficient way to activate electroless copper plating. Near contact masks could be utilized to produce patterns with high resolution on the 1 µm scale.

4.15 Silver

Silver can be employed in plasmonics to harness surface plasmons the properties of which can be modified via patterning of the surface.[143] Due to the exceptionally low resistivity of silver (1.59 µΩcm), it can be utilized in interconnects for microelectronics. LCVD enables the direct deposition of silver lines potentially simplifying the production of interconnects. The application of silver is restricted because of the chemical instability of the films that can, however, be improved by a protective barrier layer.

Itsuki *et al*. deposited silver thin films using (BTMSE)Ag(hfac) (BTMSE = bis(trimethyl-silyl)ethene) and a XeCl excimer laser emitting 308 nm photons.[144] Thermal CVD from the same precursor was also investigated. Several silver complexes with absorption at 308 nm

were synthesized but (BTMSE)Ag(hfac) exhibited the most promising properties in terms of thermal stability and vaporization. The depositions were carried out in a horizontal quartz CVD reactor. The conventional CVD process was investigated in the temperature region of 180–220 °C. With the aid of laser stimulation silver films could be deposited at lower temperatures of 80–220 °C. A mixture of argon and hydrogen was used as the carrier gas for both processes.

Figure 47 shows the growth rate of silver as a function of temperature by both thermal and laser CVD.[144] A growth rate of 3 nm/min was reached with both processes but a constant value was attained at a lower temperature when a laser was employed (120 °C versus 180 °C for the thermal process). Film formation in the LCVD process was observed already at a temperature of 80 °C but when only thermal activation was applied, a substrate temperature of 150 °C was required for the film growth.

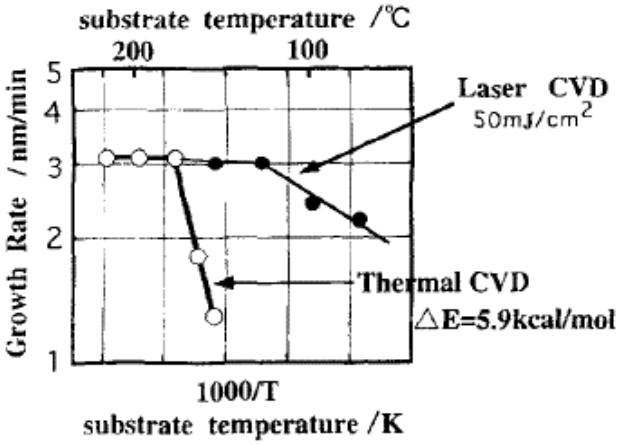

Figure 47. Growth rate of silver as a function of substrate temperature.[144] Reproduced with permission from Itsuki, A., Uchilda, H., Satou, M. and Ogi, K. *Nucl. Instrum. Methods Phys. Res., Sect. B* ***121*** 116. Copyright 1997 Elsevier.

Irradiation also had an effect on film morphology. Films deposited by thermal CVD consisted of irregularly distributed 1 mm granular islands. When laser activation was applied, particle size could be reduced down to 10 nm and the grains became uniformly distributed. However, even with laser CVD, the particle size increased to 1 mm at higher temperatures. The films deposited via laser CVD had less impurities compared to the thermal

CVD silver films (Figure 48).[144] The carbon and oxygen contents, for example, were reduced from ~10 at.% down to 3–5 at.%.

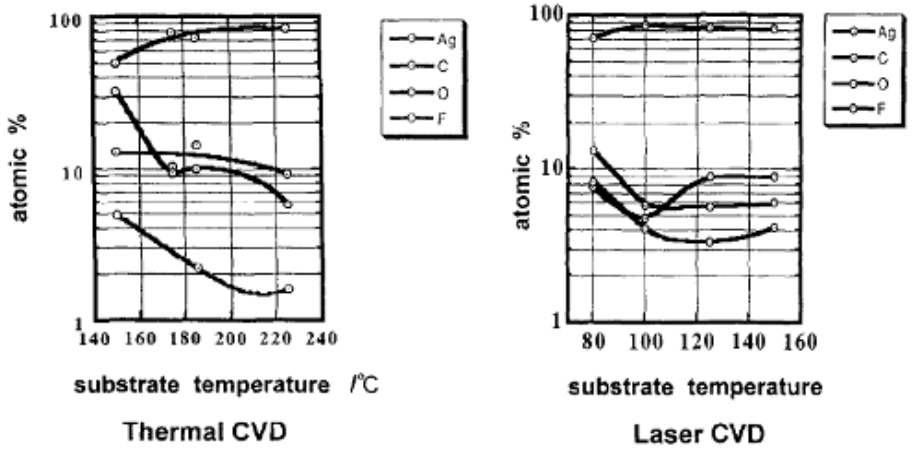

Figure 48. Impurity contents of silver thin films deposited by both thermal and laser CVD.[144] Reproduced with permission from Itsuki, A., Uchilda, H., Satou, M. and Ogi, K. *Nucl. Instrum. Methods Phys. Res., Sect. B* ***121*** 116. Copyright 1997 Elsevier.

The resistivity of the deposited silver films depended on film morphology and impurity contents. Values of the order of 10^{-3} Ωcm were achieved by conventional CVD (Figure 49).[144] However, with the aid of irradiation resistivity was reduced down to the order of 10^{-6} Ωcm being very close to the bulk value.

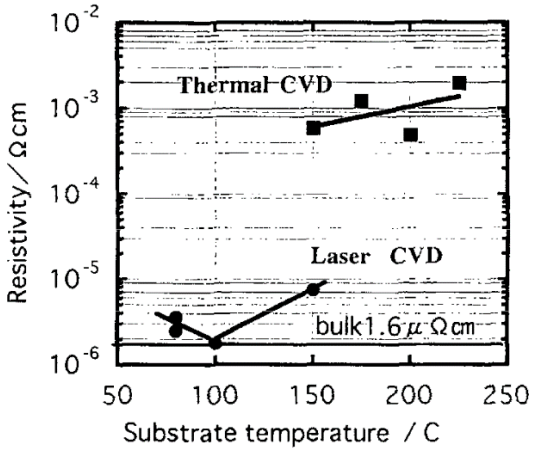

Figure 49. Resistivity of silver films deposited by both thermal and laser CVD as a function of temperature.[144] Reproduced with permission from Itsuki, A., Uchilda, H., Satou, M. and Ogi, K. *Nucl. Instrum. Methods Phys. Res., Sect. B* ***121*** 116. Copyright 1997 Elsevier.

In conclusion, silver thin films of improved purity and resistivity were deposited with LCVD using (BTMSE)Ag(hfac) as the precursor. Laser stimulation also enabled film formation at lower deposition temperatures with comparison to conventional CVD.

4.16 Cadmium

Alongside aluminum, cadmium was one of the very first materials deposited via LCVD.[50] Metallic cadmium is utilized as a photoresist material and for mask repair applications.[1] The LCVD of cadmium has been investigated only from dimethylcadmium (DMCd) the absorption spectrum of which is illustrated in Figure 50.[145]

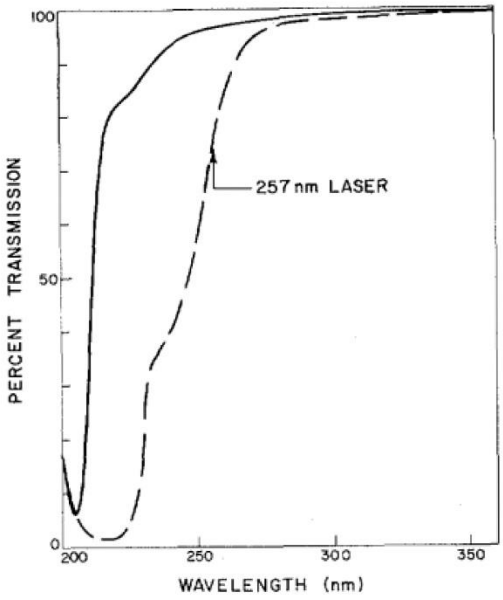

Figure 50. Absorption spectrum of DMCd (dashed line) and TMA vapor.[145] Reproduced with permission from Ehrlich, D.J., Osgood Jr., R.M. and Deutsch, T.F. *IEEE J. Quantum Electron.* ***16*** 1233. Copyright 1980 IEEE.

Deutsch *et al.* studied the LCVD process of cadmium from DMCd buffered with helium using a frequency-doubled Ar^+ laser emitting photons at 257.2 nm as well as a pulsed ArF excimer laser at 193 nm. No metal formation was observed without frequency doubling from 514.5 to 257.2 nm suggesting a photolytic growth mechanism. However, the use of a pulsed radiation source may cause localized hot spots on the surface at high enough energy densities

leading to a combination of both photolysis and pyrolysis. The effect of pyrolysis was amplified as the deposition proceeded and absorption increased along with the growing metal film. When using the cw Ar^+ laser, a modest temperature rise of only 5 °C was measured at the substrate. The linear dependence of the growth rate on both laser flux and precursor pressure is illustrated in Figure 51.[145] The low temperature and linear variation together indicate the process to occur by a photolytic gas-phase absorption mechanism.

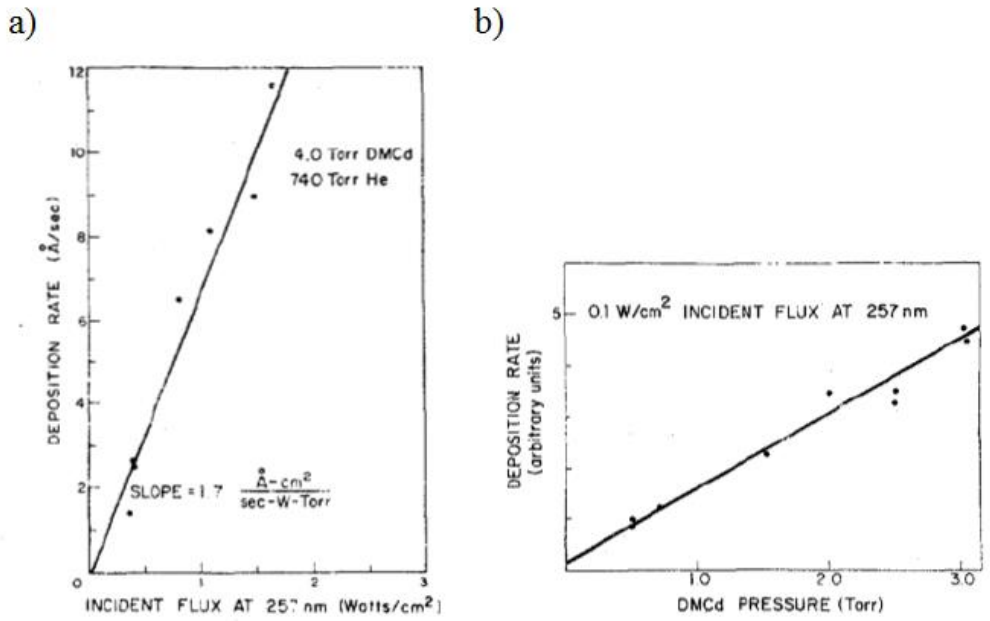

Figure 51. Deposition rate of cadmium as a function of a) laser flux and b) DMCd pressure.[145] Reproduced with permission from Ehrlich, D.J., Osgood Jr., R.M. and Deutsch, T.F. *IEEE J. Quantum Electron.* ***16*** 1233. Copyright 1980 IEEE.

Rytz-Froidevaux and coworkers deposited cadmium from DMCd by locally heating GaAs substrates with a Kr^+ laser operating at 520.8–568.2 nm. The depositions were carried out under hydrogen at atmospheric pressure. The precursor partial pressure was held at 0.14 Torr. Film formation occurred between laser powers of 70 and 300 mW translating into temperatures ranging from 235 to 1000 °C.

In summary, cadmium has been deposited by both photolytic and pyrolytic means using DMCd and radiation from different laser sources. Deposition rates together with the growth mechanisms have been speculated but little information is provided concerning film quality.

4.17 Tin

The first studies on the LCVD of tin thin films were carried out by Deutsch *et al.* using $Sn(CH_3)_4$ and a frequency-doubled Ar^+ laser (257.2 nm).[50] The same precursor was also utilized by Mingxin and coworkers who carried out their depositions using an Ar^+ laser at 514.5, 454.5, and 257.3 nm (frequency-doubled) as well as a mercury lamp at 253.7 nm.[146] Due to the temperature gradients at the substrate and the low melting point of tin, the laser deposited films were non-uniform consisting of different areas: a sputtering zone, a melting zone, and a crystallized zone. The deposition rate was linearly dependent on the precursor vapor pressure and the laser intensity. The tin films deposited with the mercury lamp appeared uniform and adhesive. The growth rate was measured to be 0.1 Å/s.

Braichotte and van den Bergh employed an Ar^+ laser at 514.5 and 257.3 nm in their depositions.[147,148] The tin films were deposited at room temperature, and the $Sn(CH_3)_4$ vapor pressure was held at 30 Torr. For the films deposited pyrolytically at a wavelength of 514.5 nm, the average particle size was found to increase as a function of increasing irradiation time and laser power density. No film formation was observed at power densities below 20 kW/cm^2. At high laser intesities, volcano-type growth occurred due to the significant temperature increase at the center of the laser beam leading to evaporation of the deposited material. The photolytic growth of tin was obtained at 257.3 nm and at a laser power density of as low as 0.5 kW/cm^2. Contrary to the pyrolytic deposition process, the films grown via photodissociation of $Sn(CH_3)_4$ were homogeneous and amorphous.

Weigmann *et al.* applied the photodissociation of $Sn(CH_3)_4$ at 257.3 nm for the repair of gold masks utilized in x-ray lithography.[149] As a low-temperature process, the LCVD of tin was considered a promising method since excess heating of the mask would result in changes in the internal stress and consequent deformation of the electroplated gold layer. To avoid excess heating, low laser powers between 2 and 4 mW were used. At first, a modest growth rate of 50 Å/s was recorded; however, an increase of one order of magnitude was observed with the addition of a carrier gas. AES measurements revealed a metal content of about 90 %. No carbon was detected but an oxygen content of 10 %, most likely originating from the impurities present in the precursor, was measured.

To conclude, only a handful of reports on the LCVD of tin exist. The deposited films exhibited uneven morphology including separate zones and volcano-type growth, low growth rates, as well as high impurity contents.

4.18 Tungsten

Tungsten is a hard metal with the highest melting point of all metals (3410 °C), and it is relatively inert even at high temperatures.[1] Tungsten films are utilized e.g. as coatings against wear and corrosion as well as for microelectronic applications like gate metallization, diffusion barriers, ohmic contacts, and interconnects. The photo-CVD of tungsten has been studied using only two precursors: $W(CO)_6$ and WF_6. The use of $W(CO)_6$ produces films with a high degree of carbon and oxygen resulting in high resistivities. WF_6 provides better quality but requires a reducing agent such as H_2 or SiH_4. Fang *et al.* deposited tungsten by photo-CVD using WF_6 and Hg vapor sensitization, a topic not assessed further in this thesis.[150]

$W(CO)_6$ is by far the most studied precursor for the LCVD of tungsten.[44,86,89,91,92,110,130,133–135,151–156] Analogous to both $Cr(CO)_6$ and $Mo(CO)_6$, similar trends could be observed in tungsten deposition. Solanki *et al.* investigated the process at room temperature using a number of different wavelengths and observed the highest deposition rate of 170 nm/min at 248 nm.[89] As shown in Figure 52, $W(CO)_6$ absorbs strongly at around 230 nm.[82] Using an Ar^+ laser operating at 350–360 nm and a laser power of 60 mW, Gilgen *et al.* measured a tungsten growth rate of 2100 nm/min on glass and 1080 nm/min on GaAs.[130] These results differ vastly from the ones reported by Solanki *et al.* and can be explained by pyrolysis; namely, a laser power of 60 mW induced a temperature of 700 and 300 °C on glass and GaAs, respectively. The high laser power generated lines with a resistivity of twice the bulk value of 5.3 μΩcm. In contrast, the films deposited by Solanki and coworkers were contaminated with oxygen (< 7 %) and carbon (0.7 %) resulting in a resistivity of 20 times the bulk value, at best. Although, the purity obtained by Solanki *et al.* was fairly good when compared to some other reports. For instance, Jackson and Tyndall determined a tungsten content of only 36 at.% when using a frequency-doubled Ar^+ laser operating at 257 nm and a power of 15 mW.[152] A conclusion can be drawn that photolysis is inadequate for the complete removal of the carbonyl ligands and in order to produce high quality deposits,

pyrolytic means are required. According to Houle and Singmaster, a surface temperature of only ~180 °C is sufficient to produce pure metal deposits once the deposition has proceeded from nucleation to a steady growth regime.[156]

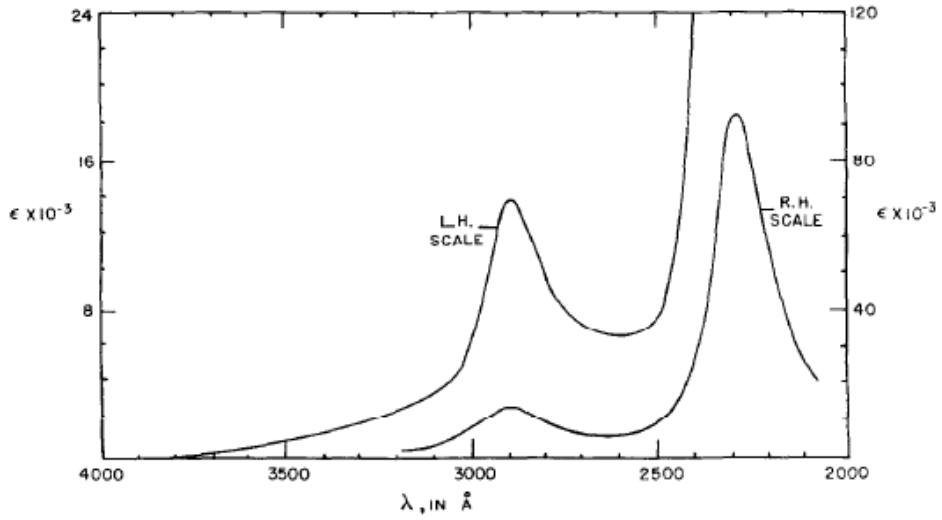

Figure 52. Absorption spectrum of $W(CO)_6$ in cyclohexane solution. (L.H. = left hand scale, R.H. = right hand scale).[82] Reproduced with permission from Alderdice, D.S. *J. Mol. Spectrosc.* ***14*** 509. Copyright 1965 Elsevier.

Liu and coworkers studied the photo-CVD of tungsten using the WF_6/Si system.[157] Tungsten lines were deposited on silicon substrates by the surface reduction of WF_6 vapor at room temperature (Equation 12).

$$2\ WF_6\ (g) + 3\ Si\ (s) \rightarrow 2\ W\ (s) + 3\ SiF_4\ (g) \qquad (12)$$

An Ar^+ laser beam was focused to a spot size of ~20 μm.[157] The precursor vapor pressure was varied from 50 to 100 Torr, and argon was used as a buffer gas. The deposition mechanism was essentially similar to thermal CVD, only a laser was utilized to locally heat the substrate. Line widths of 3 μm could be obtained depending on the applied laser power and scan speed. The film thickness was approximated at 200 Å. Similar to thermal CVD, the process was self-terminating and surface selective. Analyses showed WSi_2 formation in the

center portion of the lines suggesting the presence of hot spots with temperatures above 600 °C.

In order to obtain thicker films than restricted by the self-limiting growth mechanism of the WF_6/Si system, another reducing agent is required. Most of the research has focused on the WF_6/H_2 system using either an ArF excimer laser or an Ar^+ laser at 193 and 514 nm, respectively.[158–168] The mechanism for the thermal CVD process is depicted in Equation 13.

$$WF_6\,(g) + 3\,H_2\,(g) \rightarrow W\,(s) + 6\,HF\,(g) \qquad (13)$$

Deutsch *et al.* along with Sinke's group were able to deposit pure tungsten on SiO_2 by photon activation using 193 nm from an ArF laser.[158,162] Deutsch and coworkers observed no film formation without irradiation at temperatures below 440 °C. According to Sinke's group, H_2 is not dissociated on SiO_2, and atomic H required for the deposition is formed only by irradiation as depicted in Equations 14 and 15.[160,162]

$$WF_6 + h\nu \rightarrow WF_5 + F \qquad (14)$$

$$F + H_2 \rightarrow H + HF \qquad (15)$$

Deutsch *et al.* observed tungsten deposition on SiO_2 already at 240°C, but good adhesion was obtained only at temperatures above 440 °C.[158] The experiments were carried out at a laser power ranging from 4 to 7 W and a repetition rate of 50 Hz. Irradiation was used to reduce the activation energy of the process from 18 kcal/mol to only 9.7 kcal/mol. Along with enabling deposition on SiO_2, the deposition rate was significantly increased as opposed to thermal CVD (Figure 53).[158]

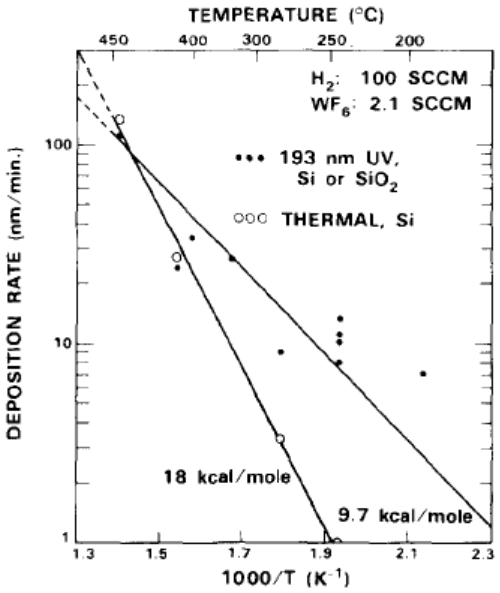

Figure 53. Deposition rate of both photolytic and thermal tungsten CVD from WF_6 and H_2 as a function of temperature.[158] Reproduced with permission from Deutsch, T.F. and Rathman, D.D. *Appl. Phys. Lett.* ***45*** 623. Copyright 1984 AIP Publishing LLC.

Deutsch *et al.* measured a resistivity of 17 μΩcm for a film deposited at 440 °C.[158] As shown in Figure 54, the phase of tungsten changes when the temperature is increased.[158] Higher deposition temperatures produce α-W consisting of large crystallites and thus less grain boundaries explaining the drastic decrease in resistivity with increasing temperature. Similar results with respect to phase change were also obtained by Mogyorósi and Carlsson who studied the LCVD of tungsten on silicon using the WF_6/H_2 system and an ArF laser at 193 nm.[163] For a film deposited at 350 °C, a resistivity of as low as 8 μΩcm was measured. The deposition rate increased linearly with increasing WF_6 partial pressure. The deposition rate increased also with increasing hydrogen partial pressure but only to a molar ratio of WF_6/H_2 1:40. The photolytic contribution independent of substrate temperature was estimated at 80–100 Å/s. The activation energy for the combined thermal and photolytic process was approximated at 16 kcal/mol. In this analysis, the low-temperature depositions arising solely from photolysis were excluded explaining the contrast with the low value of 9.7 kcal/mol determined by Deutsch *et al*.

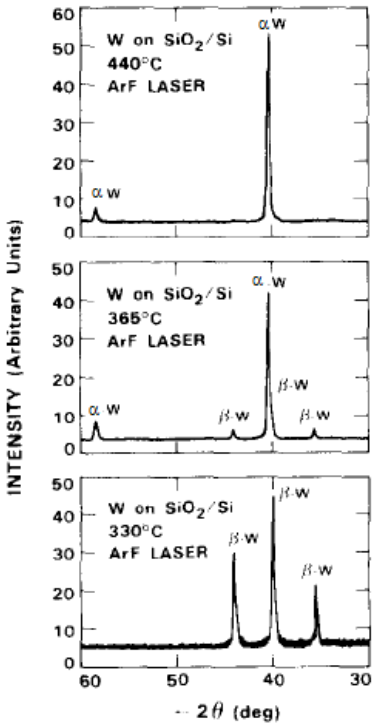

Figure 54. X-ray diffractograms of LCVD tungsten deposited at different temperatures.[158] Reproduced with permission from Deutsch, T.F. and Rathman, D.D. *Appl. Phys. Lett.* ***45*** 623. Copyright 1984 AIP Publishing LLC.

The LCVD of tungsten using the WF_6/H_2 system was studied also by several other groups, but in these cases deposition was achieved via pyrolysis using an Ar^+ laser either at 488 or at 514 nm.[159,161,164–166] High quality deposits were obtained without detectable amounts of impurities resulting in low resistivities of 13 μΩcm.

If it is necessary to avoid the formation of corrosive HF, SiH_4 can be utilized to reduce WF_6 into metallic tungsten as depicted in Equation 16. No HF was detected at temperatures below 600 °C.[169] Another advantage of the WF_6/SiH_4 system is the lower operating temperature enabling the use of thermally sensitive substrates.

$$2\ WF_6\ (g) + 3\ SiH_4\ (g) \rightarrow 2\ W\ (s) + 6\ H_2\ (g) + 3\ SiF_4\ (g) \qquad (16)$$

The photo-CVD of tungsten using the WF_6/SiH_4 system was first introduced by Black *et al.*[169] An Ar^+ laser operating at a wavelength of 488 nm and a power of 30–60 mW was utilized to induce local heating of polyimide coated silicon. A temperature of 150 °C was sufficient for the initiation of deposition. For safety measures, the reactants were diluted with argon adding up to a total pressure of 380 Torr. The film composition could be controlled by varying the reactant gas ratio. By increasing the amount of WF_6 to at least twice the amount of SiH_4, pure tungsten deposits were obtained, and the formation of WSi_2 was circumvented. At a scan speed of 300–400 μm/s, a resistivity of 12 μΩcm was measured. Meunier and colleagues also utilized the WF_6/SiH_4 system but instead of pure tungsten, their goal was to deposit WSi_x.[161,164]

In summary, the LCVD of tungsten has been studied using either $W(CO)_6$ or WF_6 as the precursor. As per usual, the films deposited using the hexacarbonyl precursor were highly contaminated, and low resistivities were obtained only via pyrolysis. The use of WF_6 produced deposits of better quality but required the presence of a reducing agent.

4.19 Iridium

Due to its chemical stability, iridium has several applications including microchannel and Freznel zone plates in X-ray optics, inductive grid filters for IR rejection, catalysis, as well as diffusion barriers and seed layers for copper electrodeposition.[170]

Cohan *et al.* have developed an LCVD process for the deposition of iridium thin films using $CpIr(C_2H_4)_2$ as the metal precursor.[139] The films were deposited in a glass cell with a quartz window under an atmosphere of H_2 and He. The glass cell was kept at room temperature and atmospheric pressure. The substrate was irradiated with a XeCl excimer laser operating at 308 nm. The laser frequency was 20 Hz, and the beam was focused to a circular area with a diameter of 1 cm. The wavelength response of the precursor was not studied since the absorption spectrum showed only one broad peak at 270 nm. The precursor was fed into the system simultaneously with irradiation for 20 minutes, after which a mirror-like iridium film had formed on glass and quartz, and a yellowish film on silicon was observed. Irradiation was continued after the deposition for another 20 minutes in order to remove all the Cp units from the surface. The deposited films were of high purity since no carbon contamination was

detected in the XPS measurements. Figure 55 represents the X-ray diffractogram of the iridium sample.[139] The peaks at 2θ = 41° and 47° indicate crystallinity of the film.

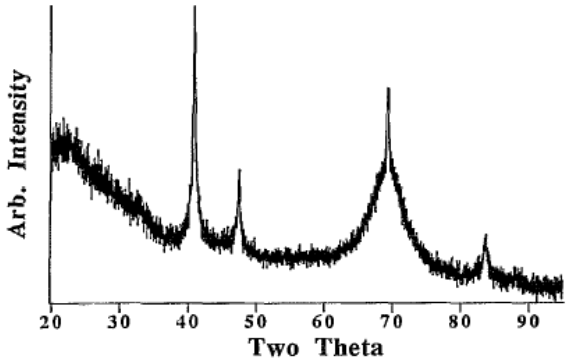

Figure 55. X-ray diffractogram of iridium deposited from $CpIr(C_2H_4)_2$. The intense peak at 2θ = 70° corresponds to the silicon substrate.[139] Reproduced with permission from Cohan, J.S., Yuan, H., Williams, R.S. and Zink, J.I. *Appl. Phys. Lett.* ***60*** 1402. Copyright 1992 AIP Publishing LLC.

4.20 Platinum

On the grounds of its chemical inertness, platinum is an attractive metal for metallic contacts in integrated circuits and for anticorrosion layers. In addition, platinum is suitable for silicide formation. The photo-CVD of platinum has mainly revolved around $Pt(hfac)_2$ but studies involving $Pt(PF_3)_4$ and Cp complexes have also been published.[130,146–148,171–179]

Van den Bergh has published a comprehensive set of studies on the deposition of platinum films from $Pt(hfac)_2$.[146–148,172,173,175,176,178] The depositions were carried out using an Ar^+ laser at 257.3 (frequency-doubled), 351–363, 458, and 514.5 nm as well as a mercury lamp at 253.7 nm. As can be depicted from Figure 56, the absorption of $Pt(hfac)_2$ vapor has a maximum at ~260 nm but extends up to wavelengths of 500 nm.[178]

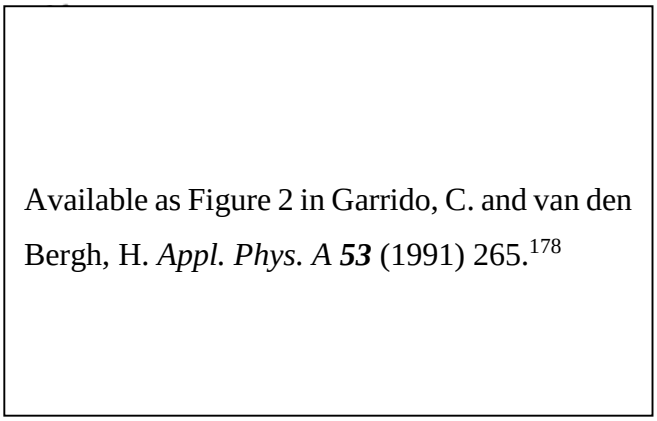

Figure 56. Absorption spectrum of $Pt(hfac)_2$ vapor.[178]

Van den Bergh investigated both the photolytic and pyrolytic LCVD of platinum and observed interesting trends regarding the line dimensions. In the pyrolytic process (at wavelengths of 458 and 514 nm), the line height increased linearly with both increasing precursor vapor pressure and laser power (Figure 57).[172] The line width, however, increased only with increasing laser power and remained more or less constant even if the precursor vapor pressure was increased. Hence, the most efficient way to produce high yet narrow lines is to increase the $Pt(hfac)_2$ vapor pressure rather than the laser power.

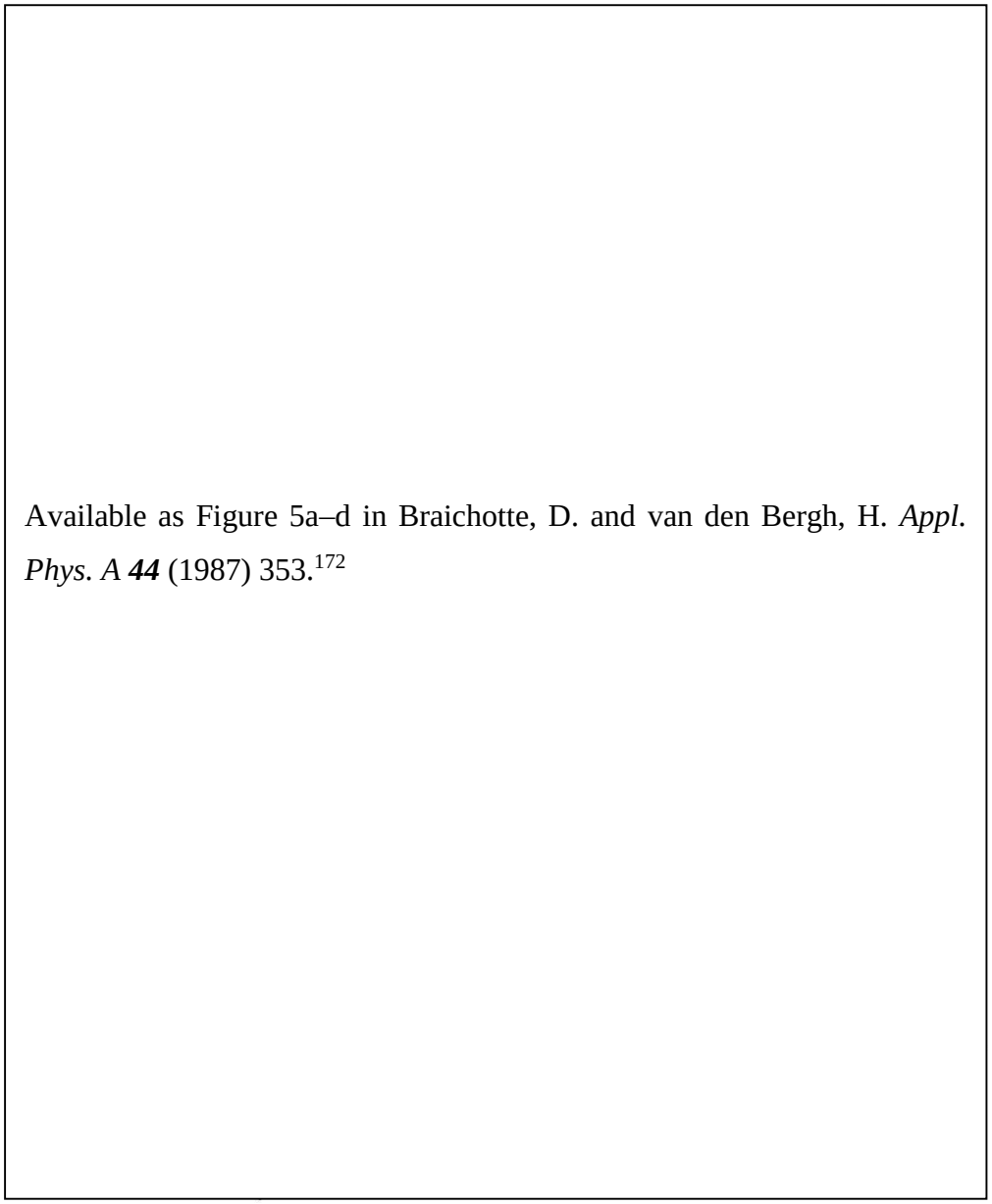

Figure 57. Platinum stripe a) height and b) width as a function of precursor vapor pressure as well as c) height and d) width as a function of laser power.[172]

In the photolytic process at 351–363 nm, three growth regimes can be distinguished (Figure 58).[175] At low laser powers, the growth is dominated by surface adlayer photolysis. At intermediate laser powers, desorption of the adlayer increases causing a decrease in the deposition rate. Between laser powers of 5 and 100 mW, the deposition rate increases again because the deposition occurs by gas-phase photolysis and is no longer affected by

desorption of the adlayer. Once the transmission of the deposit drops below 80 %, absorption increases drastically causing a temperature rise inducing pyrolysis.

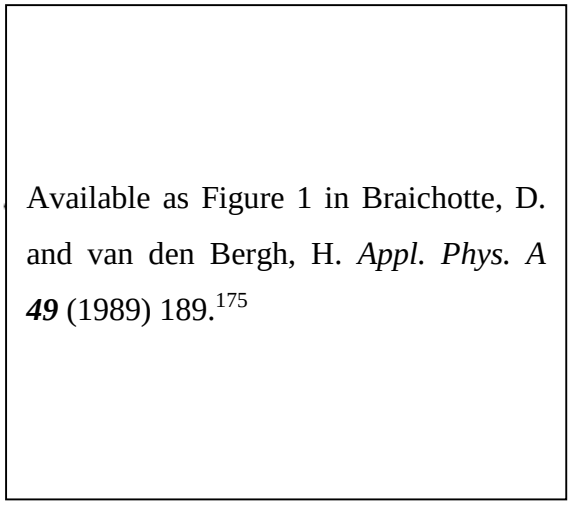

Figure 58. Platinum deposition rate as a function of laser power at different transmissions.[175]

In the wavelength region of 351–363 nm, a vapor pressure of ~0.1 Torr, a substrate temperature of 95 °C, and a laser power below 110 mW, AES measurements showed a film composition of 96 % Pt with a presence of carbon and oxygen impurities. At laser powers above 110 mW, the film composition was essentially 100 % platinum once the deposition process had proceeded from the initial photolytic stage to the pyrolytic stage. Figure 59 shows the resistivity ratio as a function of laser power for a set of $Pt(hfac)_2$ vapor pressures at a writing speed of 2 μm/s.[176] At high enough laser powers, the deposition process changes from photolytic to pyrolytic. A high enough temperature is required for obtaining smooth lines, but too high temperatures cause evaporation of the deposited material deteriorating line morphology, thereby increasing the resistivity.

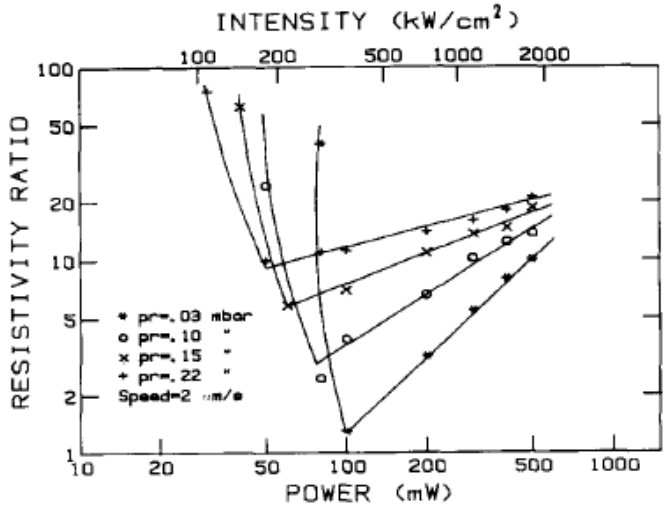

Figure 59. Resistivity ratio as a function of laser power at a number of precursor vapor pressures and a writing speed of 2 µm/s.[176] Reproduced with permission from Garrido, C., Braichotte, D., van den Bergh, H., Leon, B. and Pérez-Amor, M. *Appl. Surf. Sci.* ***43*** 68. Copyright 1989 Elsevier.

Gilgen *et al.* also employed $Pt(hfac)_2$ to deposit platinum lines using an Ar^+ laser emitting 350–360 nm photons.[130] The laser power density was varied from 0.15 to 1 MW/cm^2. The precursor was heated to 90 °C corresponding to a vapor pressure of 0.3 Torr. The reaction cell was heated to 110 °C in order to avoid condensation. Due to the well-defined line dimensions, the authors suspected the deposition to proceed via a layer of precursor adsorbed on the substrate surface. The high quality of the lines was attributed to the low deposition rates of 1–2 nm/s facilitating the removal of impurities. Furthermore, the inertness of platinum inhibits the formation of oxides, carbides, or other stable compounds that might be incorporated into the deposits. The deposited lines exhibited low resistivities of approximately twice the bulk value of 10.6 µΩcm.

Schröder and coworkers studied the reaction pathway of UV-induced platinum deposition from $Pt(PF_3)_4$.[171] 248 nm radiation from a pulsed KrF laser was applied perpendicularly to various substrates. The laser fluence was varied from 10 to 200 mJ/cm^2. The $Pt(PF_3)_4$ vapor pressure was held at about 0.5 Torr. Irradiation of the substrate was proposed to generate electrons that are captured by the precursor molecules initiating their dissociation. $Pt(PF_3)_3^-$ fragments diffuse in vapor phase and adsorb on the surface where the decomposition process is completed. The substrate was found to have a significant impact on the deposition rate,

decreasing in the order of: Si > Al > C > SiO_2 > Cu. At a laser fluence of 200 mJ/cm^2, 0.6 monolayers of material was deposited on aluminum per pulse. Thermal decomposition of $Pt(PF_3)_4$ requires a temperature of ~130 °C. Since the temperature rise of e.g. aluminum at 100 mJ/cm^2 was calculated at 120 °C, thermal contribution to the process is not to be omitted altogether. However, taking into account the short duration of a single pulse, the surface is rapidly cooled and the process was suspected to be essentially photolytic.

$Pt(PF_3)_4$ was also utilized by Shaver *et al.* who investigated the modification and repair of integrated circuits.[179] An Ar^+ laser operating at 488 nm and a power of 50 mW was focused to a ~1 µm spot size. The precursor vapor pressure was maintained at 5 Torr. Typically, lines were deposited at a writing rate of 250 µm/s and were of 5 µm width and 1 µm thickness. On polyimide, however, writing rates up to 5 mm/s were utilized. Resistivities equal to the bulk value (10–11 µΩcm) were obtained. Furthermore, good step coverage was achieved without excessive damage to the underlying material.

Koplitz *et al.* deposited platinum from $CpPtMe_3$ on various substrates using 308 nm radiation from a XeCl excimer laser as well as 351 and 364 nm radiation from an Ar^+ laser.[174] The excimer laser emitted radiation at a power of 2.6 mJ/pulse and a frequency of 10 Hz focused to a 1 mm radius spot. The Ar^+ laser was operated at 4–5 mW/mm^2. Depositions were carried out at room temperature and atmospheric pressure. The precursor was heated to 56 °C resulting in a vapor pressure of ~0.33 Torr. The precursor was transported to the substrate in a mixture of argon and hydrogen. Shiny deposits at a growth rate of 100 Å/min were obtained only in the presence of hydrogen. Without hydrogen the films appeared black. No film formation was observed at visible wavelengths of 488 and 514 nm indicating the process to be of photochemical nature. AES measurements showed the shiny deposits to be almost free of impurities, but a carbon content of approximately 20 at.% was detected in the black films produced without hydrogen. The shiny films exhibited good adhesion properties unlike the black deposits that were easily removed in the tape test. According to XRD, the shiny deposits are a mixture of crystalline and amorphous platinum (Figure 60).[174] Figure 61 shows scanning electron microscope (SEM) images from the surface of both shiny and black deposits.[174] The shiny films appear smooth and continuous whereas the black deposits show cauliflower-like structure.

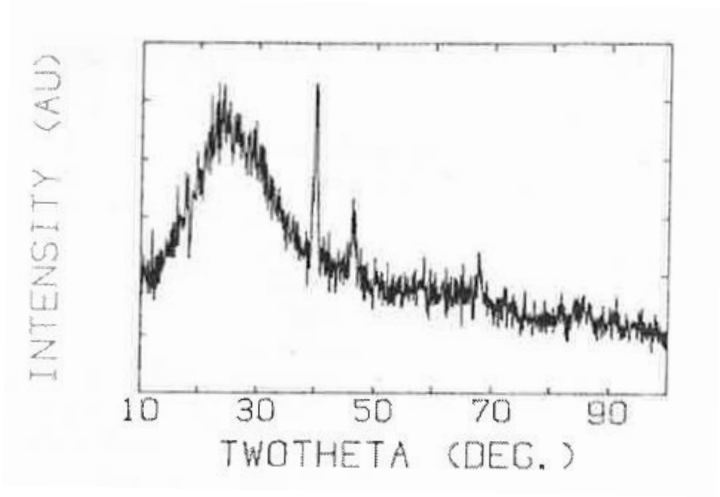

Figure 60. X-ray diffractogram of a shiny Pt film showing peaks at 39.7°, 46.2°, and 67.4° as well as a broad peak at 20–30°.[174] The substrate was either glass, fused silica, sapphire, Si, or GaAs. Reproduced with permission from Koplitz, L.V., Shuh, D.K., Chen, Y.-J., Williams, R.S. and Zink, J.I. *Appl. Phys. Lett.* ***53*** 1705. Copyright 1988 AIP Publishing LLC.

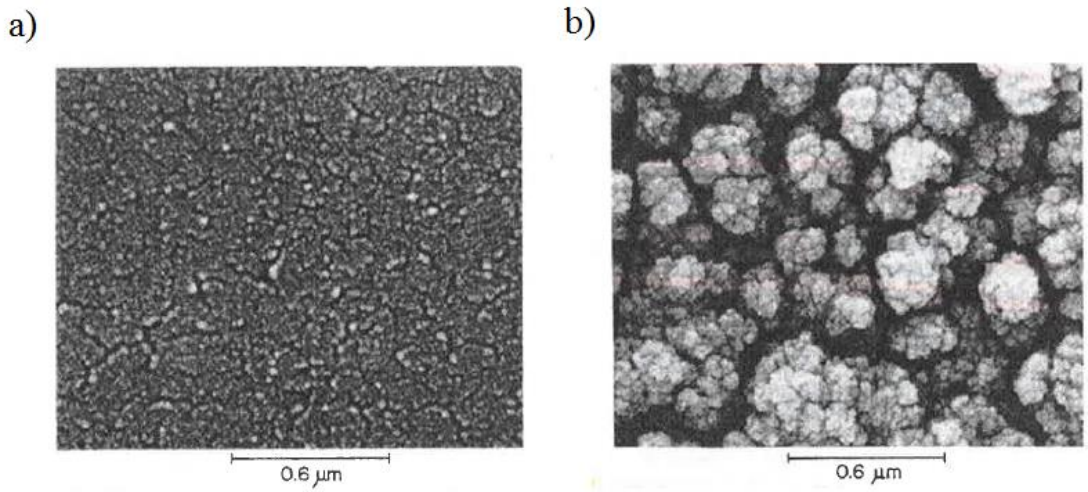

Figure 61. SEM image of a) a shiny and b) a black platinum deposit.[174] Reproduced with permission from Koplitz, L.V., Shuh, D.K., Chen, Y.-J., Williams, R.S. and Zink, J.I. *Appl. Phys. Lett.* ***53*** 1705. Copyright 1988 AIP Publishing LLC.

The LCVD of platinum from a Cp complex was also studied by Rooney *et al*. whose attempt was to develop transparent platinum electrodes using CpPt(allyl) and a XeCl laser at 308 nm.[177] Photon pulses of 20 mJ energy were directed to a rectangular area of 1.4 × 0.6 cm

at a repetition rate of 10 Hz. The depositions were carried out at a temperature of ~57 °C resulting in a precursor vapor pressure of about 0.2 Torr. Film formation was observed only on areas exposed to irradiation. The deposits exhibited high carbon contents that could be reduced by annealing in air at ~550 °C. For a film of 300–400 Å thickness, the composition was changed from 10 % Pt, 90 % C to 70 % Pt, 30 % C upon annealing. Annealing was also important for improving film properties such as resistivity. For a 550 Å film with a carbon content of 40 %, a resistivity of 72 $\pm$ 12 mΩcm was measured.

The LCVD of platinum has been studied from $Pt(hfac)_2$, $Pt(PF_3)_4$, $CpPtMe_3$, and CpPt(allyl). By varying the deposition parameters, such as laser power, precursor vapor pressure, and writing speed, the line dimensions could be quite accurately controlled using the $Pt(hfac)_2$ process. Apart from some anomalies, such as the CpPt(allyl) process, impurity levels were low and resistivities close to bulk were measured.

4.21 Gold

The LCVD of gold has been primarily studied for selective metallization and direct circuit repair without having to utilize masks or lithography techniques. The investigated precursors include $Me_2Au(acac)$ and its fluorinated derivatives as well as methyl and trimethyl(trialkylphosphine) complexes.[180–191] Alongside new processes for gold deposition, these studies provided data supporting theoretical models on LCVD surface chemistry in general.

Baum *et al.* investigated the LCVD of gold using $Me_2Au(acac)$ and radiation at 193, 248, 308, and 514 nm obtained from ArF, KrF, and XeCl excimer lasers as well as an Ar^+ laser, respectively.[180–182] All depositions were carried out at room temperature providing a precursor vapor pressure of ~9 mTorr. At 514 nm, gold was formed at laser power densities above 9×10^4 W/cm^2. At 4×10^5 W/cm^2, a growth rate of 1 µm/s was measured. After an initial nucleation phase, the film thickness increased linearly with time. By increasing the temperature to 43 °C, the growth rate increased by an order of magnitude due to the increased vapor pressure of the precursor. The addition of a buffer gas (argon) produced deposits at a lower rate due to limited diffusion. The presence of a buffer gas also induced volcano-type growth supposedly due to collisional cooling, deactivation of the activated fragments, and

changes in the sticking coefficient of the precursor. The line composition was determined as 97 at.% gold, 2.3 at.% carbon, and 0.7 at.% oxygen. A resistivity of ~10 μΩcm was obtained at the lowest being about 4 times the bulk value of 2.44 μΩcm. The lower the scan rate, the lower the resistivity showing a systematic correlation between film quality and temperature. High scan rates were proposed to cause more structural defects which could be eliminated by annealing. Since the annealing atmosphere was of no importance, the resistivity improvement was attributed to the coalescence of metal grains. Final resistivities were usually 2–3 times the bulk value. The photolytic approach using UV radiation produced lines with higher impurity contents. The highest gold content of 76 at.% was obtained at 248 nm. The gold content of lines deposited at 193 and 308 nm was below 30 at.%.

Kodas and coworkers deposited gold at room temperature using $Me_2Au(hfac)$ as the precursor and an Ar^+ laser operating at 514 nm as the irradiation source.[183,185–187] At precursor vapor pressures of both 0.35 and 0.11 Torr, the vertical deposition rate was independent of the applied laser power ranging from 100 to 1000 mW. The growth rate increased linearly with increasing precursor vapor pressure. The growth rate decreased in the presence of a buffer gas due to limited transport of the precursor to the substrate surface. The shape of the deposit was also strongly influenced by the type and partial pressure of the buffer gas. The gold content of these photothermally grown deposits was over 95 at.%. Dagata *et al.* examined the photochemistry of adsorbed $Me_2Au(hfac)$ employing a KrCl excimer laser operating at 222 nm.[184] Desorbing photoproducts were determined using time-of-flight electron ionization mass spectrometry (TOF-EI-MS). The deposition was found to initiate by dissociation of the precursor into Me_2Au and hfac fragments followed by successive loss of the methyl groups. The hfac ligand was observed to recombine with the methyl radicals on the substrate surface.

Jubber *et al.* studied the pyrolytic LCVD of gold from $MeAu(PEt_3)$.[188,189] 514 nm radiation from an Ar^+ laser was focused to a spot size of 12 μm. The depositions were carried out at room temperature (27 °C) resulting in a precursor vapor pressure of about 5 mTorr. At a scan rate of 4.5 μm/s, a laser power density of at least 0.8 MW/cm^2 was required for visible film formation. A too high power density (above 2 MW/cm^2) resulted in irregularities in the line morphology. EDS showed a high gold content of over 98 % correlating with the low resistivity of ~4 μΩcm, independent of the laser power.

Reminiscent of Jubber's experiments, Suhr's group investigated the LCVD of gold using $MeAu(PMe_3)$, $Me_3Au(PMe_3)$, and $Me_3Au(PEt_3)$ combined with 514 nm radiation from an Ar^+ laser.[190,191] The complexes do not absorb light at the applied wavelength, which refers to a process relying solely on the localized heating of the substrate accomplished with the laser. The deposition temperatures were varied in the range of 32–75 °C depending on the evaporation properties of the precursor. The stripe heights and widths varied from 0.1 to 1 µm and from 40 to 160 µm, respectively. The deposition rate increased with increasing laser power and decreasing writing speed. The use of a buffer gas led to decreased deposition rates and irregularities in morphology. In the case of $Me_3Au(PMe_3)$, the deposition rate increased linearly with increasing temperature. A decrease was observed with $MeAu(PMe_3)$ caused by decomposition of the precursor at temperatures above 50 °C. The deposition rate from $MeAu(PEt_3)$ decreased abruptly at 65 °C, which was assigned to a possible change in the decomposition pathway. Resistivities ranging from 1.5 to 7 times the bulk value were obtained using all three precursors. The deposits were of high quality almost regardless of the deposition parameters indicating high adaptability of the processes.

Gold stripes from a variety of precursors, including $Me_2Au(acac)$, $Me_2Au(hfac)$, and $Me_3Au(PMe_3)$, have been deposited by LCVD. Pyrolytic deposition employing an Ar^+ laser at 514 nm produced lines of high purity with resistivities close to the bulk value. The photolytic approach at 222 nm produced highly contaminated deposits and thus high resistivities which could, however, be decreased by annealing.

4.22 Lead

The photo-CVD of lead has been investigated from $PbEt_4$ by both Chiu *et al.* and Rigby.[192,193] Both groups carried out their experiments at room temperature. Lead thin films have little use as such but can be converted to e.g. lead chalcogenides utilized in optoelectronic applications. The absorption spectrum of $PbEt_4$ vapor is presented in Figure 62.[192]

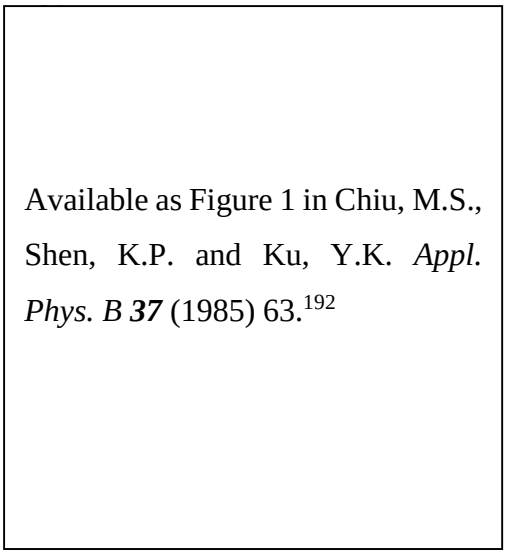

Figure 62. Absorption spectrum of $PbEt_4$ vapor.[192]

The first report on photodeposition of metallic lead from $PbEt_4$ vapor was published in 1968 by Rigby.[193] The experiments were carried out using UV radiation either from a 200 W short arc Wotan lamp (wavelength not reported) or a 6 W low pressure mercury arc lamp operating at 253.7 nm. The films were deposited at room temperature, and the precursor vapor pressure was maintained at 0.24 Torr. The deposition was observed to be driven by a gas-phase reaction followed by a secondary photolytic surface reaction. Oxygen was utilized to improve the growth rate by a secondary surface route and also to decrease the degree of film contamination. With the addition of oxygen, the carbon content was decreased from 30 at.% down to 5 at.%. The oxygen content was below 1 at.%.

Chiu *et al.* employed a frequency doubled Ar^+ laser operating at 257.3 nm to investigate the room temperature deposition of lead from $PbEt_4$. As depicted in Figure 63, the deposition rate increased linearly with increasing precursor vapor pressure and light intensity.[192] In contrast, the deposition rate decreased with increasing helium pressure due to the suppression of diffusion of the precursor molecules. At an intensity of 470 W/cm^2 and a $PbEt_4$ vapor pressure of 1.5 Torr, the deposition rate was measured to be 24 Å/s on quartz.

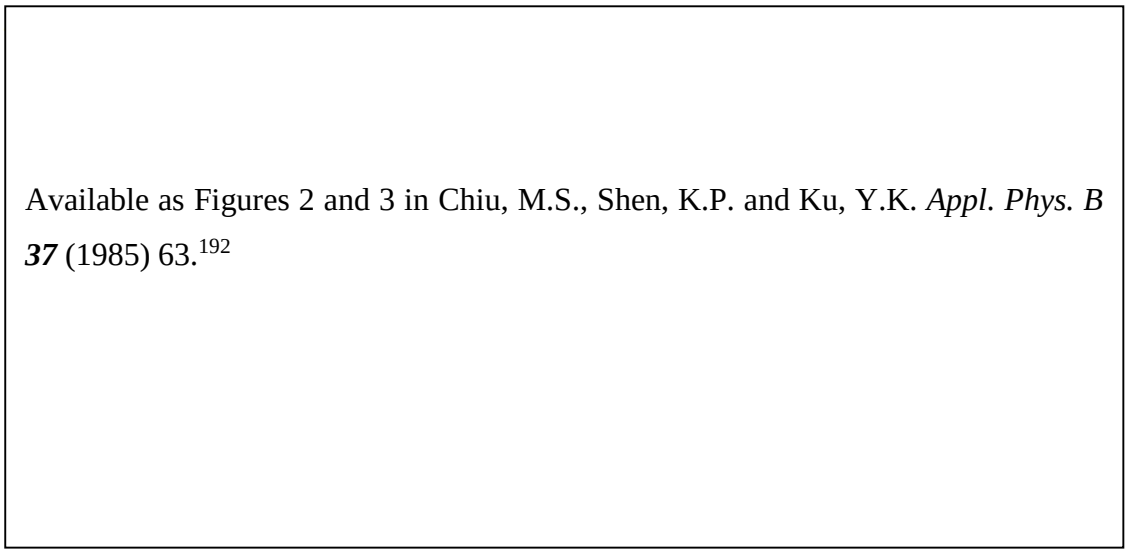

Figure 63. Deposition rate of lead as a function of a) $PbEt_4$ pressure and b) light intensity.[192]

5 Photo-assisted atomic layer deposition

5.1 Fundamentals of atomic layer deposition

The ALD method, which is a modification of the CVD technique, has been of great interest since the 1970s when it was first introduced and patented for depositing high-quality ZnS films and dielectric materials for electroluminescent displays.[194,195] ALD relies on sequential precursor pulses which are separated by gas purges in order to remove excessive precursor molecules and possible by-products from the reactor.[2–6] The deposition of material continues in a cyclic manner (Figure 64) where ideally each cycle produces one monolayer of material.[196] However, in practice one deposition cycle produces less than a monolayer of thin film material due to steric hindrances or a limited number of reactive sites such as hydroxyl groups.

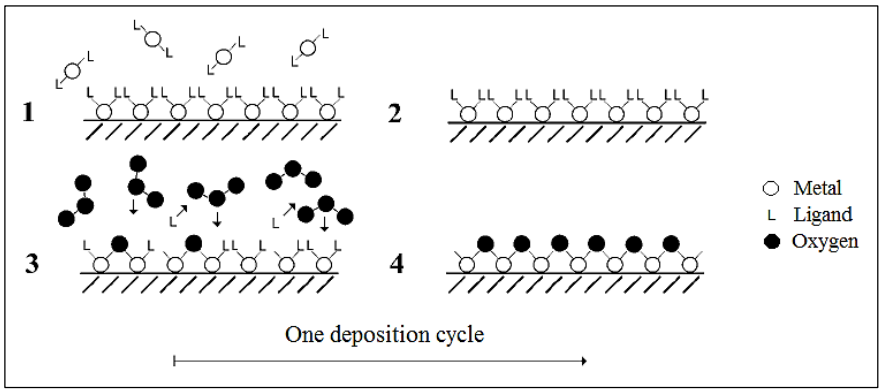

Figure 64. Formation of a hypothetical metal oxide monolayer.[196] Reproduced with permission from Niinistö, L., Päiväsaari, J., Niinistö, J., Putkonen, M. and Nieminen, M. *Phys. Status Solidi A* ***201*** 1443. Copyright 2004 John Wiley and Sons.

In order for the film formation to be an ALD-type process, each reaction step must be irreversible and saturating meaning that each adsorption site on the substrate surface is to be occupied. Surface saturation ensures the self-limiting growth mechanism where the growth rate of the film is not dependent on the precursor dose when it exceeds a minimum required for the saturated layer. The growth rate per cycle is said to be saturated as a function of pulse

time or precursor dose (Figure 65).[3] Variations from the saturated growth rate may occur due to possible precursor decomposition or etching reactions.

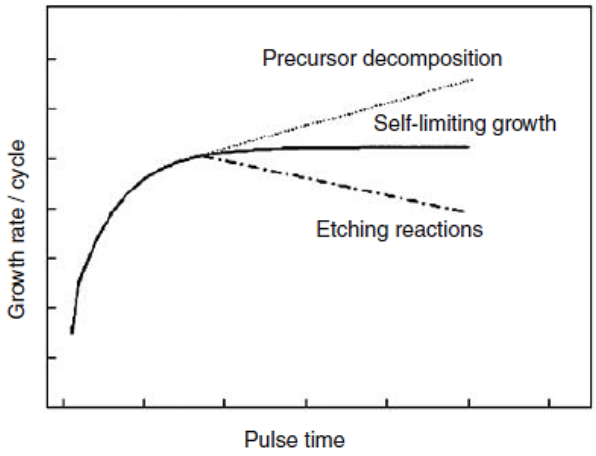

Figure 65. Growth rate as a function of pulse time.[3] Reproduced with permission from Ritala, M. and Niinistö, J. in *Chemical Vapor Deposition: Precursors, Processes and Applications*, chapter 4, p. 158. Copyright 2009 Royal Society of Chemistry.

ALD can be employed to deposit a plethora of materials such as metals, oxides, nitrides, and fluorides. One of the greatest advantages of ALD is the ability to control film formation at an atomic level. The saturated surface reactions guarantee high degree of conformality meaning it is possible to have uniform film growth even at the bottom of high-aspect-ratio trenches. This unique feature of the ALD method unachievable by other deposition techniques is demonstrated in Figure 66.[8] The ALD-type growth mechanism enables the formation of dense, uniform, and homogenous films over large substrates with complex structure. A significant limitation of ALD is slowness the effect of which can be minimized by shortening the precursor pulse lengths. Process efficiency can also be improved via batch deposition and by using larger substrates or more efficient reactors. Another major drawback of ALD is the limited amount of suitable precursors; thus, the development of precursor chemistry is essential.

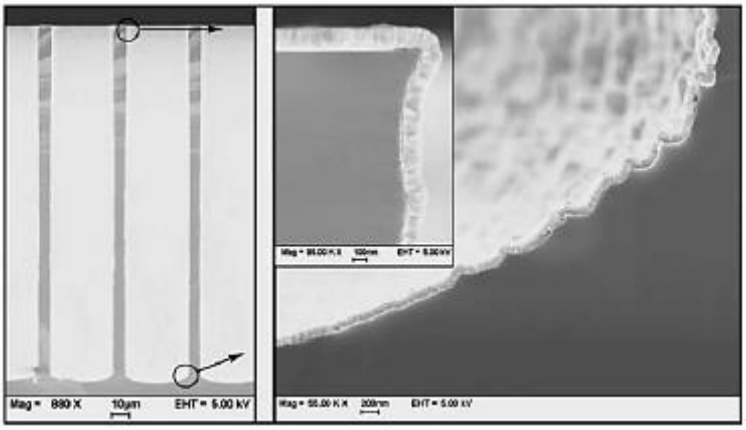

Figure 66. Demonstration of the excellent conformality of a Ru film deposited by ALD.[8] Reproduced with permission from Aaltonen, T. in *Atomic Layer Deposition of Noble Metal Thin Films*, doctoral dissertation, University of Helsinki. Copyright 2005.

5.2 Introduction to photo-assisted atomic layer deposition

5.2.1 Background

Conventionally ALD processes are divided into thermal and plasma-assisted processes. In thermal ALD, the occurring surface reactions rely on thermal energy. Typically deposition temperatures vary between 200–500 °C. In some cases the film growth is constant in a certain temperature range, which facilitates process reproducibility. The deposition temperature should be high enough to guarantee efficient surface saturation but not too high to cause precursor decomposition. Plasma-assisted processes can be carried out at lower temperatures due to reactive species generated by the plasma discharge.[10] The presence of plasma species produces thin films of increased purity and density. Limitations of the PEALD method involve complex reaction chemistry, challenging reactor design and, in some cases, decreased conformality as well as film damage caused by the energetic species in the system. Also, the PEALD method is difficult to apply in batch mode.

Photo-ALD is a modification of the ALD method where reactions are enhanced with UV radiation and/or visible light. Only a handful of articles have been published regarding photo-ALD, most likely because of problematic reactor design, limited knowledge on the photochemical reactions occurring in the system, and a lack of suitable precursors. The

method has been employed to deposit GaAs, ZnO, Ta_2O_5, ZrO_2, Al_2O_3, TiO_2, and BN thin films.[11–23] The processes have been more thoroughly discussed by the author in her B.Sc. Thesis.[197] Ruthenium has been deposited by flash-enhanced ALD which relies on rapid heating of the very surface of the film causing pyrolytic decomposition of the precursor.[198] Most of the previously mentioned depositions are enhancements of existing thermal ALD processes and only for Ta_2O_5 new ALD chemistry has been developed. Also, many of these depositions rely on the local heating of the substrate surface caused by intensive irradiation leading to CVD-type growth. A process is also more likely to show CVD character if the precursor molecules are irradiated in the gas phase rather than after the adsorption.

Photo-ALD is also a route to single-source ALD processes. Another major benefit of the method is the possibility of selective ALD which can be achieved either with a shadow mask combined with a UV lamp or without a mask if a laser is used as the radiation source. Because of the lower deposition temperatures, photo-ALD also enables the coating of substrates with poor thermal stability (e.g. polymers) and the exploitation of some thermally unstable precursors. Surface saturation is typically faster due to the additional energy provided by photons. Thus, the cycle times are shorter and process efficiency increases. Irradiation may also have an effect on film properties. For instance, the leakage current density of Ta_2O_5 films deposited via photo-ALD was decreased by several orders of magnitude as opposed to the films deposited with the thermal process using $Ta(OEt)_5$ and H_2O.[19] Unlike energetic plasma species, photons do not cause substantial film damage although some electronically active defects may appear. The effect of light is anisotropic causing decreased conformality, which should be considered when choosing a substrate for photo-assisted depositions.

5.2.2 Precursors for photo-assisted atomic layer deposition

The selection of proper precursors is essential for an ALD process.[2,3] A number of precursor properties are common to all ALD processes. In addition to these general requirements, photo-assistance sets some additional requirements for the precursors that can, for the most part, be derived from photo-CVD (Section 2.2).[30] All the requirements for photo-ALD precursors are collected in Table 6.

Table 6. Requirements for photo-ALD precursors.

Essential	**Desirable**
Sufficient volatility	Preferably high vapor pressure liquids or gases to ensure simple delivery with a constant flux
Stability before reaction, no self-decomposition	Unreactive volatile byproducts
Aggressive and complete reactions	Easy to synthesize and handle
No etching of the film or substrate	Nontoxic and environmentally friendly
No dissolution into the film or substrate	
Sufficient purity (application dependent)	
Absorption at wavelengths emitted by the irradiation source	
High extinction coefficient	
Absorption must lead to a reaction path resulting in film formation	

β-diketonates are promising candidates for the formation of metal thin films by photo-ALD since they have been exploited in both photo-CVD and thermal ALD processes, and their photochemistry has received extensive scrutiny.[7,30] The processes employing metal β-diketonates revolve mainly around the deposition of copper and platinum. The deposition of metals from metal β-diketonates typically requires a reducing agent. Metal carbonyls are another group frequently utilized in photo-CVD, especially for the deposition of refractory metals such as chromium, molybdenum, and tungsten. The complete removal of the carbonyl ligands is, however, somewhat challenging resulting in a high degree of carbon and oxygen impurities.

$Ta(OEt)_5$ and $Zr(O^tBu)_4$ have been used to deposit their respective oxides by photo-ALD.[18,19,21] The depositions were carried out with the aid of an oxidizing precursor although Ta_2O_5 film formation was also observed without a second component. The mechanism for the photolytic dissociation of alkoxides into oxides is indefinite but considering the success with $Ta(OEt)_5$, similar chemistry may also apply to other alkoxide precursors as well.

Another approach to photo-ALD is the gas-phase irradiation of reactants, such as oxygen or acetone, in an attempt to generate more reactive species and induce film formation. This method was employed by e.g. Chalker and coworkers who deposited Al_2O_3 using TMA and ozone produced by irradiation of O_2.[23]

5.2.3 Reactors for photo-assisted atomic layer deposition

The most prominent explanation for the miniscule number of articles published on photo-ALD lies in the challenging reactor design. Figure 67 represents the schematics of the most common photo-ALD reactor where the gas flows are horizontal, and light is directed into the system through a quartz window above the substrate.[18] Aoyagi *et al.* employed a perpendicular-flow reactor which is more tolerant to various non-idealities that would result in CVD-type growth mechanism (Figure 68).[13] In this case, the light source is placed at a 45° angle with respect to the substrate leading to an elliptical irradiation area.

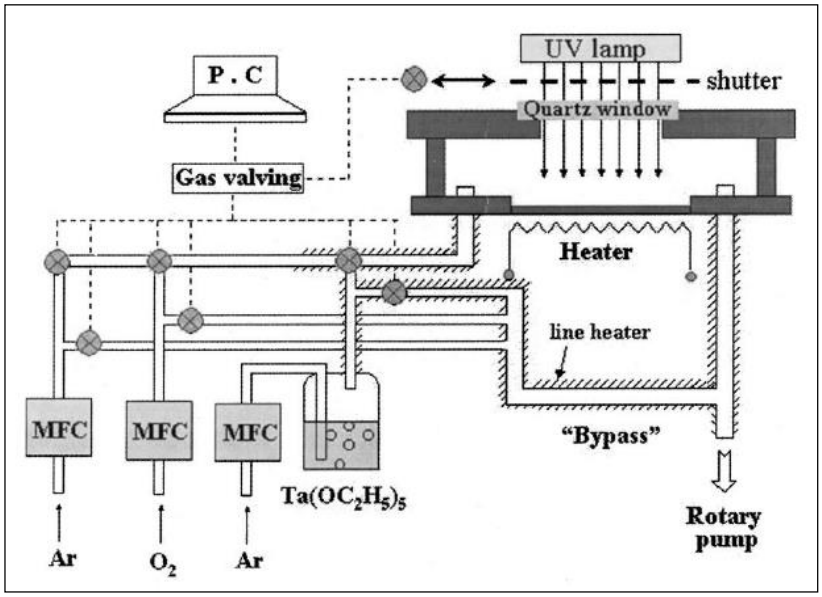

Figure 67. A typical photo-ALD reactor.[18] Reproduced with permission from Lee, Y.-H., Kwak, J.-C., Gang, B.-S., Kim, H.-C., Choi, B.-H., Jeong, B.-K., Park, S.-H. and Lee, K.-H. *J. Electrochem. Soc.* ***151*** C52. Copyright 2004 The Electrochemical Society.

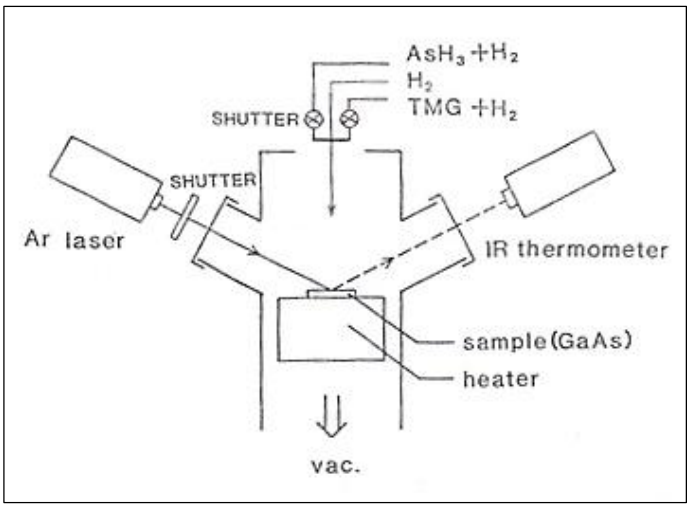

Figure 68. A photo-ALD reactor utilized in GaAs depositions.[13] Reproduced with permission from Aoyagi, Y., Meguro, T., Iwai, S. and Doi, A. *Mater. Sci. Eng., B* ***10*** 121. Copyright 1991 Elsevier.

Photo-assisted depositions are usually carried out in cold-wall reactors where only the substrate is heated. This may cause steep temperature gradients leading to severe convection, incomplete purging, and non-uniform coatings. On the other hand, local heating minimizes the deposition on reactor walls, which is particularly vital in photo-ALD in order to avoid constant cleaning of the light permeable window. Film deposition on the window surface leads to changes in the intensity of the transmitted radiation between or even during depositions. Formation of a mirror-like metal film on the window would block light permeation altogether. Olander *et al.* deposited BN films in a hot-wall reactor but the undesired deposition on the window surface was avoided by introducing the precursors to the substrate via separate routes (Figure 69).[20]

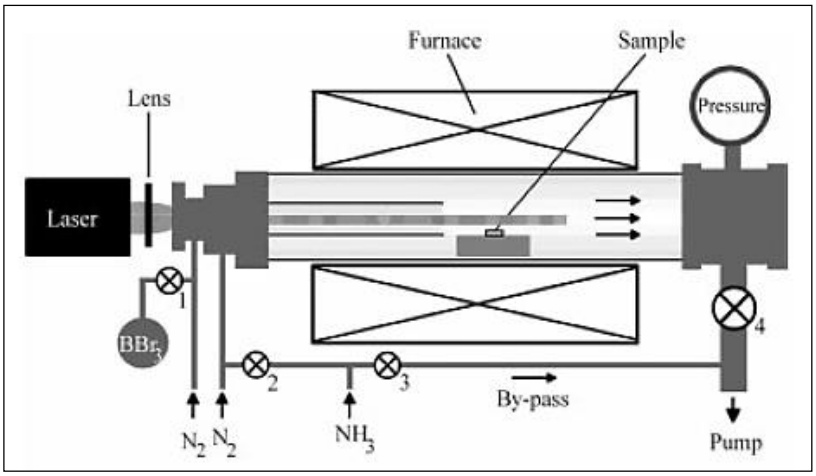

Figure 69. A hot-wall reactor employed to deposit BN films.[20] Reproduced with permission from Olander, J., Ottosson, L.M., Heszler, P., Carlsson, J.-O. and Larsson, K.M.E. *Chem. Vap. Deposition* ***11*** 330. Copyright 2005 John Wiley and Sons.

Analogous to photo-CVD, a variety of supplementary methods have been used in order to reduce undesired film formation on the window surface. Chen *et al.* utilized an additional H_2 flow to prevent precursor molecules and possible by-products from rising to the window.[14] Henke *et al.* deposited Al_2O_3 and Ru thin films in a reactor with a readily removable sacrificial glass window to protect the actual quartz window (Figure 70).[198] Film growth on the removable window, on the other hand, was suppressed with an argon flow.

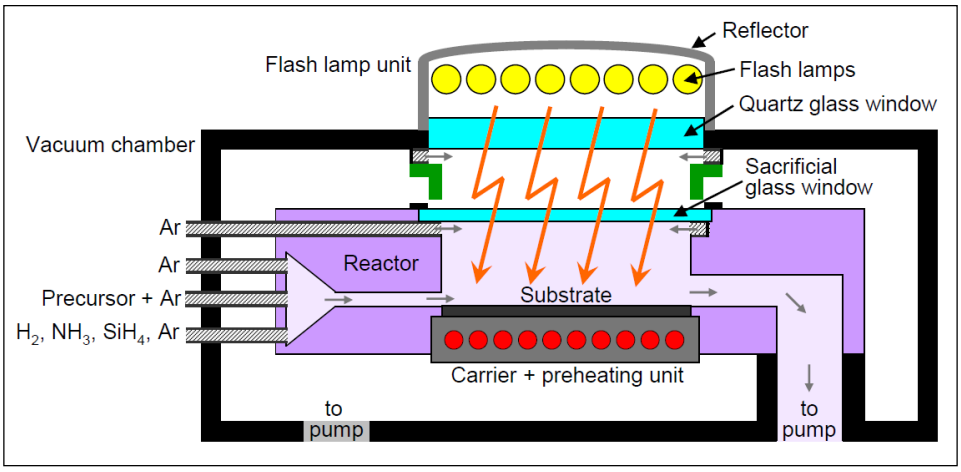

Figure 70. Schematics of a reactor used to deposit Al_2O_3 and Ru films.[198] Reproduced with permission from Henke, T., Knaut, M., Hossbach, C., Geidel, M., Rebohle, L., Albert, M., Skorupa, W. and Bartha, J.W. *ECS J. Solid State Sci. Technol.* ***4*** P277. Copyright 2015 The Authors, published by The Electrochemical Society.

6 Conclusions

Atomic layer deposition is the most promising method for confronting the technological challenges set by future microelectronics. The development of more efficient devices requires miniaturization of electronic components, which in turn calls for accurate deposition techniques. Due to its self-limiting growth mechanism, ALD is superior to the other methods with respect to accuracy and has thus been of considerable scientific and industrial interest in recent years. Despite numerous efforts, metal deposition is still quite lacking in viable ALD processes. Thermal ALD is mainly suitable for the deposition of noble metals, and plasma-enhancement often compromises film quality and conformality. Photo-assistance provides an alternative route to film deposition. The removal of ligands is achieved via photodissociation enabling lower process temperatures, the use of single-source precursors, and area-selective deposition. Since no metal photo-ALD processes exist up to date, the aim of this literature review was to gain insight into the photochemistry that occurs in metal photo-CVD and possibly use the gathered data to create general guidelines for metal photo-ALD as well.

Although the hype around photo-CVD has subsided since then, it was an area of extensive scrutiny in the ‘80s and ‘90s. The main motivation behind the development of metal photo-CVD was to create metal interconnects in a straightforward manner without multiple lithographic steps. Thus, the vast majority of the studies presented in this thesis revolve around laser-assisted processes which rely on the rapid heating of the substrate inducing localized pyrolysis. The pyrolytic approach is not that desirable from the ALD point of view because decomposition of the precursor can deteriorate the self-limiting growth mechanism if the substrate is not cooled back to the original temperature before the next pulse. Although not always exploited in LCVD, many of the precursors do undergo electronic transitions at shorter wavelengths and may thus be suitable for photo-ALD. The short lifetimes of the excited states complicate their systematic examination emphasizing the role of theory as well as trial-and-error research.

Photo-CVD processes have been developed for metals ranging from aluminum to lead implying almost endless possibilities for photo-ALD, and yet the amount of reports is scarce. The limiting factor of purely photolytic deposition lies in its complexity arising from the

large quantity of variables; attention is to be paid to precursor chemistry, reactor design, irradiation wavelength, type of light source, and substrate effects, among others. Furthermore, since ALD relies solely on surface reactions, the information acquired from photo-CVD articles cannot be directly applied to photo-ALD complicating the initial research. Prosperity requires consideration of every detail highlighting the importance of a solid background, and while this literature review provides a good start, ongoing research is essential for the development of photo-ALD and further on, accurate metal deposition.

Experimental

7 Experimental methods

7.1 Film deposition

All depositions were carried out in a modified Picosun R-200 reactor equipped with a light source placed perpendicularly with respect to the substrate. Schematics of the reactor are illustrated in Figure 71. The proper functioning of the reactor was first verified with several metal oxide processes (Section 8) employing Setup 1 (Figure 72a). The same configuration was utilized to deposit metals but after several unsuccessful attempts, the reactor was upgraded to Setup 2 (Figure 72b) operating at shorter wavelengths supposed to be more compatible with the photochemistry of metal complexes. The reactor pressure during all depositions was ~5 mbar. Metal precursors that required external heating were evaporated from a Picohot^{TM} 200 Booster source. Prior to deposition, the air-sensitive precursors were handled under N_2 in a glovebox (MBraun LABstar). The photochemical behavior of some of the metal precursors in solution was qualitatively examined by photolysis using a pulsed Xenon Corporation LH-810 with a C-type lamp.

Both metal and metal oxide films were deposited on a number of different substrates, including Si, soda lime and borosilicate glass, Al_2O_3, TiO_2, TiN, as well as Ir and Ru coated glass. Conformality studies of Ta_2O_5 were carried out on patterned trench substrates. All substrates were cleaned from particles prior to deposition using compressed N_2 (99.999 %, AGA). The deposition mechanism was examined by placing a strip of silicon wafer in near-contact (a few millimeters) with the substrate during deposition. If no film was deposited under the mask, the process was concluded to be light induced. The photolytic nature of the Ta_2O_5 process was verified using lateral high-aspect-ratio (LHAR) structures obtained from VTT Techincal Research Centre of Finland Ltd, more comprehensively described in literature.[199] The potential heating effect of the light source was monitored by placing a thermocouple in direct contact with the backside of the substrate.

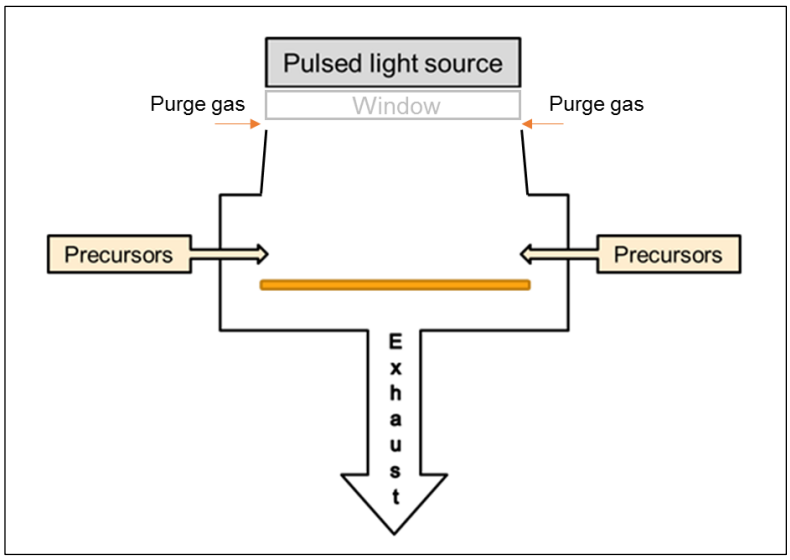

Figure 71. Schematics of the photo-ALD reactor. Irradiation was pulsed either by using a flash lamp or by combining a cw lamp with a gate valve.

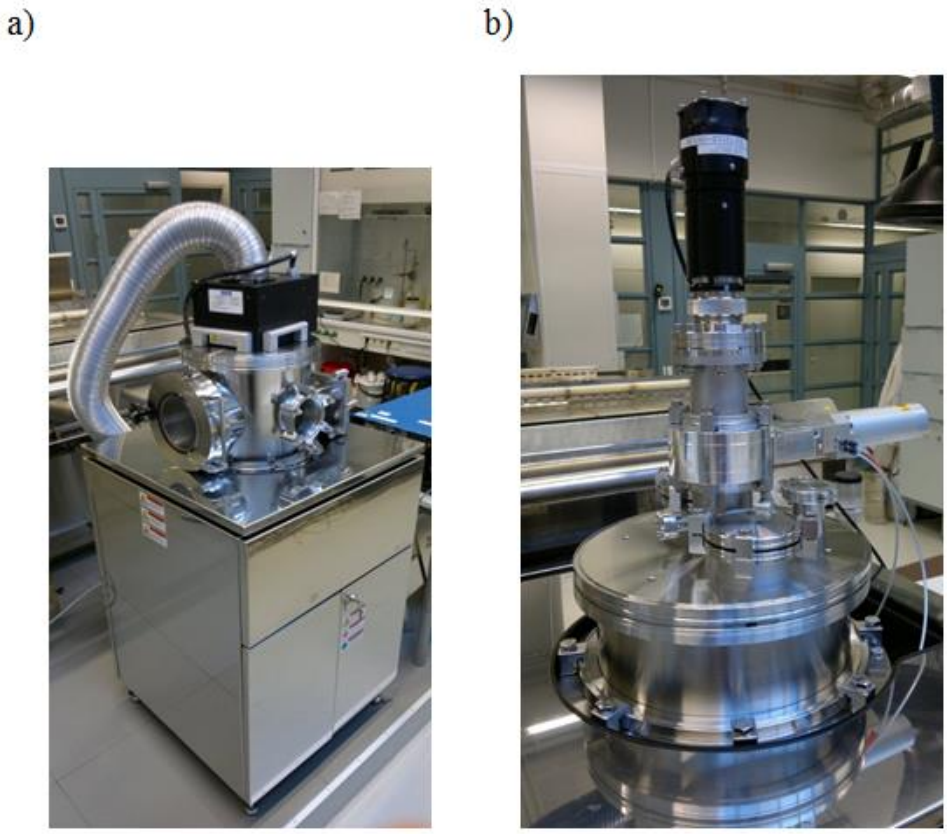

Figure 72. a) Setup 1 equipped with a pulsed Xenon Corporation LH-810 with a C-type lamp and b) Setup 2 consisting of a cw H_2D_2 L11798 lamp (Hamamatsu Photonics) and gate valve for pulsing the irradiation.

The key difference between the two reactor configurations was the light source. Setup 1 was equipped with a pulsed LH-810 lamp obtained from Xenon Corporation (Figure 73a).[200] The main advantage of using a flash lamp is that no mechanical shutter is required for pulsing the irradiation. The output spectrum of the C-type lamp is illustrated in Figure 73b.[200] The emission starts at 190 nm and extends to wavelengths in the visible region. To ensure efficient admittance of photons, fused silica, which is highly transparent at 190 nm, was chosen as the window material. The pulse energy of the lamp was 207 J/pulse, and the maximum pulsing rate was 15 Hz. Because the emission spectrum is nearly symmetrical and has a maximum at ~430 nm, the average photon energy can be estimated at 4.6×10^{-19} J. Based on the pulse energy provided by the manufacturer, the quanta/pulse can thus be approximated at 4.5×10^{20} using the Planck-Einstein relation. Finally, assuming that the irradiated area at the substrate is the same as the opening of the lamp (~150 cm^2), the number of photons arriving at the substrate per pulse is approximately 2.9×10^{18} quanta/cm^2pulse. The lamp-to-substrate distance was originally 420 mm but was reduced down to 255 mm to increase the light intensity at the substrate. The revised version of Setup 1 is depicted in Figure 74. Nitrogen was utilized as the carrier gas. A 1000 sccm N_2 flow was employed to protect the optical window from film growth.

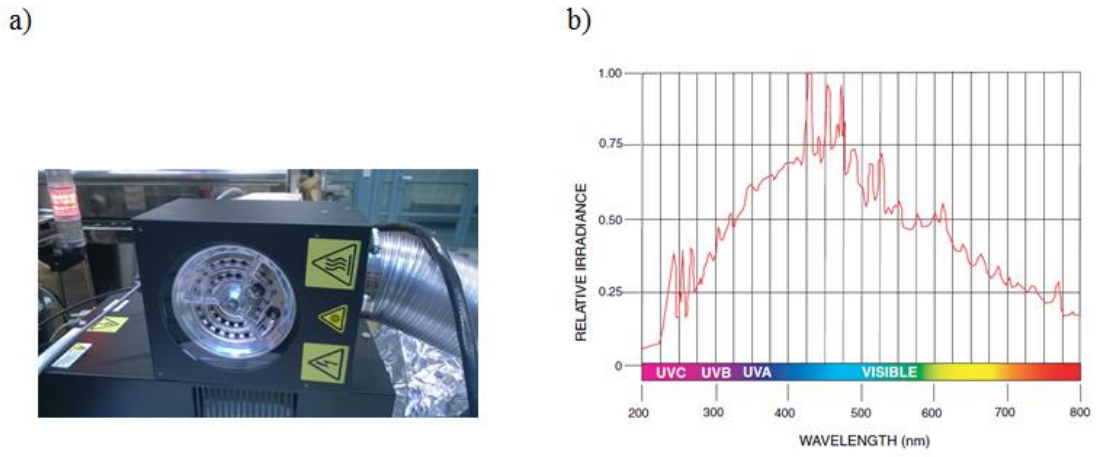

Figure 73. a) Xenon Corporation LH-810 with C-type lamp and b) its output spectrum.[200] Reproduced with permission from Xenon Corporation.

Figure 74. Lowered version of Setup 1.

None of the studied metal depositions were successful using Setup 1; thus, modifications had to be made to the reactor system. The most logical step was to try shorter wavelengths potentially more suitable for metal deposition, which is why Setup 2 was equipped with a cw H_2D_2 L11798 light source provided by Hamamatsu Photonics (Figure 75a).[201] Figure 75b illustrates the spectral range of the utilized H_2D_2 lamp.[201] Pulsing of the irradiation was accomplished using a pneumatically controlled gate valve. Light was admitted into the reaction chamber through a MgF_2 window. The lamp-to-substrate distance was 660 mm. At this distance, the radiant intensity over the spectral range of 115–200 nm is ~220 µW/cm^2. So during a second of irradiation, the number of emitted photons is in the order of 10^{14} quanta/cm^{2}s. The irradiated area was ~430 cm^2. Since nitrogen absorbs radiation at wavelengths below 150 nm (Figure 76), argon (99.999 %, AGA) was utilized as both the carrier and the window protection gas to avoid the formation of excited N_2 species leading to possible side reactions.[202] The absorption spectrum illustrated in Figure 76 is measured from solid nitrogen; however, the data is in correspondence with the spectral lines reported for gaseous N_2.[203]

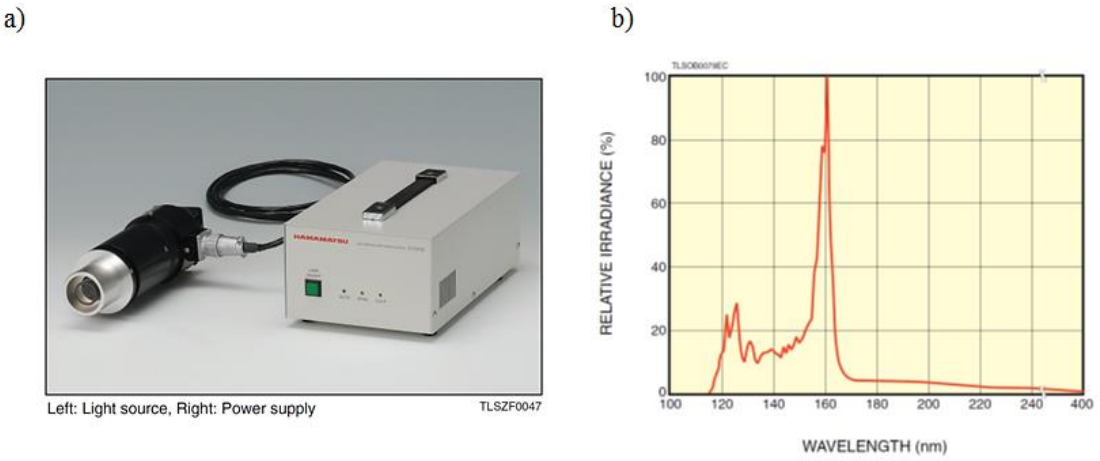

Figure 75. a) Hamamatsu H_2D_2 L11798 light source and b) its output spectrum.[201] Reproduced with permission from Hamamatsu Photonics.

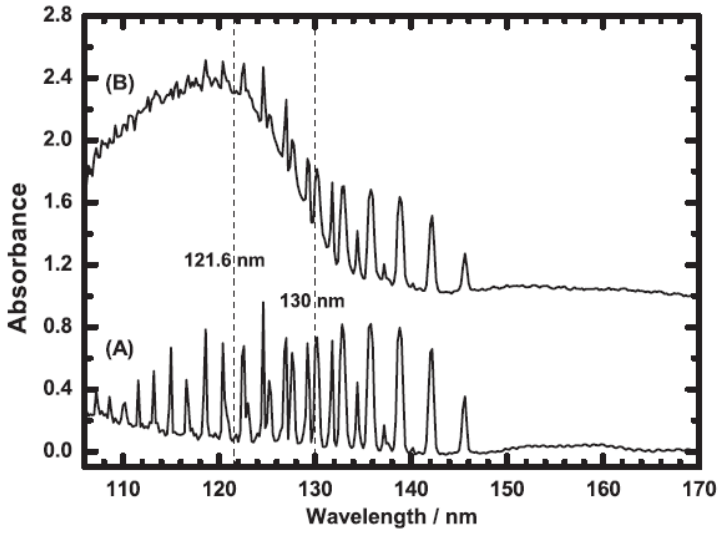

Figure 76. Absorption spectra of solid N_2 (curve A) and CH_4/N_2 (curve B).[202] Reproduced with permission from Wu, Y.-J., Wu, C.Y.R., Chou, S.-L., Lin, M.-Y., Lu, H.-C., Lo, J.-I. and Cheng, B.-M. *Astrophys. J.* ***746*** 1. Copyright 2012 The American Astronomical Society.

7.2 Film characterization

Film thicknesses were measured on Si substrates with X-ray reflectivity (XRR, PANalytical X'Pert Pro MPD). The same instrument was also utilized to determine the crystallinity of the films using grazing incidence XRD (GIXRD). The incidence angle of the CuK_α (λ = 1.54 Å) beam was 1°. The diffractograms were analyzed with PANalytical Highscore Plus 4.1 software.

Film conformality and morphology were studied by SEM imaging combined with thickness analysis using EDS (Oxford INCA 350 Energy spectrometer connected to a Hitachi S-4800 field emission SEM). For the analysis of the LHAR samples, the membrane of the substrate was partly removed with carbon tape. The SEM images were taken by M. Kemell and V. Miikkulainen (Laboratory of Inorganic Chemistry, University of Helsinki).

Film composition was determined by time-of-flight elastic recoil detection analysis (TOF-ERDA). The analyses were done by K. Mizohata at the Department of Physics, University of Helsinki. The measurements were carried out by employing either a 50 MeV $^{79}Br^{9+}$ ion beam or a combination of two beams: 35 MeV $^{35}Cl^{6+}$ and 50 MeV $^{127}I^{9+}$. The incidence angle of the beam with respect to the sample surface was 20°. The angle between the beam and the detector was 40°.

The resistivities of the deposited ruthenium and Nb_2O_5 films were determined using a four-point probe (CPS Probe Station, Cascade Microtech combined with Keithley 2400 source meter). The measured resistance value was first multiplied by 4.5324 to obtain the sheet resistance which was then multiplied by film thickness to obtain the resistivity.

8 Oxide processes

8.1 Ta_2O_5, Nb_2O_5, and V_2O_5

Prior to the metal depositions, the photo-ALD reactor was tested with a single-source photo-ALD process known from literature.[18] Ta_2O_5 films were deposited using 99.99 % $Ta(OEt)_5$ (Strem Chemicals Inc.) and Setup 1 (Xenon Corporation lamp). The precursor was evaporated at 140 °C. A typical pulsing sequence consisted of a 1.6 s metal precursor pulse followed by 5 s of purge, after which the substrate was exposed to 20–40 flashes of UV irradiation. Film growth was observed on various substrates in the temperature range of 150–245 °C.

Figure 77 depicts the growth rate as a function of both substrate temperature and the number of flashes at a pulsing rate of 5 Hz. The growth rate increased with increasing temperature when the number of applied flashes was 30 during a 6 s irradiation period. The reduction of the lamp-to-substrate distance from 420 to 255 mm had no significant effect on the growth rate. At 245 °C, the growth rate saturated at ~0.12 Å/cycle with respect to the flash count. As shown in Figure 78, the film thickness increased linearly with increasing cycle count.

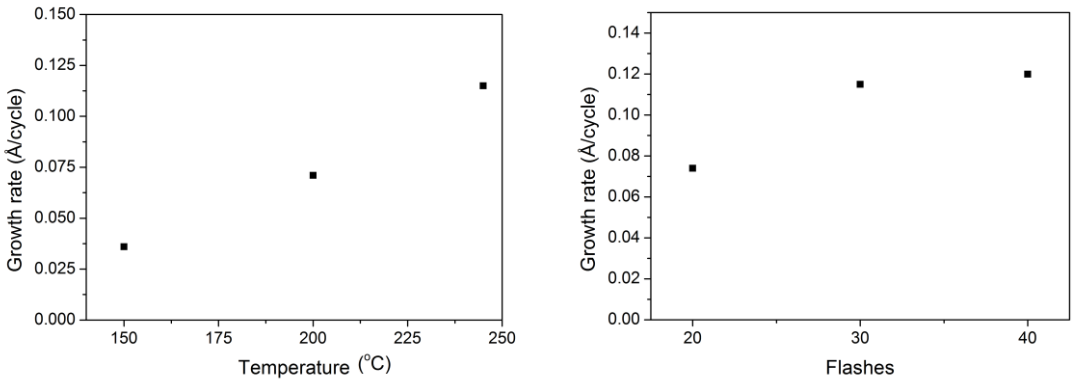

Figure 77. Ta_2O_5 growth rate as a function of temperature (left) and the number of flashes at 245 °C (right).

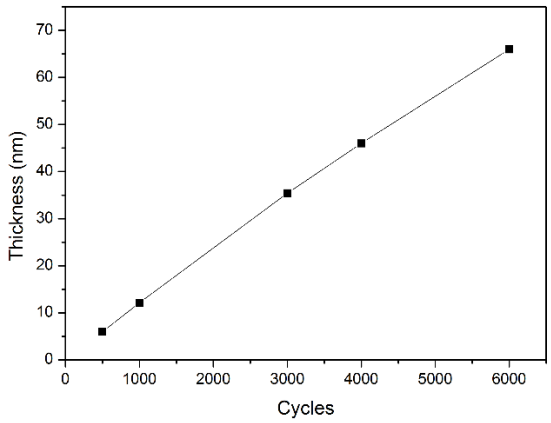

Figure 78. Ta_2O_5 film thickness as a function of cycle count (245 °C, 30 flashes/cycle).

The saturated growth rate of 0.12 Å/cycle was significantly lower compared to the growth rate of 0.27 Å/cycle determined by Lee *et al.* (Figure 79).[18] The difference may arise from the dissimilar irradiation wavelengths; Lee *et al.* used a lamp operating at 185 nm as opposed to the 190–800 nm radiation obtained from the Xenon Corporation lamp. Also, since Lee and coworkers purged the system only for 0.5 s before starting irradiation, there might have been residual precursor molecules left in the reaction chamber causing CVD-type growth and thus increased deposition rates. The growth rate in the thermal ALD process of Ta_2O_5 from $Ta(OEt)_5$ + H_2O saturated at 0.42 Å/cycle in the temperature region of 220–300 °C.[204]

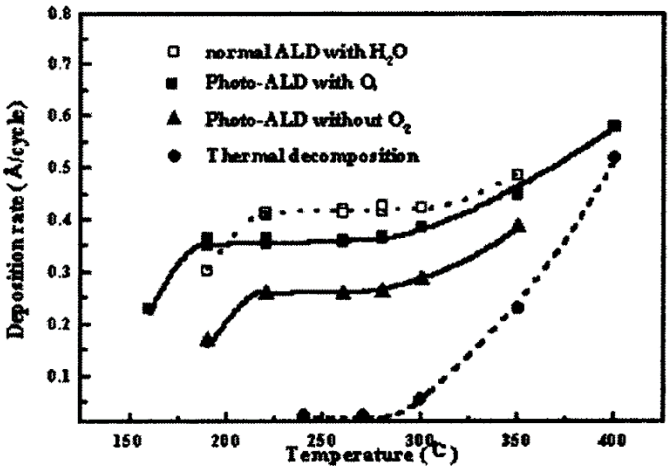

Figure 79. Ta_2O_5 growth rate as a function of deposition temperature.[18] Triangles correspond to the single-source Ta_2O_5 process of interest. Reproduced with permission from Lee, Y.-H., Kwak, J.-C., Gang, B.-S., Kim, H.-C., Choi, B.-H., Jeong, B.-K., Park, S.-H. and Lee, K.-H. *J. Electrochem. Soc.* ***151*** C52. Copyright 2004 The Electrochemical Society.

The effective wavelengths responsible for the Ta_2O_5 deposition were determined by optical filtering. Pieces of both soda lime and borosilicate glass were placed on a strip of silicon ~5 mm above the substrate (Figure 80). After the deposition, the masks were removed, and film was observed only on areas exposed to the unfiltered irradiation. Knowing the absorption spectra of the filters and the emission spectrum of the lamp, the effective wavelength region for the photo-ALD of Ta_2O_5 could be deduced as 200–350 nm. Supporting data was obtained when a B-type lamp with a cut-off point at 240 nm was used instead of the C-type lamp; Ta_2O_5 was deposited at a significantly lower rate. The fact that the longer wavelengths were redundant in terms of film deposition provides convincing evidence of the photolytic mechanism of the process. If the mechanism was pyrolytic, all the wavelengths emitted by the light source would contribute to the film growth.

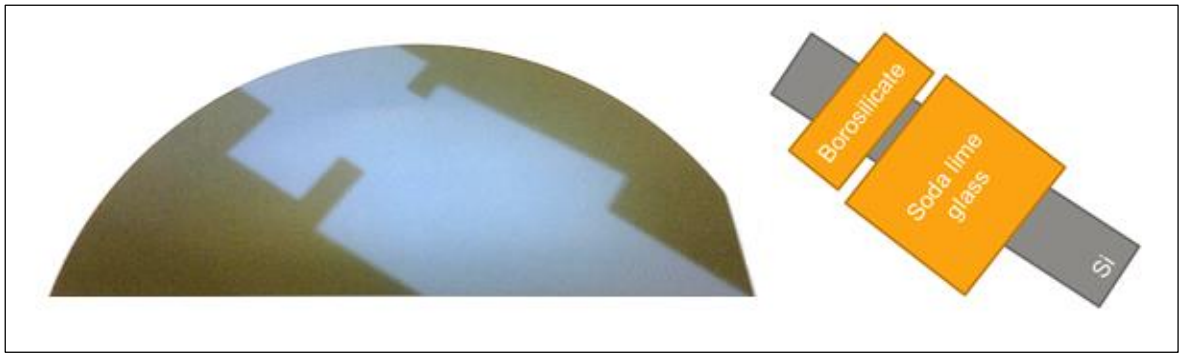

Figure 80. Ta_2O_5 film deposited with optical filters at 245 °C and with 30 flashes/cycle (4000 cycles).

Near-contact masking could also be employed to deposit complicated patterns as illustrated in Figure 81. Both masks were made of aluminum and held 0.3 mm above the substrate. The set of depositions was carried out at 245 °C and with 30 flashes during 6 s irradiation periods. First, the flame mask was utilized to produce 36 nm of Ta_2O_5 during 3000 cycles, after which the mask with three squares was used for another 7000 cycles giving additional 84 nm in thickness.

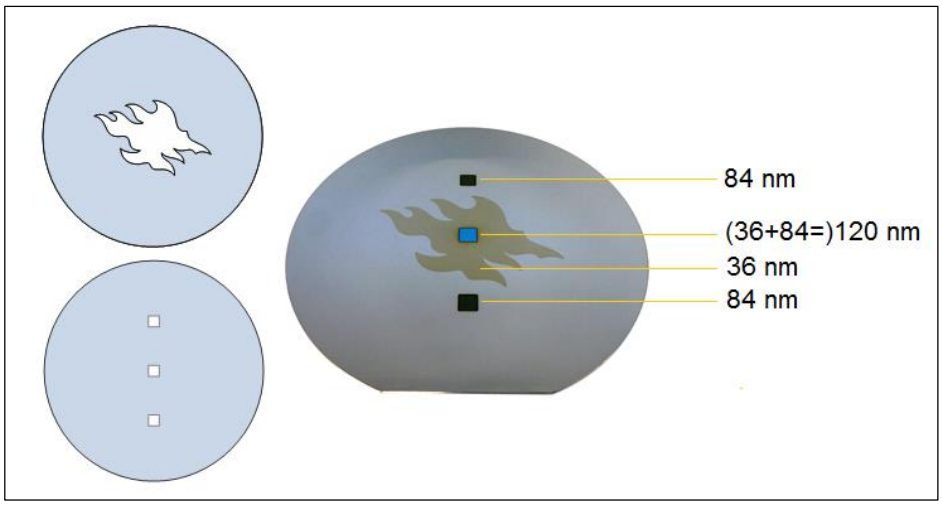

Figure 81. Demonstration of the area-selectivity of the Ta_2O_5 photo-ALD process.

The conformality of the process was examined by depositing 4000 cycles of Ta_2O_5 on patterned silicon at 245 °C and with 30 flashes during 6 s irradiation periods. The film thickness on both flat silicon and at the bottom of the trench was ~50 nm (Figure 82). In contrast, on surfaces parallel to the incident light, i.e. the pillar walls, the film thickness was only about 20 nm due to the lower light intensity. These observations are quite different from the ones made by Henke *et al.* who deposited Al_2O_3 from TMA and H_2 by flash-enhanced ALD (Xenon flash lamps) on Si structures exhibiting an aspect ratio of 40:1.[198] The formation of Al_2O_3 instead of metallic Al was attributed to oxidation in air after the deposition. Conformal deposition of a 30 nm film (2500 cycles) was obtained only on the upper parts of the substrate; at the bottom of the trench the film was barely visible by SEM. The thickness variation was explained by the uneven illumination of the structure causing a temperature gradient. Another possibility was the inadequate purging of by-products in the narrow trenches; the by-products were proposed to occupy the adsorption sites blocking subsequent film deposition.

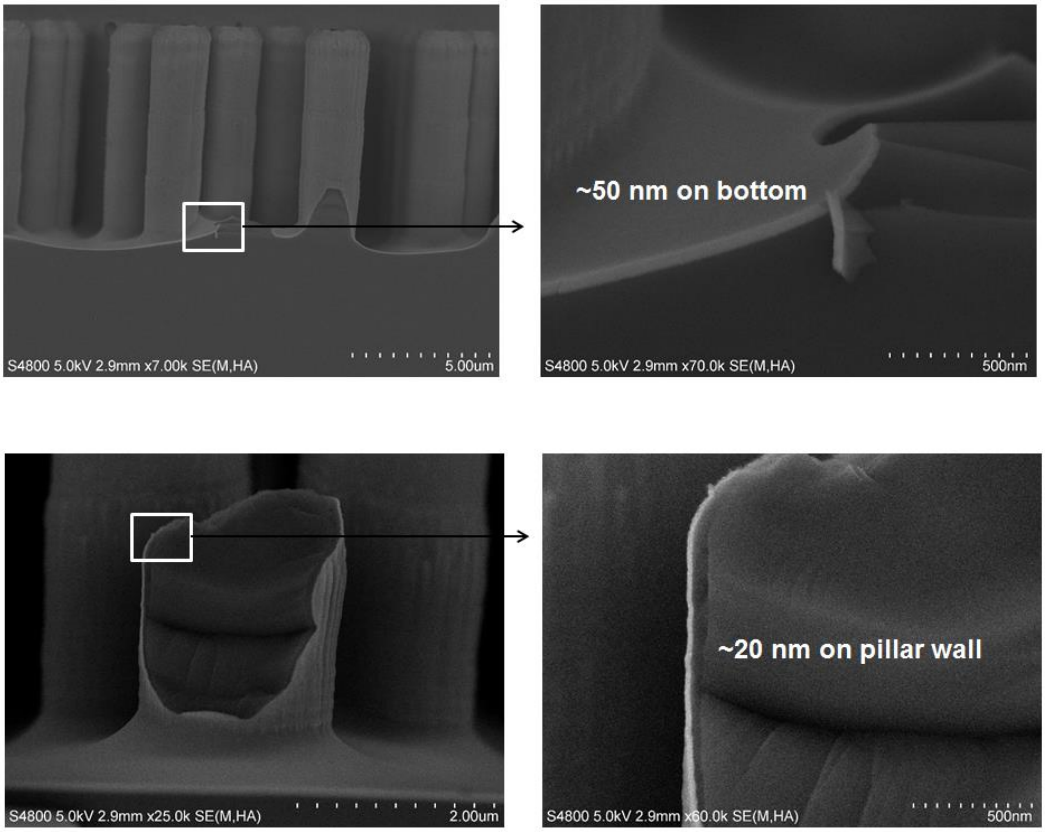

Figure 82. Ta_2O_5 deposited on patterned Si at 245 °C with 4000 cycles and 30 flashes/cycle.

Although the area-selectivity realized with the use of glass filters gives convincing evidence of the photolytic nature of the Ta_2O_5 process, further experiments were done using LHAR structures (Figure 83).[199] 4000 cycles of Ta_2O_5 was deposited on the LHAR substrate at 245 °C and with 30 flashes per irradiation period. Since the top membrane of the structure is only ~1.4 µm in thickness, and silicon conducts heat well, the temperature can be expected to be essentially the same both at the surface of the substrate and inside the cavity. The number of photons penetrated into the cavity through the uppermost silicon membrane is too low to induce film formation. Thus, film deposition inside the cavity would be a consequence of thermal decomposition and not photodissociation. After the deposition, the uppermost membrane was removed with a piece of carbon tape (Figure 84). No Ta signal was observed from the ceiling of the cavity by EDS analysis; thus, no Ta_2O_5 was deposited in the cavity, and the deposition mechanism can be stated as photolytic.

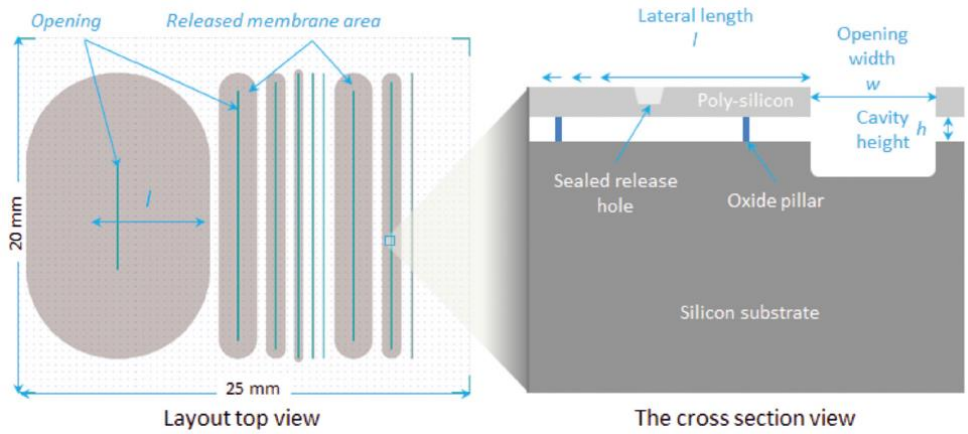

Figure 83. Schematics of the LHAR structure.[199] Reproduced with permission from Gao, F., Arpiainen, S. and Puurunen, R.L. *J. Vac. Sci. Technol. A* ***33*** 010601. Copyright 2015 American Vacuum Society.

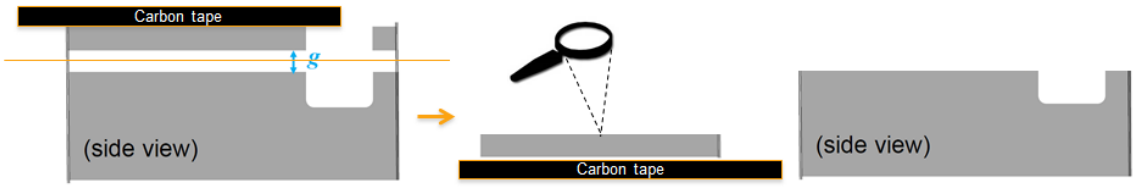

Figure 84. Preparation scheme for the EDS analysis of the LHAR structure.

According to XRD, all the Ta_2O_5 films were amorphous. Hydrogen was identified as the major impurity (7.2 at.%) by TOF-ERDA analysis (Figure 85). Prior to the reduction of the lamp-to-substrate distance, a much higher hydrogen content of 19.2 at.% was measured.

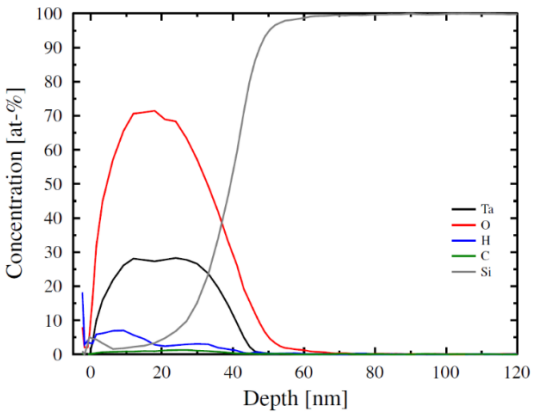

Element	at.%	Error
Ta	24.98	0.24
O	66.41	1.77
C	1.41	0.27
H	7.20	0.70
Stoichiometry	$Ta_2O_{5.3}$	
	$Ta_2O_{4.8}(OH)_{0.6}$	

Figure 85. TOF-ERDA analysis of a photo-ALD Ta_2O_5 film deposited at 245 °C and with 30 flashes per 6 s irradiation period (5000 cycles).

Analogous to Ta_2O_5, films of Nb_2O_5 could be deposited from 99.9 % $Nb(OEt)_5$ (Strem Chemicals Inc.) using the single-source approach of photo-ALD. The precursor has been previously reported in thermal ALD.[205] The photo-ALD process was examined between substrate temperatures of 180 and 245 °C. The precursor was evaporated at 130 °C. All depositions were carried out using a 1.6 s metal precursor pulse followed by 5 s of purging. After the purge, the system was exposed to 30–70 flashes at a pulsing rate of 12.5 Hz.

Uniform films with a distinct shadow effect were deposited in the investigated temperature region. Similarly to Ta_2O_5, the deposition rate of Nb_2O_5 increased with increasing substrate temperature when 60 flashes during 4.8 s periods were applied (Figure 86). The density of the films increased as a function of substrate temperature as well. The film density was higher than that of bulk, which is in agreement with the TOF-ERDA results showing a minor oxygen deficiency in the 49 nm film deposited at 245 °C and with 70 flashes during 5.6 s irradiation periods (Figure 87). Both the higher density and the oxygen deficiency were most likely caused by partial reduction of Nb from the +V oxidation state to +IV. In contrast, the density of Ta_2O_5 was slightly below the bulk value of 8.2 g/cm^3 and showed no substantial variation as a function of temperature. A 27 nm Nb_2O_5 film deposited at 225 °C and with 30 flashes per 2.4 s irradiation periods exhibited a resistivity of 2.1 × 10^8 μΩcm. Saturation with respect to the number of flashes at 225 °C was not as obvious as for Ta_2O_5. As shown in Figure 88, the growth rate increased gradually from 0.05 to 0.1 Å/cycle with increasing flash count possibly due to an incomplete reaction or moderate heating of the substrate caused by the relatively high pulsing frequency of 12.5 Hz. The growth rate in the thermal ALD process of Nb_2O_5 from $Nb(OEt)_5$ + H_2O is ~0.3 Å/cycle in the temperature region of 230–260 °C.[205] According to XRD, the Nb_2O_5 films grown by photo-ALD were amorphous.

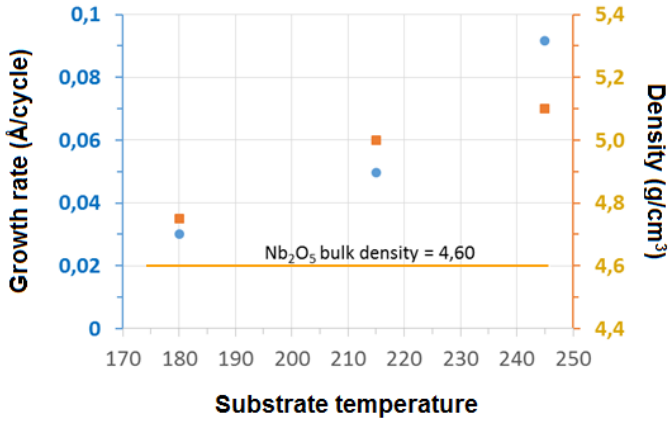

Figure 86. Growth rate and density of Nb_2O_5 as a function of substrate temperature.

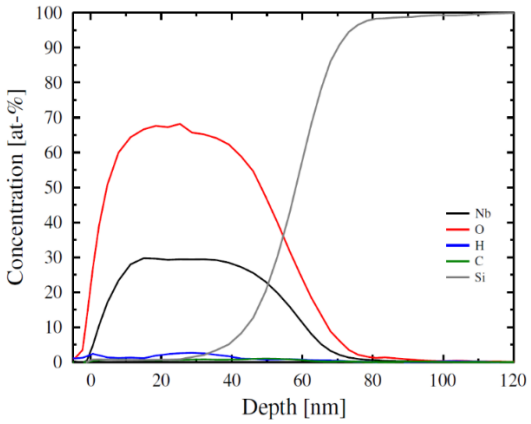

Element	at.%	Error
Nb	28.38	0.38
O	67.30	1.48
C	1.17	0.20
H	3.16	0.38
Stoichiometry	$Nb_2O_{4.7}$	
	$Nb_2O_{4.5}(OH)_{0.2}$	

Figure 87. TOF-ERDA depth profiles from photo-ALD Nb_2O_5 deposited at 245 and with 70 flashes during 5.6 s irradiation periods. Film thickness was 49 nm.

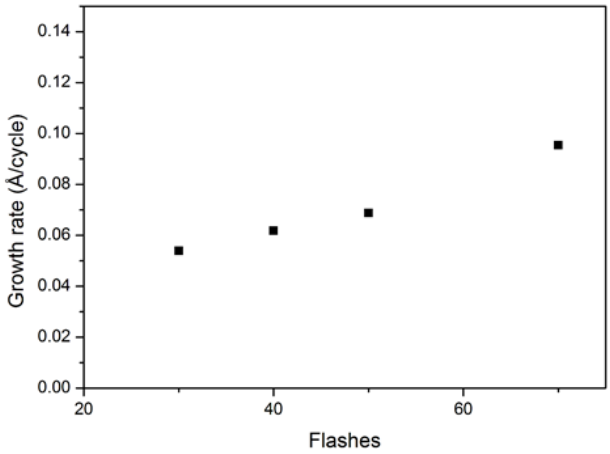

Figure 88. Growth rate of Nb_2O_5 as a function of flash count at a temperature of 225 °C.

In addition to Ta_2O_5 and Nb_2O_5, several attempts were made to deposit V_2O_5 from $VO(O^iPr)_3$ (Sigma-Aldrich) using the single-source approach. The same precursor has previously been utilized in thermal ALD together with water for the deposition of V_2O_5.[206–209] The precursor was evaporated at 60 °C and pulsed for 1.6 s followed by a 5 s purge. The experiments were carried out at 150 °C, and the number of flashes per irradiation period was varied from 5 to 30. The pulsing frequency was fixed at 12.5 Hz. The cycle count was 5000. 5 flashes per irradiation period was insufficient for film formation. 20 and 30 flashes, on the other hand, produced thick, non-uniform deposits over the entire 6” Si wafer, despite the use of a shadow mask. Thus, due to the uncontrollable behavior of the process, V_2O_5 could not be deposited from $VO(O^iPr)_3$ by photo-ALD.

8.2 TiO_2, ZrO_2, and HfO_2

The photo-ALD of TiO_2 was studied using 97 % $Ti(O^iPr)_4$ (Sigma-Aldrich) which is an abundantly utilized precursor in both photo-CVD and thermal ALD.[210–216] $Ti(O^iPr)_4$ has also been used in photo-ALD together with water.[22] In the photo-ALD experiments presented here, the precursor was evaporated at 60 °C and pulsed for 1.6 s followed by 5 s of purge. The depositions were carried out between temperatures of 200 and 250 °C. The temperature dependence of the process was studied with 30 flashes during 6 s irradiation periods. Growth rate with respect to the flash count was studied at 225 °C and at a pulsing rate of 5 Hz. Each deposition was composed of 5000 cycles.

The growth rate of TiO_2 was studied as a function of both substrate temperature and the number of flashes (Figure 89). The growth rate remained relatively constant between 200 and 225 °C (0.077 and 0.065 Å/cycle, respectively) but was significantly higher at 245 °C (0.12 Å/cycle). The growth rate increased with increasing flash count at a temperature of 225 °C. The growth rate in the thermal ALD process of TiO_2 from $Ti(O^iPr)_4$ and H_2O saturates at 0.3 Å/cycle in the temperature window of 250–325 °C.[216]

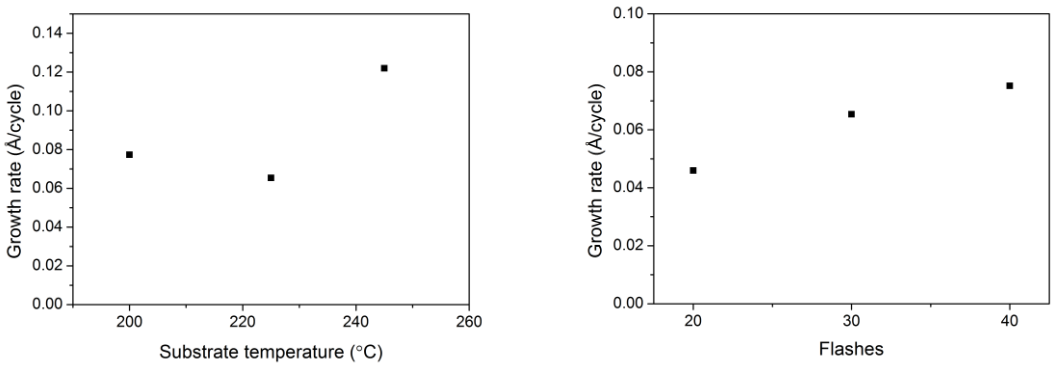

Figure 89. Growth rate of TiO_2 as a function of temperature with 30 flashes during 6 s irradiation periods (left) and flash count at 225 °C (right).

As illustrated in Figure 90, the TiO_2 films deposited at 245 °C and with 30 flashes per 6 s irradiation periods as well as at 225 °C and with 40 flashes per 8 s irradiation periods exhibited weak reflections corresponding to the rutile phase. The films deposited at lower temperatures or with less flashes were amorphous. The thermal ALD process of TiO_2 from

$Ti(O^iPr)_4$ and H_2O produces films with the anatase structure.[216] The anatase structure was also observed by Kim *et al.* who combined UV light to the existing thermal process.[22] Typically, the rutile structure is observed only upon annealing at high temperatures or in photo-CVD when lasers with high intensity are employed to heat the substrate. Composition analysis of the photo-ALD TiO_2 films by TOF-ERDA is in progress.

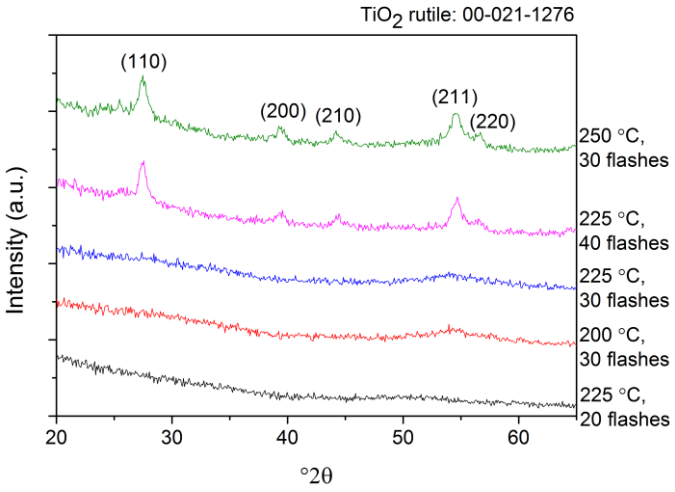

Figure 90. X-ray diffractogram of TiO_2 deposited at various temperatures and with different flash counts.

As in the case of Ta_2O_5, optical filtering with soda lime and borosilicate glasses was utilized to determine the effective wavelength region of the process (Figure 91). At 200 °C, no film was deposited under either of the glasses; thus, the effective spectrum for the surface chemistry was 200–350 nm. Indeed, as shown in Figure 92, $Ti(O^iPr)_4$ absorbs strongly in the aforesaid wavelength region.[214]

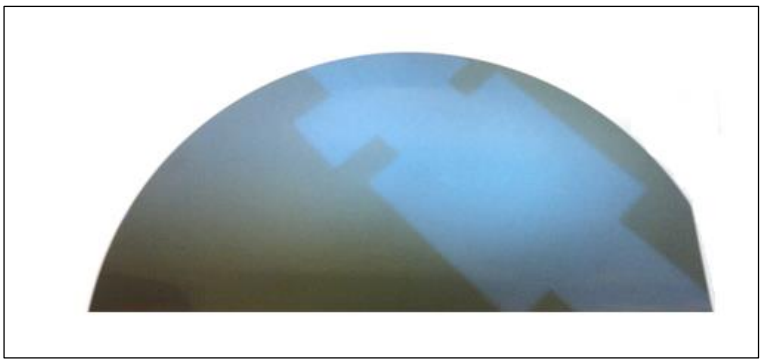

Figure 91. TiO_2 deposited with optical filters at 200 °C and with 30 flashes per irradiation period (5000 cycles).

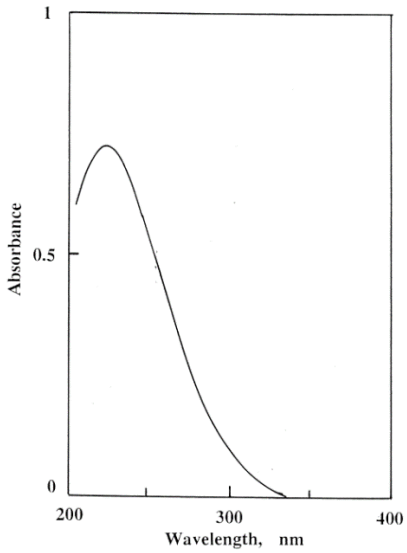

Figure 92. Absorption spectrum of $Ti(O^iPr)_4$ in ethanol.[214] Reproduced with permission from Watanabe, A. and Imai, Y. *Thin Solid Films* ***348*** 63. Copyright 1999 Elsevier.

Photo-ALD was also employed to deposit both ZrO_2 and HfO_2 from 99 % $Zr(O^tBu)_4$ and 99.9 % $Hf(O^tBu)_4$, respectively. Both chemicals were obtained from Strem Chemicals Inc. The same precursors have also been previously reported in both photo-CVD and thermal ALD.[217–222] In the photo-ALD experiments, the precursors were evaporated at room temperature and pulsed for 1.6 s followed by 5 s of purge. The processes were studied at substrate temperatures of 150 and 245 °C and with 30 flashes during 2.4 s irradiation periods. The cycle count was 5000.

As illustrated in Figure 93, the growth rate for both processes increased significantly with increasing substrate temperature. The high growth rates at 245 °C were possibly

consequence of precursor decomposition. According to Kukli *et al.*, thermal decomposition of $Zr(O^tBu)_4$ begins at around 300 °C.[220] Another indication of precursor decomposition in the photo-ALD experiments was film growth beneath the shadow mask at 245 °C. Saturation with respect to the number of flashes per irradiation period was not studied. The growth rates in the thermal ALD processes of ZrO_2 and HfO_2 from the corresponding tetra-tert-butoxides and H_2O at 250 °C are 0.7 and 1.1 Å/cycle, respectively.[220,221] The growth rate of thermal ALD ZrO_2 reaches a maximum at 200 °C (2 Å/cycle) and gradually decreases until no film is deposited at 320 °C.

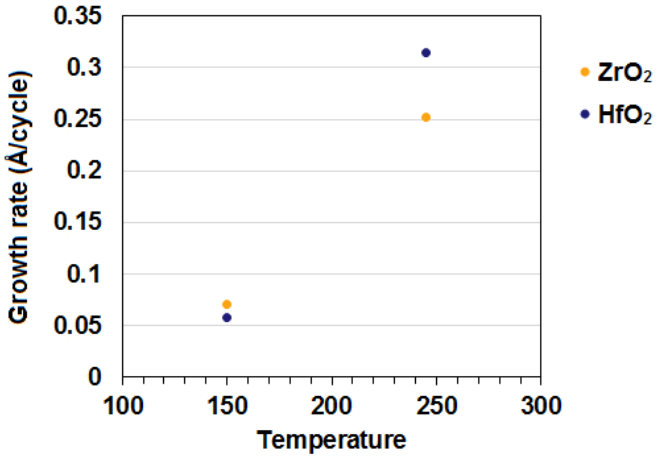

Figure 93. Growth rates of ZrO_2 and HfO_2 as a function of substrate temperature (30 flashes during 2.4 s irradiation periods).

Figure 94 depicts the X-ray diffractograms of both ZrO_2 and HfO_2 deposited at 245 °C and with 30 flashes per 2.4 s irradiation periods. ZrO_2 was mostly cubic but due to the reflection at 24°, presence of the monoclinic phase could not be excluded altogether. The slight peak broadening is a consequence of nanocrystallinity and possibly also the monoclinic phase. HfO_2 was identified as monoclinic. Compositions of the films deposited at 150 °C were determined by TOF-ERDA. The results are summarized in Table 7. Hydrogen was identified as the main impurity in both ZrO_2 and HfO_2. A similar hydrogen content (6–8 at.%) was also reported for the thermally grown ZrO_2 films.[200]

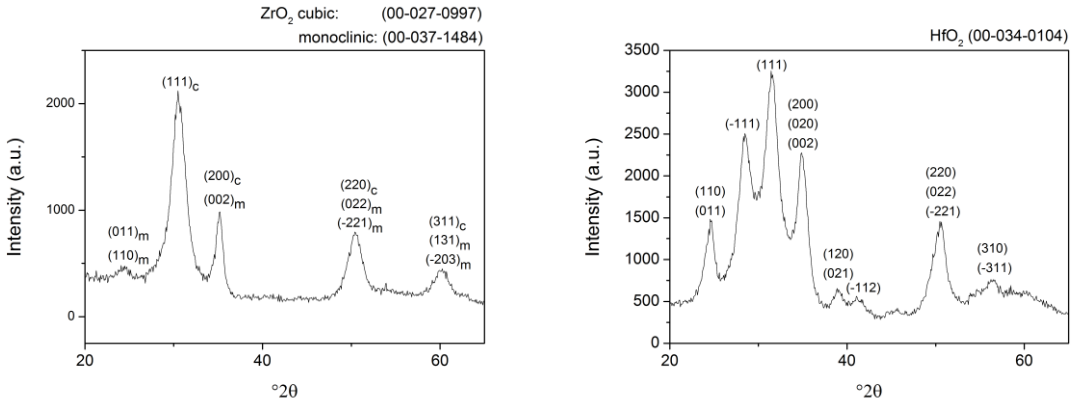

Figure 94. X-ray diffractograms of ZrO_2 (left) and HfO_2 (right) films deposited at 245 °C and with 30 flashes during 2.4 s irradiation periods. ZrO_2 was identified as mostly cubic and HfO_2 as monoclinic.

Table 7. TOF-ERDA results of ZrO_2 (left) and HfO_2 (right) films deposited at 150 °C and with 30 flashes during 2.4 s irradiation periods.

Element	**at.%**	**Error**
Zr	29.5	0.9
O	61.3	1.7
H	6.3	0.6
C	2.6	0.4
F	0.32	0.12
Stoichiometry	$ZrO_{2.1}$ $ZrO_{1.9}(OH)_{0.2}$	

Element	**at.%**	**Error**
Hf	28.6	0.8
O	66.8	2.1
H	2.7	0.5
C	1.6	0.3
F	0.30	0.15
Stoichiometry	$HfO_{2.3}$ $HfO_{2.2}(OH)_{0.1}$	

9 Metal processes

9.1 Silver

The photo-ALD of silver was studied from 98 % Ag(fod)(PEt_3) (fod = 2,2-dimethyl-6,6,7,7,8,8,8-heptafluorooctane-3,5-dionato) obtained from Strem Chemicals Inc. due to its previous usage in PEALD.[143] The molecular structure of the precursor is illustrated in Figure 95.[143] Prior to deposition, photoreactivity of the precursor was qualitatively examined by photolysis in isopropanol solution using the Xenon Corporation flash lamp. Visual changes were observed after only 50 flashes both in solution and on a piece of filter paper moistened with the precursor solution. Further irradiation produced a more intense color change from the original light yellow to gray together with the formation of a black precipitate.

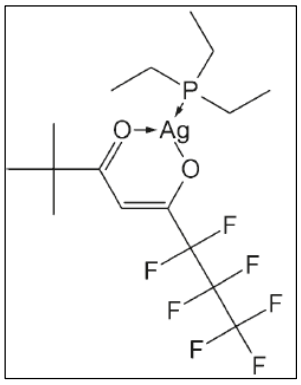

Figure 95. Molecular structure of Ag(fod)(PEt_3).[143] Reproduced with permission from Kariniemi, M., Niinistö, J., Hatanpää, T., Kemell, M., Sajavaara, T., Ritala, M. and Leskelä, M. *Chem. Mater.* ***23*** 2901. Copyright 2011 American Chemical Society.

Several deposition schemes using both light sources were tested. The silver precursor was evaporated at 140 °C. The substrate temperature was maintained at 140 °C as well in order to avoid condensation or decomposition of the precursor at any lower or higher temperatures, respectively. A typical cycle consisted of the silver precursor pulse (1.6 s) followed by purge (5 s) and an irradiation period (2.4–6 s). The system was irradiated either without a second

reactant or in the presence of hydrogen (H_2, 99.999 %, AGA), water, dried acetone, 97 % 1,4-cyclohexadiene (chd) or anhydrous 99.5 % isopropanol. The latter two were both obtained from Sigma-Aldrich. Typically, a very thin, yellow film exhibiting poor adhesion to the substrate was formed. Reliable thickness analysis was infeasible by XRR. In all experiments, however, a distinct shadow effect was observed indicative of the photolytic nature of the process. According to literature, isopropanol is an effective hydrogen atom donor supposedly facilitating the reduction of metals.[223,224] Indeed, the most promising results in the case of silver were obtained when using isopropanol as a reactant. Irradiation from the H_2D_2 light source was applied both during the isopropanol pulse (3 s) and the following purge (5s). The cycle count was 3000. Growth was observed on glass, Si, and Al_2O_3. Shiny, metallic film was deposited only on Al_2O_3. On glass and Si, the deposit appeared yellow, consistent with all the other attempts.

Figure 96 illustrates the X-ray diffractograms measured of silver films deposited on both Si and glass at the aforesaid deposition conditions. The film deposited on glass exhibited only modest crystallinity but reflections corresponding to cubic silver were identified for both samples.

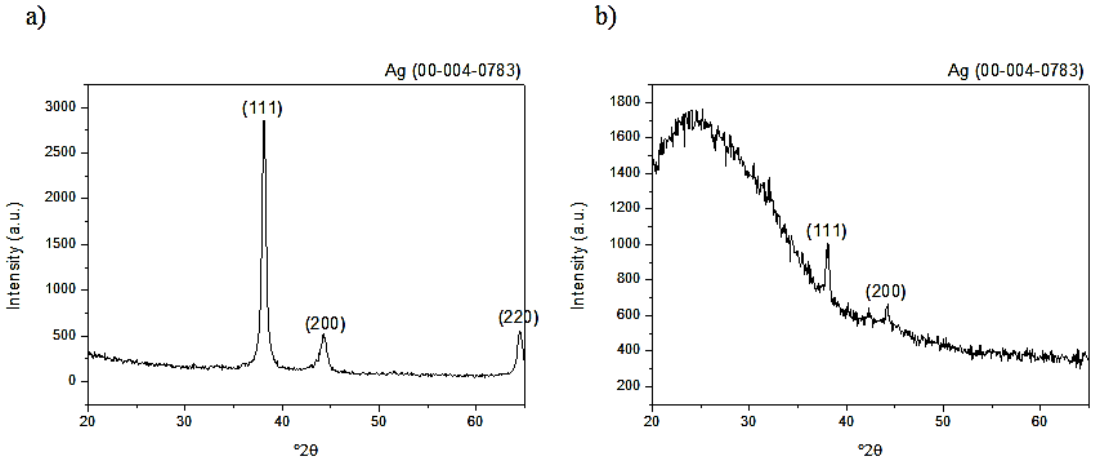

Figure 96. X-ray diffractograms for silver films deposited at 140 °C and with 8 s of irradiation on a) Si and b) glass.

Figure 97 depicts SEM images of the most promising silver films on various, essentially oxide substrates. Distinct island growth was observed on all substrates. As shown in Figure 98, the density of silver nuclei is considerably lower on Ru and TiN as opposed to

the oxide surfaces. Similar behavior was also observed for ruthenium as discussed in the following section.

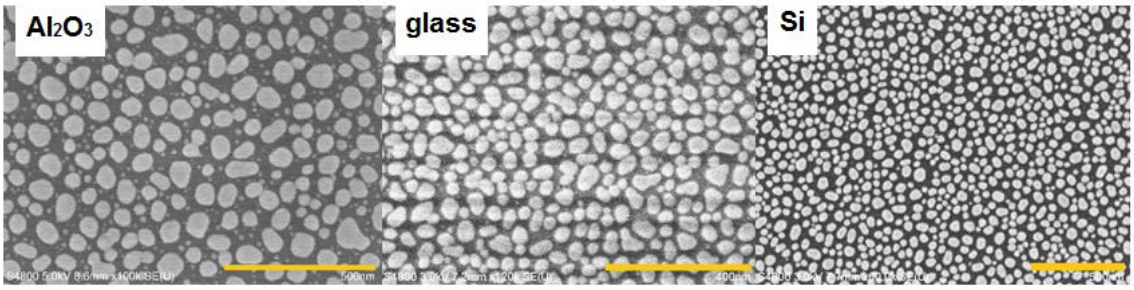

Figure 97. SEM micrographs of silver films deposited on Al_2O_3, soda lime glass, and Si. Scale bar is 500 nm for Al_2O_3 and Si, 400 nm for glass.

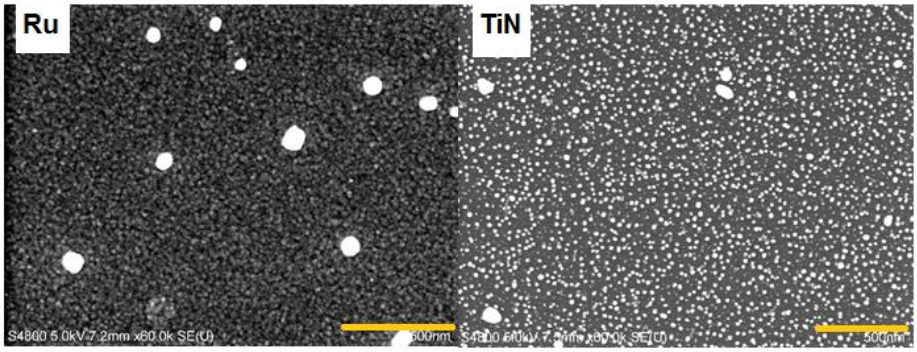

Figure 98. SEM images of silver deposits grown on Ru and TiN. Scale bar is 500 nm.

9.2 Ruthenium

The photo-ALD of ruthenium was studied using both Setups 1 and 2 from a variety of different precursors. The first set of experiments was carried out with Setup 1 using $Ru(hfac)_2(CO)_2$, $Ru(thd)_2(CO)_2$, and $Ru_3(CO)_{12}$ (99 %) as well as (ethylbenzyl)(1-ethyl-1,4-cyclohexadienyl)Ru(0) (EBECHRu). The first two were synthesized in house and the latter two obtained from Strem Chemicals Inc. and Hansol Chemical, respectively. The carbonyl-containing precursors have been successfully utilized in thermal CVD to deposit both Ru and RuO_2.[225–229] However, their poor thermal stability restricts their applicability in ALD. For example, $Ru_3(CO)_{12}$ decomposed already in the source. EBECHRu has been utilized to

deposit metallic ruthenium in thermal ALD.[230] Although initial photolysis experiments in both cyclohexane and isopropanol solution were promising, no proper metal deposition from any of the precursors was observed. The precursors, deposition conditions, and results for the experiments using Setup 1 are summarized in Table 8.

Table 8. Ruthenium experiments using Setup 1.

Precursor	**Reactant(s) with irradiation**	**T_{dep} (°C)**	**Result**
$Ru(hfac)_2(CO)_2$	$^{i}PrOH$, H_2, Me_2CO chd	250	No film
$Ru(thd)_2(CO)_2$	O_2	250	Brown film, no shadow effect
$Ru_3(CO)_{12}$	-	100–120	Precursor decomposed in source
EBECHRu 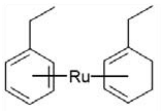	H_2, H_2O, O_2, Me_2CO	120–200	Very thin, brown film with shadow effect using excited O_2 at 120 °C

Since no auspicious results were obtained using the aforementioned precursors and Setup 1, further experiments were carried out using Setup 2. 4000 cycles of EBECHRu (1.6 s followed by 5 s purge) combined with a subsequent irradiation period (5–10 s) at 200 °C produced a very thin film exhibiting a visible shadow effect from the mask; thus, the process was confirmed as photolytic. However, no mirror-like ruthenium film was deposited.

Deposition from $Ru(CO)_3(chd)$ (ATMI Inc.) was studied by photo-ALD in the temperature region of 75–125 °C. Several papers on the thermal ALD and pulsed CVD of ruthenium using $Ru(CO)_3(chd)$ together with NH_3, N_2O, or H_2 have been published.[231–235] However, the other groups utilized a precursor with a 1,3-cyclohexadienyl ligand instead of the 1,4-cyclohexadienyl precursor employed in the experiments presented in this thesis (Figure 99). In the photo-ALD experiments, the precursor was evaporated at 50 °C and pulsed for 1.6 s followed by 5 s of purge. The irradiation period was varied between 5 and 15 s, and the cycle count was 4000. The process was also tested with Setup 1, but it produced non-uniform films due to the poor confinement of the irradiation.

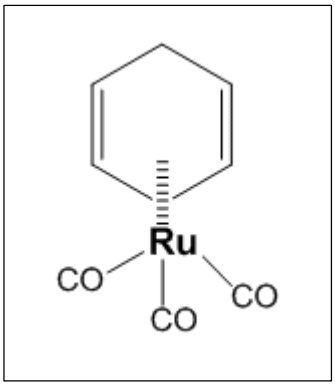

Figure 99. Molecular structure of $Ru(CO)_3(chd)$.

Mirror-like ruthenium was deposited at 100–125 °C on Al_2O_3, soda lime glass, and Si (Figure 100). All the films were uniform and exhibited a distinct shadow effect arising from the near-contact mask. An irradiation period of 5 s was enough to produce metallic ruthenium at 125 °C. The film thickness on Si was measured to be 34 nm. At a deposition temperature of 100 °C, an irradiation period of 10 s was required to produce mirror-like film (16.1 nm). The film thickness was not increased by increasing the irradiation period to 15 s (13 nm). Figure 101 depicts SEM micrographs of Ru films deposited on Si at various temperatures and with 5 s of irradiation. The films exhibited high surface roughness. Analogous to the silver experiments, Ru deposition was not observed on TiN coated Si. On TiN, film growth was obtained only after ≥ 50 cycles of TMA + H_2O deposited prior to the photodeposition (10 cycles was insufficient).

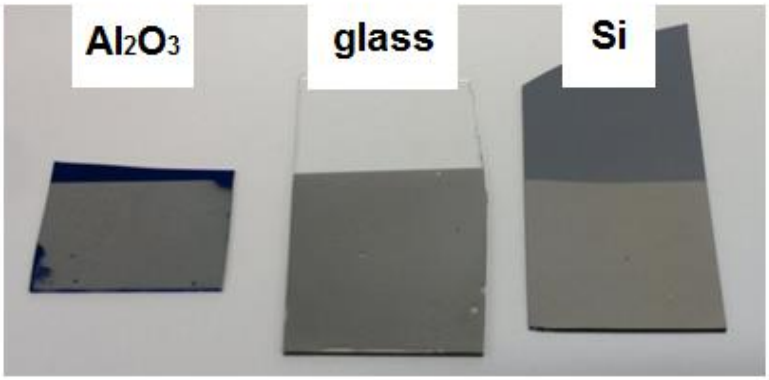

Figure 100. Ruthenium deposited on various substrates at 125 °C and with 5 s of irradiation.

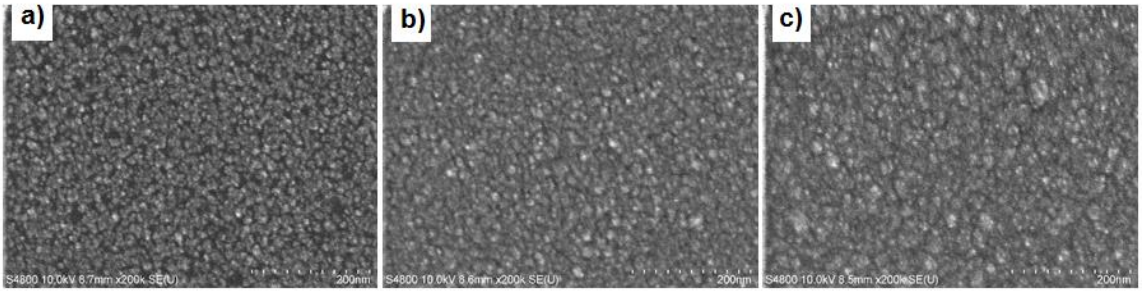

Figure 101. SEM images of Ru films deposited on Si with 5 s of irradiation at a) 75 b) 100, and c) 125 °C.

In summary, neither silver nor ruthenium were deposited on TiN coated Si. On Al_2O_3, glass, and Si the growth appeared to stop after the formation of a continuous metal film. One possible explanation for the observed behavior is that the process is actually driven by photocatalysis on the substrate surface, and the adsorbed precursor molecules on their own are passive to photolysis.[236] Another possibility is that the underlying metal surface quenches the excited species generated during irradiation inhibiting deposition after the formation of a continuous metal film. This mechanism does not, however, apply to the single-source photo-ALD processes of oxides; Ta_2O_5 was deposited with a similar thickness on both Si and Ir (51 and 45 nm, respectively, with 5000 cycles at 245 °C and with 30 flashes during 6 s irradiation periods). The third option, although unlikely, is that the precursor molecules simply do not adsorb on metallic surfaces. The adsorption properties of both $Ru(CO)_3(chd)$ and $Ag(fod)(PEt_3)$ should, namely, be quite similar here as in the thermal ALD process of ruthenium from the aforementioned precursor combined with NH_3, N_2O, or H_2 as well as in the PEALD process of silver. Since these processes can be utilized to deposit metal films beyond the formation of a continuous layer, it is doubtful that the adsorption of the precursor molecules would be the problem in photo-ALD. The lack of film deposition on metallic surfaces may be explained by only one of the aforesaid reasons, a combination of them, or by something utterly different; thus, further investigation is necessary.

According to XRD, the ruthenium films deposited on Si at 100 and 125 °C were weakly crystalline (Figure 102). Reflections at 38, 42, and 44 °2θ corresponding to crystal planes of (100), (002), and (101), respectively, were detected. Based on the observations, the crystal structure was characterized as hexagonal. Peak broadening is caused by the small grain size arising from the low deposition temperatures and high level of impurities, as measured by

TOF-ERDA analysis (Figure 103). For the film deposited at 125 °C and with 5 s of irradiation, a high carbon content of 13.5 at.% was measured. The contamination was probably caused by incomplete ligand removal or thermal decomposition, the latter of which would also explain the thickness difference between the films deposited at 125 and 100 °C (34 versus 16 nm with 5 and 10 s of irradiation, respectively). According to Song *et al.*, the decomposition of $Ru(CO)_3(chd)$ begins at temperatures above 100 °C.[231] The formation of a distinct shadow under the near-contact mask also at 125 °C would, however, be unlikely if thermal decomposition was involved.

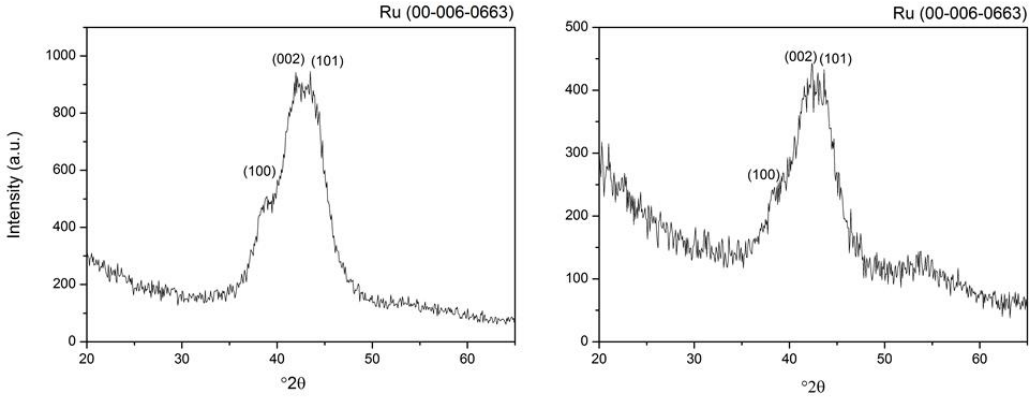

Figure 102. X-ray diffractograms of Ru deposited on Si at 125 °C (left) and 100 °C (right). Film thicknesses were 34 and 16 nm, respectively.

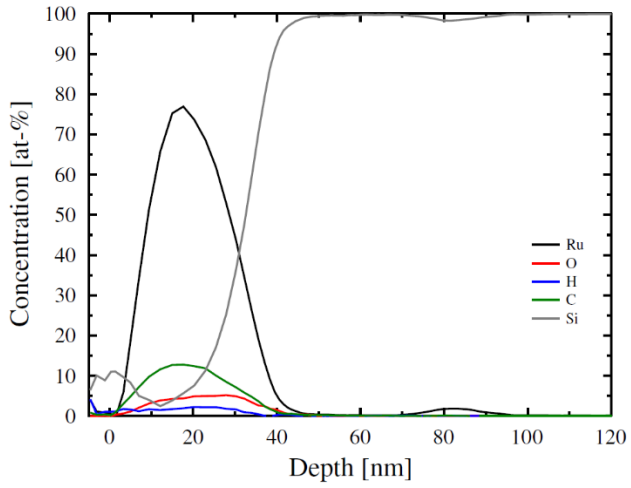

Element	at.%	Error
Ru	76.32	0.72
O	6.60	0.56
C	13.50	0.84
H	3.59	0.50

Figure 103. TOF-ERDA depth profiles obtained from Ru deposited on Si at 125 °C with 5 s of irradiation (34 nm).

According to the resistivity measurements, the 16.1 nm Ru film deposited at 100 °C with a 10 s irradiation period exhibited a relatively high resistivity of ~250 μΩcm (bulk value 7.6 μΩcm at 0 °C). For the 13 nm film deposited also at 100 °C but with a longer irradiation period of 15 s, a resistivity of ~290 μΩcm was measured. The composition of these films was not determined.

Despite the apparent self-termination of photodeposition, the $Ru(CO)_3$(chd) photo-ALD process may be of use when combined with an existing thermal ALD process. Aaltonen *et al.* studied the ALD of ruthenium using $RuCp_2$ and oxygen.[237] Metallic ruthenium was deposited at 275–400 °C on glass substrates coated with either Al_2O_3 or TiO_2 (~2 nm). Without the Al_2O_3 or TiO_2 layers, the deposits were non-uniform and exhibited macroscopic holes. Combined with the thermal process, the photo-ALD process could possibly be utilized to produce uniform ruthenium also on other substrates, such as glasses and Si, and thus act as a nucleation activator. Taking into account the selectivity and low operating temperature of the photo-ALD process, the further thermal deposition could potentially also be carried out at a lower temperature and only on selected parts of the substrate. Similar approaches regarding the previously mentioned $RuCp_2 + O_2$ process have been studied before; Aaltonen and coworkers, for example, observed that the ruthenium deposition occurred at a temperature of as low as 225 °C when using an Ir seed layer.[238] Färm *et al.*, on the other hand, studied the area-selective deposition of ruthenium from $RuCp_2$ and O_2 by using microcontact printed RuO_x as an activator to enable film growth only on selected parts of Si substrates at a temperature of 250 °C which is below the deposition temperature of Ru on Si.[239]

9.3 Miscellaneous studies

In addition to silver and ruthenium, Setup 2 was utilized to study the photo-ALD of several other metals as well. The materials, most important deposition conditions, and results are summarized in Table 9. On the grounds of their abundance in photo-CVD (Sections 4.9, 4.12), copper and molybdenum deposition was attempted from $Cu(hfac)_2 \cdot xH_2O$ and 98 % $Mo(CO)_6$, respectively. Both precursors were obtained from Sigma-Aldrich. A reducing agent was added to facilitate the reduction. No film formation was observed in either case. Irradiation might cause decomposition of the copper precursor and produce fluorine which

could possibly poison the surface and thus inhibit further adsorption of the precursor. In molybdenum photo-CVD, the carbonyl ligands are partially removed already in the gas phase possibly explaining why no film was deposited in the photo-ALD experiments relying solely on surface reactions. Molybdenum was deposited only on the chamber walls possibly due to thermal decomposition.

The experiments on titanium were based on a CVD patent by Iyer *et al.* who utilized a radio frequency source to generate reactive methyl radicals from methane.[240] The radicals attack the titanium-chlorine bonds in $TiCl_4$ producing chloromethane and metallic titanium (Equation 17). Acetone absorbs UV radiation in the region of 220–330 nm with a maximum at 280 nm. As depicted in Equation 18, the photodissociation of acetone results in the formation of methyl radicals; consequently, titanium deposition should, in theory, be possible analogous to the patent of Iyer and coworkers. However, no deposition was observed potentially caused by too low a yield of methyl radicals.

$$TiCl_4 + CH_4 \xrightarrow{plasma} TiCl_4 + \bullet CH_3 + \bullet H \rightarrow Ti + 4\ CH_3Cl + 2\ H_2 \quad (17)$$

$$CH_3C(O)CH_3 + h\nu \rightarrow \bullet CH_3CO + \bullet CH_3 \quad (18)$$

Table 9. Deposition conditions and results for processes tested with Setup 2.

Metal	**Precursor**	**Reactant**	**T_{dep} (°C)**	**Pulsing sequence (s) (prec./purge/react./purge)**	**Result**
Mo	$Mo(CO)_6$	-	150	1.6/5/-/5*	No film
Mo	$Mo(CO)_6$	H_2	180	1.6/5/2.5*/3.5*	Film only on chamber walls
Cu	$Cu(hfac)_2$	$^{i}PrOH$ and/or Me_2CO	150	1.6/5/4*/5*	No film
Ti	$TiCl_4$	Me_2CO	250	0.2/5/2*/5*	Very thin, non-metallic film

*) irradiation simultaneously with pulse and/or purge

10 Conclusions

The aim of the photo-ALD experiments was to develop low-temperature processes for the deposition of as thin, continuous, and conducting metal films as possible. Owing to the lower reaction temperatures, coarsening should be reduced and continuous films therefore formed at lower thicknesses in photo-ALD than in thermal ALD. Lower thicknesses, in turn, promote the downscaling of feature sizes potentially fulfilling the never-ending yearning for more efficient electronic devices. Moreover, photo-ALD provides a route to single-source processes and selective area deposition diversifying the field of metal deposition in the microelectronic industry.

In order to test and verify the operation of the photo-ALD reactor, the single-source process to deposit Ta_2O_5 from $Ta(OEt)_5$, first introduced by Lee *et al*., was scrutinized. In addition, analogous processes were developed for Nb_2O_5, TiO_2, ZrO_2, and HfO_2. In all cases, selective area growth was realized with the use of near-contact masks. The photolytic nature of the Ta_2O_5 process was further demonstrated with LHAR structures prepared by VTT Technical Research Centre of Finland Ltd. On the grounds of single-source chemistry, the photo-ALD of metal oxides from the corresponding metal alkoxides provides a fresh approach to metal oxide deposition. The development of the aforementioned processes also proved the proper operation of the reactor and was important preliminary work for the execution of the actual goal: metal deposition.

Based solely on the considerable amount of reports on metal photo-CVD, one might expect comparable fruitfulness for metal photo-ALD as well. However, the deposition of metals by photo-ALD turned out to be more complicated than anticipated. Various precursors were examined to deposit a wide selection of metals, including titanium, molybdenum, ruthenium, silver, and copper, but proper metallic film was obtained only for silver and ruthenium and, furthermore, only on certain substrates. Neither silver from $Ag(fod)(PEt_3)$ nor ruthenium from $Ru(CO)_3(chd)$ was deposited on TiN coated Si. Moreover, on Al_2O_3, glass, and Si the deposition appeared to stop after the formation of a continuous metal film. The underlying metallic surface possibly quenches the excited precursor species generated by irradiation and thus inhibits further deposition. This mechanism does not, however, apply to the single-source photo-ALD processes of oxides which were deposited with a similar thickness on

both Si and noble metals. It is also possible that the deposition of metals is actually driven by photocatalysis that occurs only on oxide surfaces and stops once the surface is coated with a layer of metal. Finally, the problem could be adsorption related; the precursor molecules might simply not adsorb on metallic surfaces. This is quite unlikely, however, since $Ru(CO)_3(chd)$ has been employed in thermal ALD and $Ag(fod)(PEt_3)$ in PEALD to produce films beyond the point of a continuous layer. Further investigation is required to determine whether the observed behavior is caused by only one of the three explanations, a combination of them, or by something completely different.

Due to the short lifetimes of the excited states and the lack of suitable equipment, surface photochemistry is an area seriously lacking in systematic research, and most information is based merely on speculations and theoretical calculations. Since ALD is a surface reaction method, the understanding of the surface photochemistry would be crucial for the development of metal photo-ALD. So far, all the research has relied on trial-and-error leaving any potential future breakthroughs in the hands of an educated guess. However, without methods to study the photochemistry that occurs in the system, thorough scrutiny of literature together with trial-and-error is the best, and only, asset at hand. Although there is a possibility that photo-ALD might turn out unsuitable for metal deposition in the normal sense, the method could be leveraged for e.g. the low-temperature deposition of patterned seed layers for subsequent area-selective thermal ALD. One should just look for the silver lining, or as would be more to the point in the context of photo-ALD, any metal lining.

11 References

1 Kodas, T. and Hampden-Smith, M. *The Chemistry of Metal CVD*, VCH Verlagsgesellschaft mbH, Weinheim (Federal Republic of Germany), 1994.

2 Ritala, M. and Leskelä, M. *Handbook of Thin Film Materials,* Academic Press, New York, 2002.

3 Ritala, M. and Niinistö, J. in *Chemical Vapour Deposition: Precursors, Processes and Applications*, eds. Jones, A.C. and Hitchman, M.L., Royal Society of Chemistry, Cambridge, UK, 2009, chapter 4, p. 158.

4 Steven, M.G. *Chem. Rev.* ***110*** (2010) 111.

5 Johnson, R.W., Hultqvist, A. and Bent, S.F. *Mater. Today* ***17*** (2014) 236.

6 Leskelä, M., Niinistö, J. and Ritala, M. *Compr. Mater. Process.* ***4*** (2014) 101.

7 Miikkulainen, V., Leskelä, M., Ritala, M. and Puurunen, R.L. *J. Appl. Phys.* ***113*** (2013) 021301.

8 Aaltonen, T. *Atomic Layer Deposition of Noble Metal Thin Films*, doctoral dissertation, University of Helsinki, 2005.

9 Hämäläinen, J. *Atomic Layer Deposition of Noble Metal Oxide and Noble Metal Thin Films*, doctoral dissertation, University of Helsinki, 2013.

10 Kim, H. *Thin Solid Films* ***519*** (2011) 6639.

11 Doi, A., Aoyagi, Y. and Namba, S. *Appl. Phys. Lett.* ***49*** (1986) 785.

12 Aoyagi, Y., Doi, A., Meguro, T., Iwai, S., Nagata, K. and Nonoyama, S. *Chemtronics* ***4*** (1989) 117.

13 Aoyagi, Y., Meguro, T., Iwai, S. and Doi, A. *Mater. Sci. Eng., B* ***10*** (1991) 121.

14 Chen, Q. and Dapkus, P.D. *Thin Solid Films* ***225*** (1993) 115.

15 Yamada, A., Sang, B. and Konagai, M. *Appl. Surf. Sci.* ***112*** (1997) 216.

16 Saito, K., Watanabe, Y., Takahashi, K., Matsuzawa, T., Sang, B. and Konagai, M. *Sol. Energy Mater. Sol. Cells* ***49*** (1997) 187.

17 Yamamoto, Y., Saito, K., Takahashi, K. and Konagai, M. *Sol. Energy Mater. Sol. Cells* ***65*** (2001) 125.

18 Lee, Y.-H., Kwak, J.-C., Gang, B.-S., Kim, H.-C., Choi, B.-H., Jeong, B.-K., Park, S.-H. and Lee, K.-H. *J. Electrochem. Soc.* ***151*** (2004) C52.

19 Kwak, J.-C., Lee, Y.-H. and Choi, B.-H. *Appl. Surf. Sci.* ***230*** (2004) 249.

20 Olander, J., Ottosson, L.M., Heszler, P., Carlsson, J.-O. and Larsson, K.M.E. *Chem. Vap. Deposition* ***11*** (2005) 330.

21 Lee, B.H., Cho, S., Hwang, J.K., Kim, S.H. and Sung, M.M. *Thin Solid Films* ***518*** (2010) 6432.

22 Kim, S.K., Hoffmann-Eifert, S. and Waser, R. *Electrochem. Solid-State Lett.* ***14*** (2011) H146.

23 Chalker, P.R., Marshall, P.A., Dawson, K., Brunell, I.F., Sutcliffe, C.J. and Potter, R.J. *AIP Adv.* ***5*** (2015) 017115.

24 Irvine, S.J.. and Lamb, D. in *Chemical Vapour Deposition: Precursors, Processes and Applications*, eds. Jones, A.C. and Hitchman, M.L., Royal Society of Chemistry, Cambridge, UK, 2009, chapter 11, p. 477.

25 Solanki, R., Moore, C. and Collins, G. *Solid State Technol.* ***28*** (1985) 220.

26 Hanabusa, M. *Mater. Sci. Rep.* ***2*** (1987) 51.

27 Herman, I.P. *Chem. Rev.* ***89*** (1989) 1323.

28 Baum, T.H. and Comita, P.B. *Thin Solid Films* ***218*** (1992) 80.

29 Maury, F., Gueroudji, L. and Vahlas, C. *Surf. Coat. Technol.* ***86-87*** (1996) 316.

30 Trundle, C. and Brierley, C.J. *Appl. Surf. Sci.* ***36*** (1989) 102.

31 Wrighton, M. *Chem. Rev.* ***74*** (1974) 401.

32 Jackson, R.L. and Tyndall, G.W. *Chemtronics* ***4*** (1989) 127.

33 Kuroda, H. *Pure Appl. Chem.* ***64*** (1992) 1449.

34 Hess, P. *Spectrochim. Acta, Part A* ***46*** (1990) 489.

35 Stauf, G.T., Driscoll, D.C., Dowben, P.A., Barfuss, S. and Grade, M. *Thin Solid Films* ***153*** (1987) 421.

36 Oshima, T., Yamada, A. and Konagai, M. *Jpn. J. Appl. Phys.* ***36*** (1997) 6481.

37 Kadokura, H., Ito, A., Kimura, T. and Goto, T. *Surf. Coat. Technol.* ***204*** (2010) 2302.

38 Fukushima, Y., Higashino, T., Matsumura, N. and Saraie, J. *Jpn. J. Appl. Phys.* ***31*** (1992) L261.

39 Conde, O. and Silvestre, A.J. *Appl. Phys. A* ***79*** (2004) 489.

40 Mercury lamp spectrum, http://www.newport.com/200---500-W-Hg-Research-Arc-Sources/378044/1033/info.aspx, Accessed August 27th, 2015.

41 Xenon lamp spectrum, https://commons.wikimedia.org/wiki/File:Xenon_arc_lamp_profile.png, Accessed August 25th, 2015.

42 D2 lamp spectrum, http://mcphersoninc.com/lightsources/model632lightsource.htm, Accessed August 27th, 2015.

43 Kuroiwa, K., Yamazaki, H., Tsuchiya, S., Kamisako, K. and Tarui, Y. *Jpn. J. Appl. Phys.* ***31*** (1992) L518.

44 Turney, W., Hung, Y.M., Starcevich, S.G., Cardinahl, P.S. and Grassian, V.H. *Chem. Mater*. ***4*** (1992) 1192.

45 Mutsukura, N., Katoh, Y. and Machi, Y. *J. Appl. Phys.* ***60*** (1986) 3364.

46 Kwak, J., Kwon, S.W., Park, S.I., Yang, J.H. and Lim, K.S. *Sol. Energy Mater. Sol. Cells* ***92*** (2008) 1081.

47 Rocheleau, R.E. and Jackson, S.C. *U.S. Pat.* 4654226 (1987).

48 Rocheleau, R.E., Hegedus, S.S., Buchanan, W.A. and Jackson, S.C. *Appl. Phys. Lett.* ***51*** (1987) 133.

49 Peters, J.W. and Gebhart, F.L. *U.S. Pat.* 4265932 (1981).

50 Deutsch, T.F., Ehrlich, D.J. and Osgood Jr., R.M. *Appl. Phys. Lett.* ***35*** (1979) 175.

51 Rytz-Froidevaux, Y., Salathé, R.P. and Gilgen, H.H. *Phys. Lett.* ***84A*** (1981) 216.

52 Calloway, A.R., Galantowicz, T.A. and Fenner, W.R. *J. Vac. Sci. Technol. A* ***1*** (1983) 534.

53 Arai, Y., Yamaguchi, S. and Ohsaki, T. *Appl. Phys. Lett.* ***52*** (1988) 2083.

54 Shanov, V., Ivanov, B. and Popov, C. *Thin Solid Films* ***207*** (1992) 71.

55 Seki, K., Frye, J.M., Okabe, H. and Halpern, J.B. *J. Cryst. Growth* ***132*** (1993) 25.

56 Shi, Z., Lu, P. and Walker, A.V. *Langmuir* ***28*** (2012) 16909.

57 Tsao, J.Y. and Ehrlich, D.J. *Appl. Phys. Lett.* ***45*** (1984) 617.

58 Higashi, G.S. and Fleming, C.G. *Appl. Phys. Lett.* ***48*** (1986) 1051.

59 Blonder, G.E., Higashi, G.S. and Fleming, C.G. *Appl. Phys. Lett.* ***50*** (1987) 766.

60 Mantell, D.A. *Appl. Phys. Lett.* ***53*** (1988) 1387.

61 Lee, H.W. and Allen, S.D. *Appl. Phys. Lett.* ***58*** (1991) 2087.

62 Baum, T.H., Larson, C.E. and Jackson, R.L. *Appl. Phys. Lett.* ***55*** (1989) 1264.

63 Foulon, F. and Stuke, M. *Appl. Phys. A* ***56*** (1993) 283.

64 Lehmann, O. and Stuke, M. *Appl. Phys. A* ***53*** (1991) 343.

65 Frugier, T., Boulahia, A., Sayah, A., Tonneau, D., Bourée, J.E., Siffre, J.M. and Mencaraglia, D. *Appl. Surf. Sci.* ***69*** (1993) 305.

66 Popov, C., Ivanov, B. and Shanov, V. *J. Appl. Phys.* ***75*** (1994) 3687.

67 Han, J., Jensen, K.F., Senzaki, Y. and Gladfelter, W.L. *Appl. Phys. Lett.* ***64*** (1994) 425.

68 Beuermann, T. and Stuke, M. *Chem. Phys. Lett.* ***178*** (1991) 197.

69 Flicstein, J. and Bourée, J.E. *Appl. Surf. Sci.* ***36*** (1989) 443.

70 Motooka, T., Gorbatkin, S., Lubben, D. and Greene, J.E. *J. Appl. Phys.* ***58*** (1985) 4397.

71 Higashi, G.S. *Appl. Surf. Sci.* ***43*** (1989) 6.

72 Higashi, G.S. *J. Chem. Phys.* ***88*** (1988) 422.

73 Okabe, H., Emadi-Babaki, M.K. and McCrary, V.R. *J. Appl. Phys.* ***69*** (1991) 1730.

74 Cacouris, T., Scelsi, G., Shaw, P., Scarmozzino, R., Osgood, R.M. and Krchnavek, R.R. *Appl. Phys. Lett.* ***52*** (1988) 1865.

75 Zhu, N., Cacouris, T., Scarmozzino, R. and Osgood Jr., R.M. *J. Vac. Sci. Technol. B* ***10*** (1992) 1167.

76 Hanabusa, M., Oikawa, A. and Cai, P.Y. *J. Appl. Phys.* ***66*** (1989) 3268.

77 Geohegan, D.B. and Eden, J.G. *Appl. Phys. Lett.* ***45*** (1984) 1146.

78 Lane, S.J. and Green, M. *J. Chem. Soc., Faraday Trans.* ***87*** (1991) 995.

79 Tsao, J.Y., Becker, R.A., Ehrlich, D.J. and Leonberger, F.J. *Appl. Phys. Lett.* ***42*** (1983) 559.

80 Izquierdo, R., Lavoie, C. and Meunier, M. *Appl. Phys. Lett.* ***57*** (1990) 647.

81 Chou, W.B., Azer, M.N. and Mazumder, J. *J. Appl. Phys.* ***66*** (1989) 191.

82 Alderdice, D.S. *J. Mol. Spectrosc.* ***14*** (1965) 509.

83 Moskalyk, R.R. and Alfantazi, A.M. *Miner. Eng.* ***16*** (2003) 793.

84 Haas, H. and Sheline, R.K. *J. Am. Chem. Soc.* ***88*** (1966) 3219.

85 Rubinson, K.A. *J. Am. Chem. Soc.* ***98*** (1976) 5188.

86 Solanki, R., Boyer, P.K., Mahan, J.E. and Collins, G.J. *Appl. Phys. Lett.* ***38*** (1981) 572.

87 Ehrlich, D.J., Osgood Jr., R.M. and Deutsch, T.F. *J. Electrochem. Soc.* ***128*** (1981) 2039.

88 Mayer, T.M., Fisanick, G.J. and Eichelberger IV, T.S. *J. Appl. Phys.* ***53*** (1982) 8462.

89 Solanki, R., Boyer, P.K. and Collins, G.J. *Appl. Phys. Lett.* ***41*** (1982) 1048.

90 Yokoyama, H., Uesugi, F., Kishida, S. and Washio, K. *Appl. Phys. A* ***37*** (1985) 25.

91 Flynn, D.K., Steinfeld, J.I. and Sethi, D.S. *J. Appl. Phys.* ***59*** (1986) 3914.

92 Gluck, N.S., Wolga, G.J., Bartosch, C.E., Ho, W. and Ying, Z. *J. Appl. Phys.* ***61*** (1987) 998.

93 Nowak, R., Konstantinov, L. and Hess, P. *Appl. Surf. Sci.* ***36*** (1989) 177.

94 Singmaster, K.A., Houle, F.A. and Wilson, R.J. *Appl. Phys. Lett.* ***53*** (1988) 1048.

95 Haight, R., Longo, P. and Wagner, A. *J. Vac. Sci. Technol. A* ***21*** (2003) 649.

96 Hitosugi, T. and Mizuno, T. *Jpn. J. Appl. Phys.* ***44*** (2005) L596.

97 Gray, H.. and Beach, N.A. *J. Am. Chem. Soc.* ***85*** (1963) 2922.

98 Tyndall, G.W. and Jackson, R.L. *J. Chem. Phys.* ***89*** (1988) 1364.

99 Kotzian, M., Rösch, N., Schröder, H. and Zerner, M.C. *J. Am. Chem. Soc.* ***111*** (1989) 7687.

100 Ray, U., Brandow, S.L., Bandukwalla, G., Venkataraman, B.K., Zhang, Z. and Vernon, M. *J. Chem. Phys.* ***89*** (1988)

101 Jackman, R.B., Foord, J.S., Adams, A.E. and Lloyd, M.L. *J. Appl. Phys.* ***59*** (1986) 2031.

102 Maxwell, J.L., Pegna, J. and Messia, D.V. *Appl. Phys. A* ***67*** (1998) 323.

103 Xu, X. and Steinfeld, J.I. *Appl. Surf. Sci.* ***45*** (1990) 281.

104 Armstrong, J.V., Enrech, M., Decrouez, C., Lunney, J.G. and Coey, J.M.. *IEEE Trans. Magn.* ***26*** (1990) 1629.

105 Allen, S.D. and Tringubo, A.B. *J. Appl. Phys.* ***54*** (1983) 1641.

106 Bottka, N., Walsh, P.J. and Dalbey, R.Z. *J. Appl. Phys.* ***54*** (1983) 1104.

107 Foord, J.S. and Jackman, R.B. *Chem. Phys. Lett.* ***112*** (1984)

108 Stauf, G.T. and Dowben, P.A. *Thin Solid Films* ***156*** (1988) L31.

109 Rothschild, M., Sedlacek, J.H.C., Shaver, D.C., Ehrlich, D.J., Bittenson, S.N., Edwards Jr., D. and Economou, N.P. *Mat. Res. Soc. Symp. Proc.* ***158*** (1989) 79.

110 Reisse, G., Gaensicke, F., Ebert, R., Illmann, U. and Johansen, H. *Appl. Surf. Sci.* ***54*** (1992) 84.

111 Allen, S.D. *J. Appl. Phys.* ***52*** (1981) 6501.

112 Kräuter, W., Bäuerle, D. and Fimberger, F. *Appl. Phys. A* ***31*** (1983) 13.

113 Petzoldt, F., Piglmayer, K., Kräuter, W. and Bäuerle, D. *Appl. Phys. A* ***35*** (1984) 155.

114 Allen, S.D., Jan, R.Y., Mazuk, S.M. and Vernon, S.D. *J. Appl. Phys.* ***58*** (1985) 327.

115 Jervis, T.R. *J. Appl. Phys.* ***58*** (1985) 1400.

116 Allen, S.D., Goldstone, J.A., Stone, J.P. and Jan, R.Y. *J. Appl. Phys.* ***59*** (1986) 1653.

117 Tonneau, D., Auvert, G. and Y, P. *J. Appl. Phys.* ***64*** (1988) 5189.

118 Beleznai, C., Nanai, L., Leppävuori, S., Remes, J., Moilanen, H. and George, T.F. *SPIE Proc.* ***3573*** (1998) 116.

119 Houle, F.A., Jones, C.R., Baum, T., Pico, C. and Kovac, C.A. *Appl. Phys. Lett.* ***46*** (1985) 204.

120 Maury, F., Vidal, S. and Gleizes, A. *Adv. Mater. Opt. Electron.* ***10*** (2000) 123.

121 Vidal, S., Maury, F., Gleizes, A. and Mijoule, C. *Appl. Surf. Sci.* ***168*** (2000) 57.

122 Wu, Y.-L., Hsieh, M.-H. and Hwang, H.-L. *Thin Solid Films* ***483*** (2005) 10.

123 Igumenov, I.K., Kuchumov, B.M., Kozlova, S.G., Koretskaya, T.P., Trubin, S.V., Sokuev, R.I., Lyakh, V.V. and Kruchinin, V.N. *ECS Trans.* ***25*** (2009) 979.

124 Zama, H., Miyake, T., Hattori, T. and Oda, S. *Jpn. J. Appl. Phys.* ***31*** (1992) L588.

125 Krchnavek, R.R., Gilgen, H.H., Chen, J.C., Shaw, P.S., Licata, T.J. and Osgood Jr., R.M. *J. Vac. Sci. Technol. B* ***5*** (1987) 20.

126 Johnson, W.E. and Schlie, L.A. *Appl. Phys. Lett.* ***40*** (1982) 798.

127 Deutsch, T.F., Ehrlich, D.J. and Osgood Jr., R.M. *Opt. Lett.* ***4*** (1979) 378.

128 Lüthy, W. *Appl. Phys. B* ***40*** (1986) 121.

129 Björklund, K.L., Heszler, P. and Boman, M. *Appl. Surf. Sci.* ***186*** (2002) 179.

130 Gilgen, H.H., Cacouris, T., Shaw, P.S., Krchnavek, R.R. and Osgood, R.M. *Appl. Phys. B* ***42*** (1987) 55.

131 Radloff, W., Hohmann, H., Ritze, H.-H. and Paul, R. *Appl. Phys. B* ***49*** (1989) 301.

132 Duty, C., Johnson, R., Bondi, S. and Lackey, W.J. *Chem. Vap. Deposition* ***9*** (2003) 298.

133 Jackson, R.L. and Tyndall, G.W. *J. Appl. Phys.* ***64*** (1988) 2092.

134 Radloff, W., Below, E., Dürr, H. and Stert, V. *Appl. Phys. A* ***50*** (1990) 233.

135 Singmaster, K.A., Houle, F.A. and Wilson, R.J. *J. Phys. Chem.* ***94*** (1990) 6864.

136 Flint, E.B., Messelhäuser, J. and Suhr, H. *Appl. Phys. A* ***53*** (1991) 430.

137 Messelhäuser, J., Flint, E.B. and Suhr, H. *Adv. Mater.* ***4*** (1992) 347.

138 Flint, E.B., Messelhäuser, J. and Suhr, H. *Appl. Surf. Sci.* ***54*** (1992) 56.

139 Cohan, J.S., Yuan, H., Williams, R.S. and Zink, J.I. *Appl. Phys. Lett.* ***60*** (1992) 1402.

140 Kuchumov, B.M., Koretskaya, T.P., Shevtsov, Y.V., Trubin, S.V., Zharkova, G.I., Danilovich, V.S., Igumenov, I.K. and Kruchinin, V.N. *ECS Trans.* ***25*** (2009) 909.

141 Cole, H.S., Liu, Y.S., Rose, J.W. and Guida, R. *Appl. Phys. Lett.* ***53*** (1988) 2111.

142 Thomas, R.R. and Park, J.M. *J. Electrochem. Soc.* ***136*** (1989) 1661.

143 Kariniemi, M., Niinistö, J., Hatanpää, T., Kemell, M., Sajavaara, T., Ritala, M. and Leskelä, M. *Chem. Mater.* ***23*** (2011) 2901.

144 Itsuki, A., Uchida, H., Satou, M. and Ogi, K. *Nucl. Instrum. Methods Phys. Res., Sect. B* ***121*** (1997) 116.

145 Ehrlich, D.J., Osgood Jr., R.M. and Deutsch, T.F. *IEEE J. Quantum Electron.* ***16*** (1980) 1233.

146 Mingxin, Q., Monot, R. and van den Bergh, H. *Sci. Sin. A* ***27*** (1984) 531.

147 Braichotte, D. and van den Bergh, H. *Springer Ser. Chem. Phys.* ***39*** (1984) 183.

148 Braichotte, D. and van den Bergh, H. *Springer Ser. Opt. Sci.* ***48*** (1985) 38.

149 Weigmann, U., Petzold, H.C., Burghause, H., Putzar, R. and Schaffer, H. *J. Vac. Sci. Technol. B* ***6*** (1988) 2170.

150 Fang, Y.K., Hwang, S.B. and Sun, C.Y. *J. Electrochem. Soc.* ***138*** (1991) 1720.

151 Chiu, M.S., Tseng, Y.G. and Ku, Y.K. *Opt. Lett.* ***10*** (1985) 113.

152 Jackson, R.L. and Tyndall, G.W. *J. Appl. Phys.* ***62*** (1987) 315.

153 Swanson, J.R., Flitsch, F.A. and Friend, C.M. *Surf. Sci.* ***226*** (1990) 147.

154 Xuebiao, L., Jie, Z. and Mingxin, Q. *Thin Solid Films* ***196*** (1991) 95.

155 Flitsch, F.A., Swanson, J.R. and Friend, C.M. *Surf. Sci.* ***245*** (1991) 85.

156 Houle, F.A. and Singmaster, K.A. *J. Phys. Chem.* ***96*** (1992) 10425.

157 Liu, Y.S., Yakymyshyn, C.P., Philipp, H.R., Cole, H.S. and Levinson, L.M. *J. Vac. Sci. Technol. B* ***3*** (1985) 1441.

158 Deutsch, T.F. and Rathman, D.D. *Appl. Phys. Lett.* ***45*** (1984) 623.

159 Gottsleben, O. and Stuke, M. *Appl. Phys. Lett.* ***52*** (1988) 2230.

160 van Maaren, A.J.P., Krans, R.L. and Sinke, W.C. *Appl. Surf. Sci.* ***46*** (1990) 138.

161 Meunier, M., Izquierdo, R., Desjardins, P., Tabbal, M., Lecours, A. and Yelon, A. *Thin Solid Films* ***218*** (1992) 137.

162 Krans, R.L., Brands, C. and Sinke, W.C. *Appl. Surf. Sci.* ***54*** (1992) 117.

163 Mogyorósi, P. and Carlsson, J.-O. *J. Vac. Sci. Technol. A* ***10*** (1992) 3131.

164 Meunier, M., Izquierdo, R., Tabbal, M., Evoy, S., Desjardins, P., Bernier, M.-H., Bertomeu, J., Elyaagoubi, N., Suys, M., Sacher, E. and Yelon, A. *Mater. Sci. Eng. B* ***45*** (1997) 200.

165 Piglmayer, K., Schieche, H. and Chabicovsky, R. *Appl. Surf. Sci.* ***154-155*** (2000) 365.

166 Björklund, K.L., Lu, J., Heszler, P. and Boman, M. *Thin Solid Films* ***416*** (2002) 41.

167 Landström, L., Lu, J. and Heszler, P. *J. Phys. Chem. B* ***107*** (2003) 11615.

168 Zhang, G.Q., Szörényi, T. and Bäuerle, D. *J. Appl. Phys.* ***62*** (1987) 673.

169 Black, J.G., Doran, S.P., Rothschild, M. and Ehrlich, D.J. *Appl. Phys. Lett.* ***56*** (1990) 1072.

170 Hämäläinen, J., Hatanpää, T., Puukilainen, E., Costelle, L., Pilvi, T., Ritala, M. and Leskelä, M. *J. Mater. Chem.* ***20*** (2010) 7669.

171 Schröder, H., Kompa, K.L., Masci, D. and Gianinoni, I. *Appl. Phys. A* ***38*** (1985) 227.

172 Braichotte, D. and van den Bergh, H. *Appl. Phys. A* ***44*** (1987) 353.

173 Braichotte, D. and van den Bergh, H. *Appl. Phys. A* ***45*** (1988) 337.

174 Koplitz, L.V., Shuh, D.K., Chen, Y.-J., Williams, R.S. and Zink, J.I. *Appl. Phys. Lett.* ***53*** (1988) 1705.

175 Braichotte, D. and van den Bergh, H. *Appl. Phys. A* ***49*** (1989) 189.

176 Garrido, C., Braichotte, D., van den Bergh, H., León, B. and Pérez-Amor, M. *Appl. Surf. Sci.* ***43*** (1989) 68.

177 Rooney, D., Negrotti, D., Byassee, T., Macero, D., Chaiken, J. and 1st Lieutenant Vastag, B. *J. Electrochem. Soc.* ***137*** (1990) 1162.

178 Garrido, C. and van den Bergh, H. *Appl. Phys. A* ***53*** (1991) 265.

179 Shaver, D.C., Doran, S.P., Rothschild, M. and Sedlacek, J.H.C. *Proc. Int. Soc. Opt. Engr.* ***1596*** (1991) 46.

180 Baum, T.H. and Jones, C.R. *Appl. Phys. Lett.* ***47*** (1985) 538.

181 Baum, T.H. and Jones, C.R. *J. Vac. Sci. Technol. B* ***4*** (1986) 1187.

182 Baum, T.H., Marinero, E.E. and Jones, C.R. *Appl. Phys. Lett.* ***49*** (1986) 1213.

183 Comita, P.B. and Kodas, T.T. *Appl. Phys. Lett.* ***51*** (1987) 2059.

184 Dagata, J.A., Villa, E. and Lin, M.C. *Appl. Phys. B* ***51*** (1990) 443.

185 Kodas, T.T., Baum, T.H. and Comita, P.B. *J. Cryst. Growth* ***87*** (1988) 378.

186 Kodas, T.T. and Comita, P.B. *J. Appl. Phys.* ***65*** (1989) 2513.

187 Kodas, T.T., Baum, T.H. and Comita, P.B. *J. Appl. Phys.* ***62*** (1987) 281.

188 Jubber, M., Wilson, J.I.B., Davidson, J.L., Fernie, P.A. and John, P. *Appl. Surf. Sci.* ***43*** (1989) 74.

189 Jubber, M., Wilson, J.I.B., Davidson, J.L., Fernie, P.A. and John, P. *Appl. Phys. Lett.* ***55*** (1989) 1477.

190 Messelhäuser, J., Flint, E.B. and Suhr, H. *Appl. Phys. A* ***55*** (1992) 196.

191 Messelhäuser, J., Flint, E.B. and Suhr, H. *Appl. Surf. Sci.* ***54*** (1992) 64.

192 Chiu, M.S., Shen, K.P. and Ku, Y.K. *Appl. Phys. B* ***37*** (1985) 63.

193 Rigby, L.J. *Trans. Faraday Soc.* ***65*** (1969) 2421.

194 Suntola, T. and Antson, J. *U.S. Pat.* 4058430 (1977).

195 Suntola, T. *Mater. Sci. Rep.* ***4*** (1989) 261.

196 Niinistö, L., Päiväsaari, J., Niinistö, J., Putkonen, M. and Nieminen, M. *Phys. Status Solidi A* ***201*** (2004) 1443.

197 Väyrynen, K. *Fotoavusteinen atomikerroskasvatus*, B.Sc. Thesis, University of Helsinki, 2013.

198 Henke, T., Knaut, M., Hossbach, C., Geidel, M., Rebohle, L., Albert, M., Skorupa, W. and Bartha, J.W. *ECS J. Solid State Sci. Technol.* ***4*** (2015) P277.

199 Gao, F., Arpiainen, S. and Puurunen, R.L. *J. Vac. Sci. Technol. A* ***33*** (2015) 010601.

200 Xenon Corporation lamp, http://www.polytec.com/fileadmin/user_uploads/Products/Lichtquellen/Xenon_Blitzlampen/Documents/PH_HL_XEN_RC-800_Series_Brochure.pdf, Accessed October 12th, 2015.

201 Hamamatsu Photonics light source, http://www.hamamatsu.com/eu/en/product/alpha/D/3025/L11798/index.html#1336991057744, Accessed October 12th, 2015.

202 Wu, Y.-J., Wu, C.Y.R., Chou, S.-L., Lin, M.-Y., Lu, H.-C., Lo, J.-I. and Cheng, B.-M. *Astrophys. J.* ***746*** (2012) 175.

203 Lofthus, A. and Krupenie, P.H. *J. Phys. Chem. Ref. Data* ***6*** (1977) 113.

204 Kukli, K., Ritala, M. and Leskelä, M. *J. Electrochem. Soc.* ***142*** (1995) 1670.

205 Kukli, K., Ritala, M., Leskelä, M. and Lappalainen, R. *Chem. Vap. Deposition* ***4*** (1998) 29.

206 Badot, J.C., Ribes, S., Yousfi, E.B., Vivier, V., Pereira-Ramos, J.P., Baffier, N. and Lincot, D. *Electrochem. Solid-State Lett.* ***3*** (2000) 485.

207 Badot, J.C., Mantoux, A., Baffier, N., Dubrunfaut, O. and Lincot, D. *J. Mater. Chem.* ***14*** (2004) 3411.

208 Groult, H., Balnois, E., Mantoux, A., Le Van, K. and Lincot, D. *Appl. Surf. Sci.* ***252*** (2006) 5917.

209 Le Van, K., Groult, H., Mantoux, A., Perrigaud, L., Lantelme, F., Lindström, R., Badour-Hadjean, R., Zanna, S. and Lincot, D. *J. Power Sources* ***160*** (2006) 592.

210 Kaliwoh, N., Zhang, J.-Y. and Boyd, I.W. *Appl. Surf. Sci.* ***186*** (2002) 241.

211 Fang, Q., Zhang, J.-Y., Wang, Z.M., Wu, J.., O'Sullivan, B.J., Hurley, P.K., Leedham, T.L., Davies, H., Audier, M.A., Jimenez, C., Senateur, J.-P. and Boyd, I.W. *Thin Solid Films* ***428*** (2003) 263.

212 Halary, E., Haro-Poniatowski, E., Benvenuti, G. and Hoffmann, P. *Appl. Surf. Sci.* ***168*** (2000) 61.

213 Halary, E., Benvenuti, G., Wagner, F. and Hoffmann, P. *Appl. Surf. Sci.* ***154-155*** (2000) 146.

214 Watanabe, A. and Imai, Y. *Thin Solid Films* ***348*** (1999) 63.

215 Kim, S.K., Hoffmann-Eifert, S., Reiners, M. and Waser, R. *J. Electrochem. Soc.* ***158*** (2011) D6.

216 Ritala, M., Leskelä, M., Niinistö, L. and Haussalo, P. *Chem. Mater.* ***5*** (1993) 1174.

217 Watanabe, A., Tsuchiya, T. and Imai, Y. *Jpn. J. Appl. Phys.* ***40*** (2001) 4051.

218 Yu, J.J. and Boyd, I.W. *Appl. Phys. A* ***75*** (2002) 489.

219 Fang, Q., Zhang, J.-Y., Wang, Z.M., Wu, J.X., O'Sullivan, B.J., Hurley, P.K., Leedham, T.L., Davies, H., Audier, M.A., Jimenez, C., Senateur, J.-P. and Boyd, I.W. *Thin Solid Films* ***427*** (2003) 391.

220 Kukli, K., Ritala, M. and Leskelä, M. *Chem. Vap. Deposition* ***6*** (2000) 297.

221 Sawkar-Mathur, M., Perng, Y.-C., Lu, J., Blom, H.-O., Bargar, J. and Chang, J.P. *Appl. Phys. Lett.* ***93*** (2008) 233501.

222 Chang, H.S., Baek, S.-K., Park, H., Hwang, H., Oh, J.H., Shin, W.S., Yeo, J.H., Hwang, K.H., Nam, S.W., Lee, H.D., Song, C.L., Moon, D.W. and Cho, M.-H. *Electrochem. Solid-State Lett.* ***7*** (2004) F42.

223 Gafney, H.D. and Lintvedt, R.L. *J. Am. Chem. Soc.* ***93*** (1971) 1623.

224 Kutal, C., Grutsch, P.A. and Ferraudi, G. *J. Am. Chem. Soc.* ***101*** (1979) 6884.

225 Lee, F.-J., Chi, Y., Liu, C.-S., Hsu, P.-F., Chou, T.-Y., Peng, S.-M. and Lee, G.-H. *Chem. Vap. Deposition* ***7*** (2001) 99.

226 Cheng, W.-Y., Hong, L.-S., Jiang, J.-C., Chi, Y. and Lin, C.-C. *Thin Solid Films* ***483*** (2005) 31.

227 Lai, Y.-H., Chen, Y.-L., Chi, Y., Liu, C.-S., Carty, A.J., Peng, S.-M. and Lee, G.-H. *J. Mater. Chem.* ***13*** (2003) 1999.

228 Chen, R.-S., Huang, Y.-S., Chen, Y.-L. and Chi, Y. *Thin Solid Films* ***413*** (2002) 85.

229 Wang, Q., Ekerdt, J.G., Gay, D., Sun, Y.-M. and White, J.M. *Appl. Phys. Lett.* ***84*** (2004) 1380.

230 Hong, T.E., Choi, S.-H., Yeo, S., Park, J.-Y., Kim, S.-H., Cheon, T., Kim, H., Kim, M.-K. and Kim, H. *ECS J. Solid State Sci. Technol.* ***2*** (2013) P47.

231 Song, Y.W., Lee, J., Lee, K., Lee, Y. and Jang, H.K. *ECS Trans.* ***2*** (2006) 1.

232 Chung, S.-H., Vasilyev, V., Gorokhov, E., Song, Y.-W. and Jang, H.-K. *Mater. Res. Soc. Symp. Proc.* ***990*** (2007).

233 Vasilyev, V.Y. *Russian Microelectronics* ***39*** (2010) 26.

234 Vasilyev, V.Y. *Russian Microelectronics* ***39*** (2010) 262.

235 Vasilyev, V.Y. *Russian Microelectronics* ***39*** (2010) 199.

236 Zhou, X.-L. and White, J.M. in *Laser Spectroscopy and Photochemistry on Metal Surfaces, Part 2*, eds. Dai, H.L. and Ho, W., World Scientific Publishing Company, Singapore, 1995, chapter 25, p. 1141.

237 Aaltonen, T., Alén, P., Ritala, M. and Leskelä, M. *Chem. Vap. Deposition* ***9*** (2003) 45.

238 Aaltonen, T., Ritala, M., Tung, Y.-L., Chi, Y., Arstila, K., Meinander, K. and Leskelä, M. *J. Mater. Res.* ***19*** (2004) 3353.

239 Färm, E., Lindroos, S., Ritala, M. and Leskelä, M. *Chem. Mater.* ***24*** (2012) 275.

240 Iyer, R. and Sharan, S. *U.S. Pat.* 5946594 (1999).